AMERICAN UNIVERSITY OF BEIRUT

CONTROLLED SYNTHESIS OF MULTIVARIATE METAL-ORGANIC FRAMEWORKS

by
FAYROUZ SALIM ABOU IBRAHIM

A thesis
submitted in partial fulfillment of the requirements
for the degree of Master of Science
to the Department of Chemistry
of the Faculty of Arts and Sciences
at the American University of Beirut

Beirut, Lebanon
June 2020

AMERICAN UNIVERSITY OF BEIRUT

CONTROLLED SYNTHESIS OF MULTIVARIATE METAL-ORGANIC FRAMEWORKS

by
FAYROUZ SALIM ABOU IBRAHIM

Approved by:

_____
Dr. Mohamad Hmadeh, Associate professor   Advisor
Chemistry

_____
Dr. Mazen Al Ghoul, Professor   Co-advisor
Chemistry

_____
Dr. Houssam El-Rassy, Associate professor   Member of Committee
Chemistry

_____
Dr. Kamal Bouhadir, Professor   Member of Committee
Chemistry

Date of thesis defense: 18 June 2020

AMERICAN UNIVERSITY OF BEIRUT

THESIS, DISSERTATION, PROJECT RELEASE FORM

Student Name: _____
　　　　　　　　　　Abou Ibrahim　　　　　　　　Fayrouz　　　　　　　　　Salim
　　　　　　　　　　　　Last　　　　　　　　　　　First　　　　　　　　　Middle

◉ Master's Thesis　　　　　○ Master's Project　　　○ Doctoral Dissertation

☐　　I authorize the American University of Beirut to: (a) reproduce hard or electronic copies of my thesis, dissertation, or project; (b) include such copies in the archives and digital repositories of the University; and (c) make freely available such copies to third parties for research or educational purposes.

☑　　I authorize the American University of Beirut, to: (a) reproduce hard or electronic copies of it; (b) include such copies in the archives and digital repositories of the University; and (c) make freely available such copies to third parties for research or educational purposes after:

One -✓- year from the date of submission of my thesis, dissertation, or project.
Two ---- years from the date of submission of my thesis, dissertation, or project.
Three ---- years from the date of submission of my thesis, dissertation, or project.

_____　　　6 July 2020

Signature　　　　　　　　　　　　　　　Date

ACKNOWLEDGMENTS

AN ABSTRACT OF THE THESIS OF

Fayrouz Salim Abou Ibrahim   for   Master of Science

Major: Chemistry

Title: Controlled Growth and Composition of Multivariate Metal-Organic Frameworks-199 via a Reaction-Diffusion Process

Metal-organic frameworks (MOFs) are robust extended structures built from an organic link and inorganic joint components. MOFs are used as rigid platforms for physical interactions such as gas storage and adsorption, as well as chemical reactions such as catalysis and post-synthetic modification. Most of MOFs reported to date are synthesized using a single type of links and inorganic joint units. Nevertheless, MOF structures incorporating more than one type of linkers (multivariate, MTV-MOFs) and more than one type of metal cations (solid solution MOFs) are rare, and their synthesis and characterization are challenging. The few reported multivariate and mixed metal MOFs exhibited an enhancement in their physical and chemical properties. Here, we outline a strategy for synthesizing MTV-MOFs in a controlled manner by using a reaction-diffusion framework (RDF) at room temperature. Our synthesis system is based on the separation of the reactants into two parts, inner and outer electrolytes. Initially, 1,3,5-benzene tricarboxylic acid (BTC) is dissolved in the gel matrix, and then the outer solution of the copper salt is added on the top of the gel matrix and allowed to diffuse through the inner electrolyte forming thereby the MOF-199 crystals. Based on this initial success, other organic linkers incorporating different functional groups, such as Isophthalic acid, 5-hydroxyisophthalic acid, 5-aminoisophthalic acid, 5-cyanoisophthalic acid and 5-sulfoisophthalic acid, have been mixed in different ratios within the gel matrix leading to the formation of multivariate MOF-199 (MTV-MOF-199). The resulting MTV-MOFs are fully characterized using powder X-ray diffraction (PXRD), Brunauer, Emmett and Teller (BET) analysis, thermogravimetric analysis (TGA), scanning electron microscopy (SEM) and nuclear magnetic resonance (NMR). We have found that several linkers can be incorporated within the same MOF-199 topology in a controlled manner. Thus, different functional groups can be implemented within the framework, leading to controlled interactions between the MOF structure and the guest molecules. Furthermore, the newly synthesized MTV-MOFs are used to remove organic pollutants from water, and their performance is optimized by changing the ratio of the different functional groups in the hetero-MOFs structures.

CONTENTS

ILLUSTRATIONS

TABLES

CHAPTER I

INTRODUCTION

A. Metal Organic Frameworks (MOFs)

1. Emergence of MOFs

"It has always been a dream of scientists to build chemical structures from molecular building blocks", states Omar Yaghi, the father of the rising field of metal-organic frameworks. Indeed, the first attempts to construct hybrid coordination solids date back to the beginning of the eighteenth century with the discovery of a pigment with the formula $Fe_4^{3+}[Fe^{2+}(CN)_6]_3.H_2O$, lately named the Prussian Blue[1]. Many trials then failed to extend the networks into rigid frameworks because the networks collapsed after the guest molecules occupying the empty voids of the structure are removed like the example of the diamond-like open structure combining copper and adiponitrile synthesized by Kinoshita et al. in 1959 in a 3D structure $[Cu((CH_2)_4(CN)_2)_2].(NO_3)$ that collapses after the removal of nitrate ions because of the weakness brought by the length of the adiponitrile binding units[2]. One more advanced trial is made by employing more rigid binding ligands by the synthesis of the same diamond-like structure by replacing adiponitrile by bipyridine yet the same outcome is obtained[3]. By 1995, the discovery of a rigid cobalt-trimesate-bipyridine coordination polymer was done by Yaghi et al. where the term metal-organic framework was first introduced to illustrate the persistence of a stable network of strong covalent metal-linker bonds[4] (Figure 1). In 1998, MOF-2 was discovered displaying a new robustness-granting feature with the assembly

of a multi-metal cluster instead of a single metal corner, later referred to as secondary building units (SBUs), yielded by the joint of Zn (II) ions and the carboxylate of the terephthalate linkers[5]. Using the same SBU approach, MOF-5 and MOF-199 were synthesized[6-7] and found to be of the most efficient and studied structures[8-11].
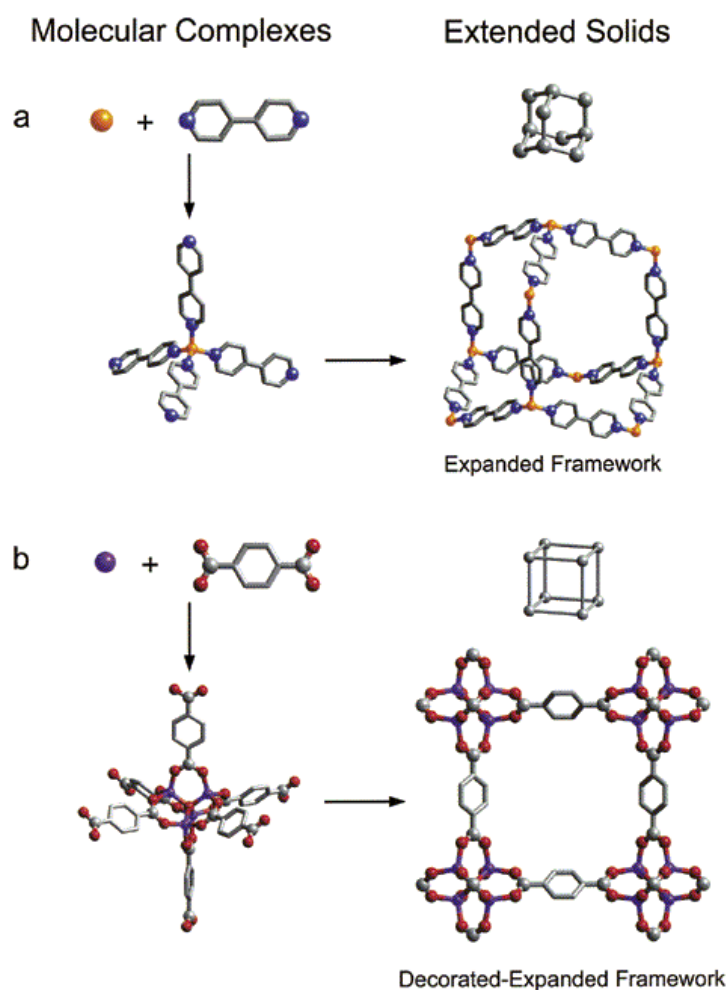
Figure 1 Assembly of metal−organic frameworks (MOFs) by the copolymerization of metal ions with organic linkers to give (a) flexible metal−bipyridine structures with expanded diamond topology and (b) rigid metal−carboxylate clusters that can be linked by benzene "struts" to form rigid extended frameworks in which the M−O−C core (SBU) of each cluster acts as a large octahedron decorating a 6-connected vertex in a cube. Reprinted with permission from Reference[12]. Copyright 2001 American Chemical society.

In fact, MOF-199 is one of the oldest well-known metal organic frameworks. It was discovered in 1999 by Williams et al[7]. It was first named HKUST-1 as an abbreviation to "Hong Kong University of Science and Technology-1" where it was synthesized by heating cupric nitrate trihydrate $Cu(NO_3)(H_2O)_3$ with trimesic acid (TMA) also known as 1,3,5-benzenetricarboxylic acid (BTC) in 50:50 H_2O:EtOH (EtOH, ethyl alcohol) at 180°C for 12 hours to form a porous 3D interconnected network with the formula $[Cu_3(BTC)_2(H_2O)_3]_n$. The topology of the HKUST-1 is characterized by one of the most common secondary building units, the square SBU also known as in our case by the cupper paddle-wheel where two copper ions Cu^{2+} are bridged by 4 dicarboxylate joints as shown Figure 2. These metal nodes forming the vertices of the net are linked together by BTC units consisting the edges of the cubic lattice of the MOF-199 framework as shown in Figure 2.
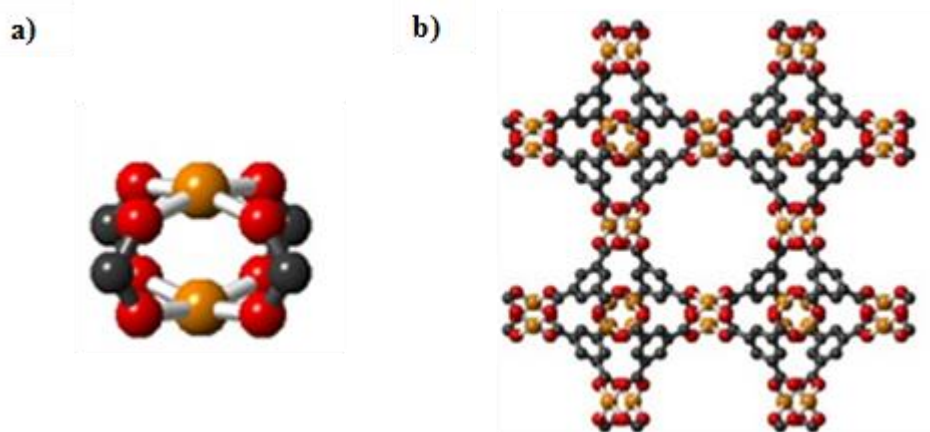
Figure 2 Copper paddle-wheel secondary building unit: Cu, gold; C, black; O, red (a), structure of the cubic metal-organic framework HKUST-199 built from linking the copper-paddle wheel SBUs by BTC (b).

This structure has granted MOF-199 a wide range of superior properties such having a thermal stability up to 300°C owing to its robust metal nodes and a relatively large surface area ranging between 1000 and 2200 m^2/g. These exceptional properties of MOF-199 along with its open metal sites structure allowed to be ideal of various types of applications such as hydrogen and carbon dioxide storage, drug delivery, and catalysis.

2. *Building units of MOFs*

After the emergence of MOFs in 1999, the field has experienced an exponential growth in terms of the number of discovered MOFs, the interested scientists and corresponding publications (Figure 3). This immense attention is owed not only to MOF's exceptional properties and tremendous range of applications but to the chemistry behind the coordination and configuration commonly named by reticular chemistry[13-15]. Reticular chemistry is the chemistry of designing new coordination materials fitted to intended specific applications[16-17]. The concept of the three dimensional architecture of such nets by means of reticular chemistry is brought to life by the knowledge of the exact geometry and connectivity of underlying components of the networks which can be divided into two main building units; the organic linkers and the secondary building units.
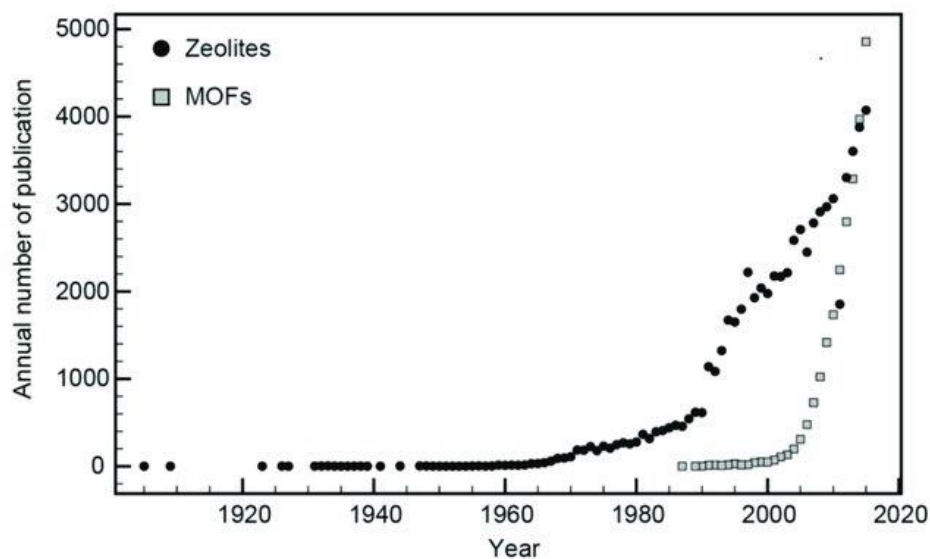
Figure 3 Annual number of publications of MOFs (grey squares) versus common porous zeolites (black circle). Reprinted with permission from reference[18]. Copyright 2017 MDPI.

a. Organic linkers

  The diversity of the synthesized MOF structures is highly relative to the numbers of organic linkers differentiated by their underlying binding groups and core structure. Organic linkers, also known as the struts or the edges of the net, provide the electron donor group forming the chelating mostly covalent bonds with the metal clusters or the net vertices[19]. The polytopic linker (e.g. ditopic, tritopic…dodecatopic) in the net directly influence the dimension and direction of the built framework (Figure 4). Carboxylate-based linkers are the most encountered donor group because of their chelating ability which favors the formation of metal clusters that results to a more rigid frameworks that are chemically and thermally stable[20], featuring permanent porosity and ultrahigh surface areas[21]. In addition to carboxylates, each of imidazolates, phosphates, pyrazolates,

tetrazolates and catecholates are also able bind to metal clusters to further enlarge the family and reveal immense diverse pool of materials with desired properties[22-26]. Moreover, the length of aromatic rings, their geometry and their backbone connectivity give rise to subfamilies of MOFs known as isoreticular MOFs (Figure 5).

Hence, the organic linker component is crucial to direct the growth as well as the rigidity of the framework. This concept leads to the fact that one same linker can be incorporated in different nets resulting a wide variety of structures and topologies (Figure 6).
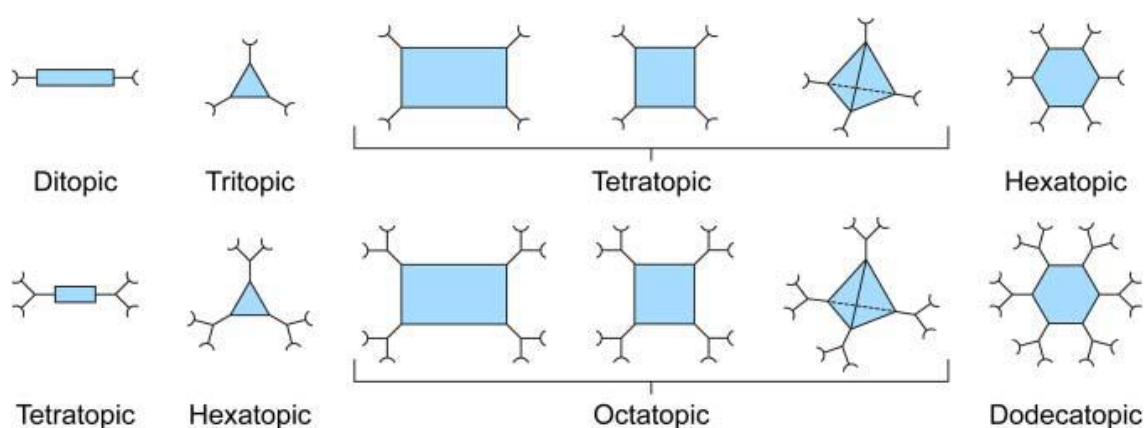
Figure 4   Illustration of the basic geometries of organic linkers used in the synthesis of MOFs typically ranging from 2 to 12 points of extension. Reprinted with permission from reference[27]. Copyright 2019 John Wiley & Sons.
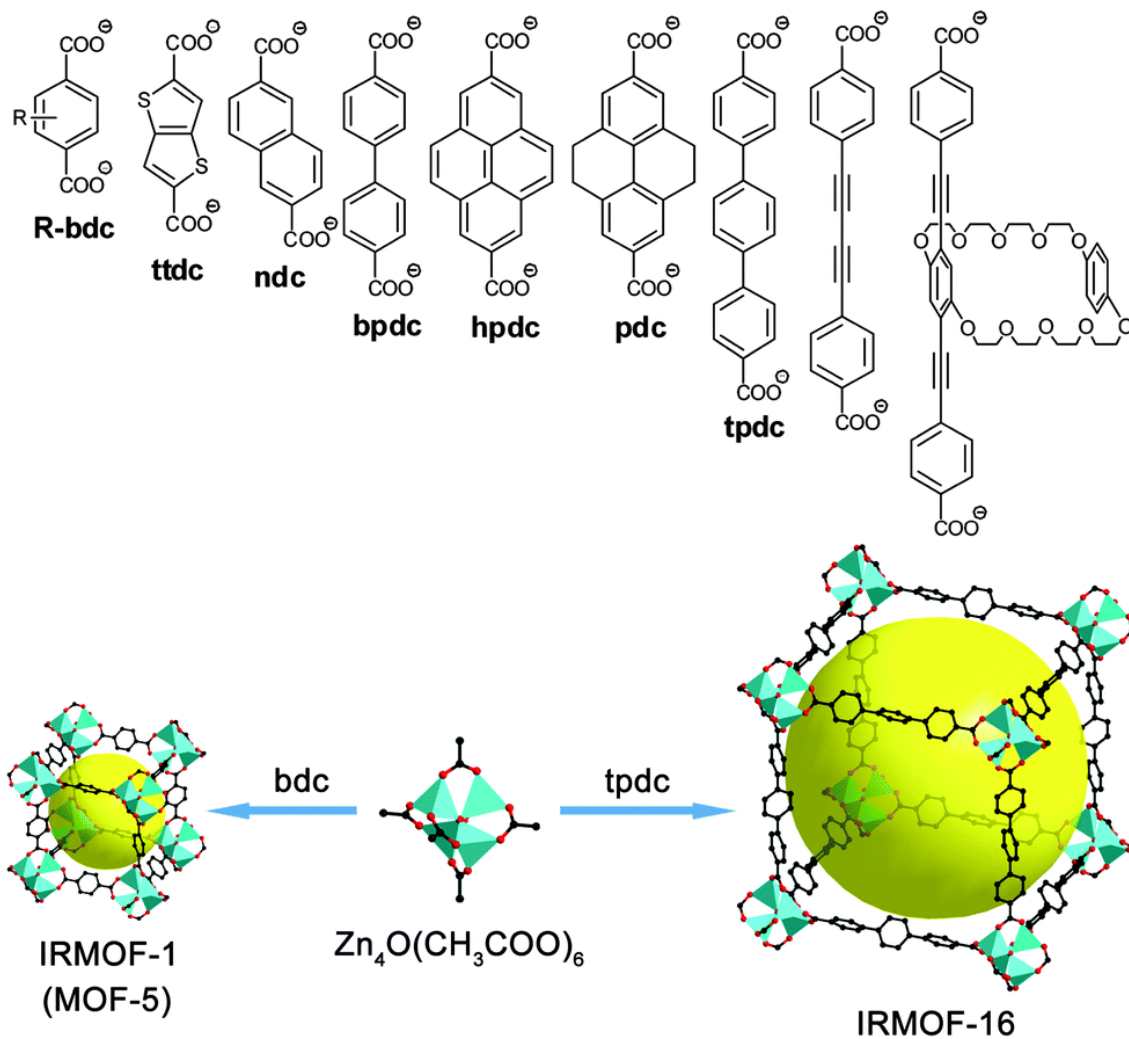
Figure 5 Some representative ditopic carboxylate linkers and illustration of formation of extended IRMOF networks by replacing acetate with rigid dicarboxylates. Color scheme: Zn (turquoise polyhedra); O (red); C (black); available pore volume (yellow ball). Reprinted with permission from reference[28]. Copyright 2014 Royal society of chemistry.
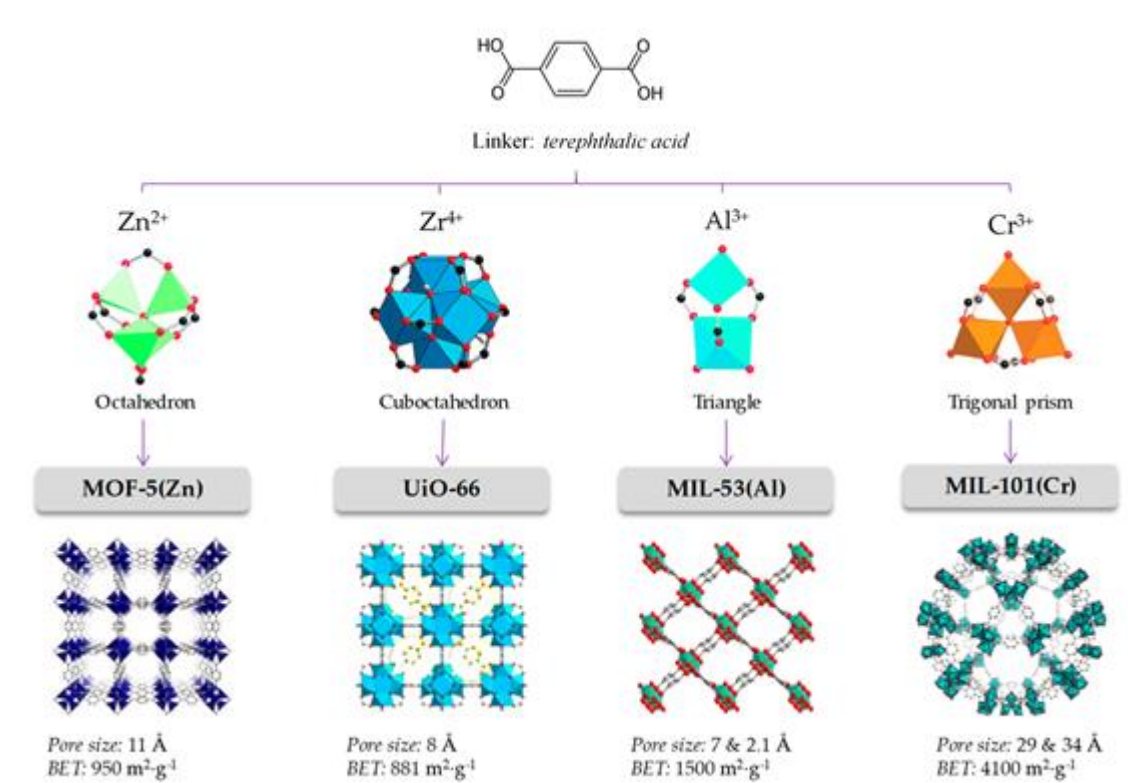
Figure 6 The node-and-connector approach to prepare MOFs. The adequate selection of the organic linker (linear in the case of terephthalic acid) and connection geometry of the metal cluster lead to the desired topology. Reprinted with permission from reference[29]. Copyright 2019 MDPI.

b. Secondary Building Units

In order to simplify highly complex structures formed by reticular chemistry, the concept of secondary building units is used by deconstructing the nets into atomic arrangements or building blocks. A secondary building unit or metal cluster is formed by the assembly of polynuclear metal ions with polydentate binding groups of linkers subsuming the inorganic components of the net[30]. The secondary building units constitute the vertices of the net that can through a wide range of geometries and a connectivity ranging from three to twelve points of extensions access a large variety of framework

structures[31]. As illustrated in Figure 7, most metal and metalloids are already incorporated in inorganic secondary building units and integrated in the several known MOF structures. Furthermore, one same metal node can be extended with different linkers yielding different distinct MOFs as illustrated in Figure 8.
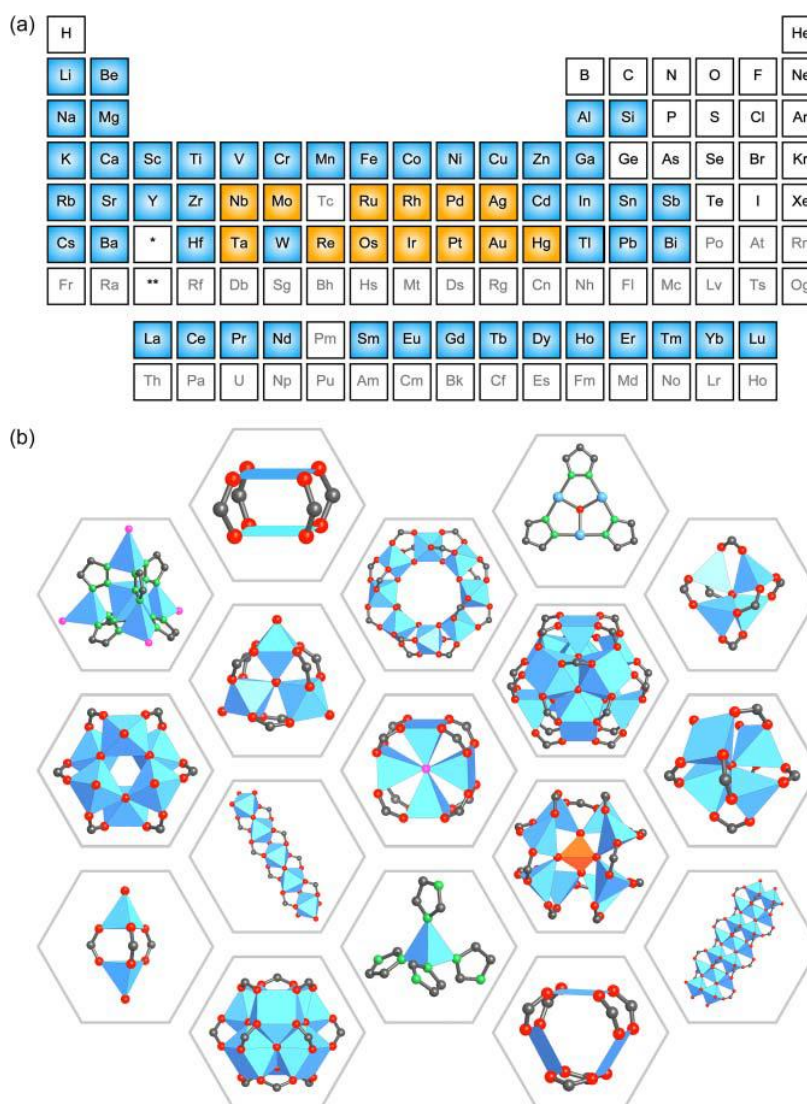
Figure 7 Periodic table showing metals that have been incorporated into MOF structures. The elements highlighted in blue can form SBUs or are part of the organic linker (metallo-linker), elements highlighted in orange have been incorporated into the structure of MOFs by metalation of the linker in the form of complexes (a). Some examples of 0D and 1D SBUs with points of extension ranging from 3 to 12 (b). Reprinted with permission from reference[27]. Copyright 2019 John Wiley & Sons.

9
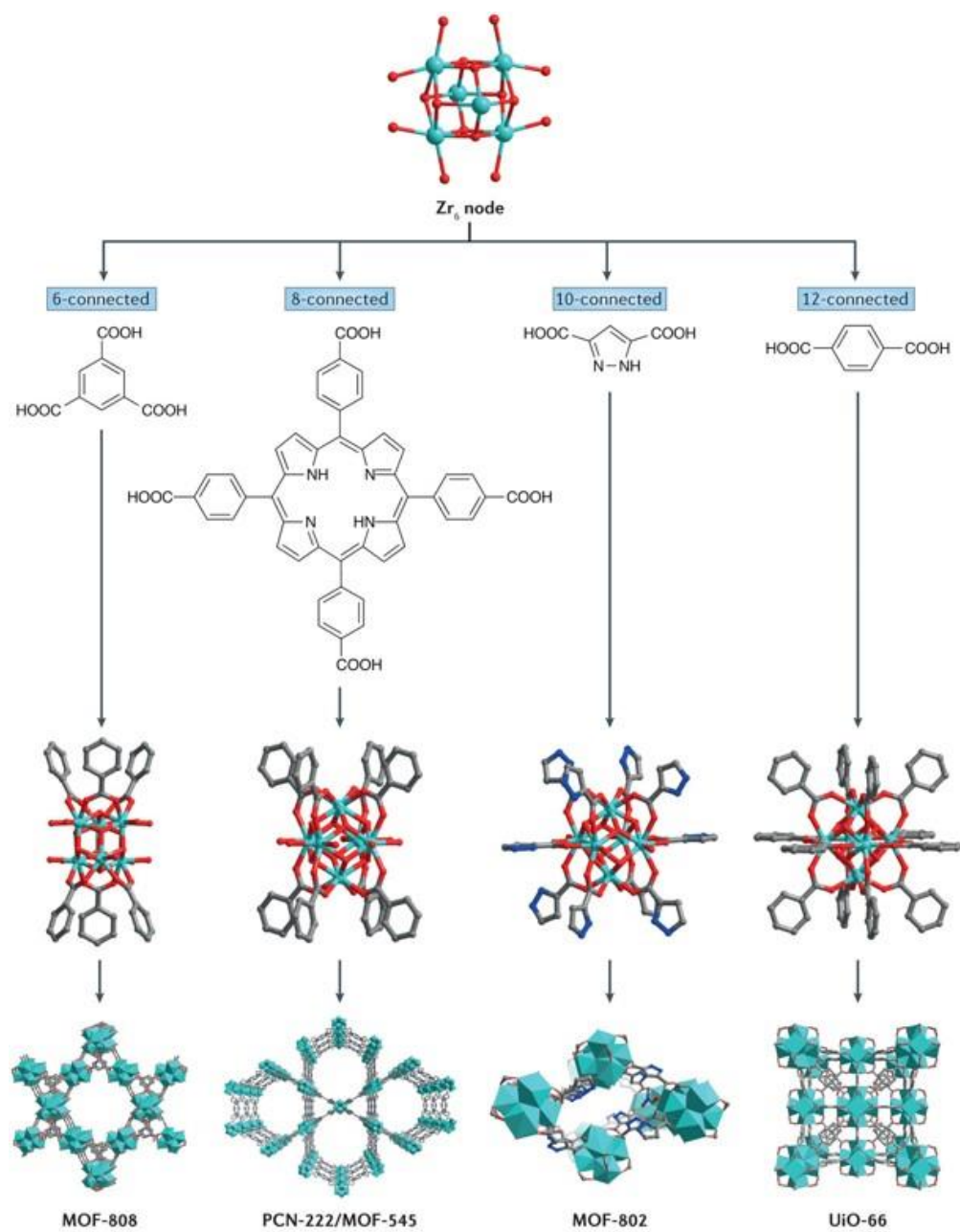
Figure 8 Connectivity of Zr6 nodes in zirconium-based metal–organic frameworks and the associated carboxylate molecules required to link nodes together. Metal–organic frameworks (MOFs) containing 12-, 10-, 8- and 6‑connected Zr6 nodes have been synthesized. This connectivity refers to the number of linker-associated carboxylates coordinated to each node. Zr, teal; C, grey; O, red; N, blue. Hydrogen atoms are omitted for clarity. PCN, porous coordination network. Reprinted with permission from reference[32]. Copyright 2016 Nature.

3. *Complexity and Heterogeneity in MOFs*

The combination of one metal cluster with one organic linker results a well-defined metal-organic framework structure. Nevertheless, the combinations are not so limited because the mixture of two or more distinct building units (SBUs or organic linkers) can lead to much more complex structures than expected. For instance, the mixing scenarios can be distinguished into two cases: "complexity" and "heterogeneity". As previously explained, any of the building units of MOFs can direct and control the structural topology. A controlled twist to the structure can be introduced if the structure's points of extension remains intact. In this case, heterogeneity will be added while maintaining the backbone intact[33]. This can be obtained by either (a) mixing multiple interchangeable linkers metrically identical and have the same binding groups, (b) mixing different metal ions that form the same SBU in the same conditions or (c) insert aperiodic vacancies into a single MOF structure., The resulting MOFs form a new subfamily of metal-organic frameworks known as multivariate metal-organic frameworks (MTV-MOFs). It was until 2010 that the first MTV-MOFs were reported[34] (Figure 9). As simple as the concept may seem, many problems were previously encountered; a phase separation is obtained in most cases instead of a homogeneous mixture inheriting the parent structure as well as a major lost in overall crystallinity[35-36].

On the second hands, mixing different distinct linkers or different metals forming distinct SBUs or both together leads to much complex, yet fully ordered and well-studied structures and creates as well what is known as complexity in MOFs, which details will not be further explained[37].

a. <u>Mixing of organic linkers</u>

In order to maintain the same backbone structure, isostructural organic linkers that present geometrical similarities such as the length of the aromatic chain, their solubility and their functional binding groups must be employed[38-39]. Such linkers that are metrically similar but chemically distinguishable are expected to mix and inherit the parent MOF structure. Many scenarios for the distribution of the linkers inside the framework can be seen either random distribution, clustering of functionalities or even alternating patterns[40]. These predictions may be more guided by molecular dynamics simulations and solid state NMR studies[34] that provide information about the overall distribution of functionalities, yet recently fluorescence lifetime imaging is found to be a powerful tool. By coupling the defect-introducing organic linker with a fluorophore, It can aid in detecting heterogeneity on the nanoscale level, between different crystals in the same sample or even within the same crystal[41]. It is found that these distributions are highly dependent on the chemical composition of the linkers[42].

b. <u>Mixing of metal ions</u>

Another route to introduce heterogeneity is by mixing different metal ions mostly having the same valence and forming the same SBU in the employed reaction conditions. This can be done by either mixing the metal ions in the starting reacting solution[43] (Figure 10) or by post synthetic metal exchange reactions[44]. The metal distribution is not easily tracked but can be elucidated by energy dispersive X-ray spectroscopy[45]. Some metals may form domains and some may mix in the same SBU. It is generally noticed that metal

12

having the same electronegativity and radius form mix-SBU while the others tend to form

more SBU with one kind of metal also known as domain distribution[46].
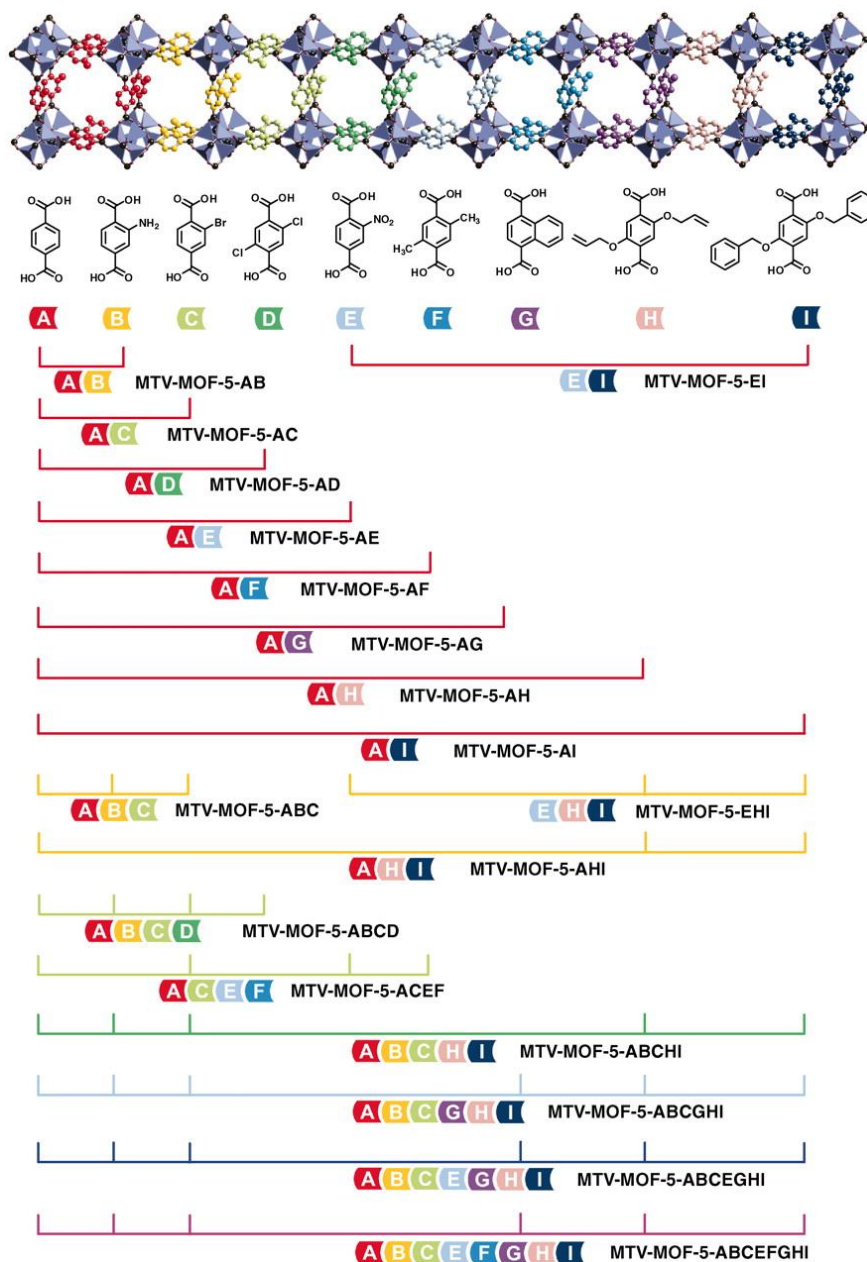
Figure 9 Cubic MOF-5 structure with the combined acid forms of 1,4-benzenedicarboxylate (BDC), NH_2-BDC, Br-BDC, $(Cl)_2$-BDC, NO_2-BDC, $(CH3)_2$-BDC, C_4H_4-BDC, $(OC_3H5)_2$-BDC, and $(OC_7H_7)_2$-BDC links (A to I, respectively) forms the corresponding sets of 18 MTV-MOFs, each having two or more different functionalities [two: MTV-MOF-5-AB, -AC, -AD, -AE, -AF, -AG, -AH, -AI, and -EI; three: MTV-

13

MOF-5-ABC, -AHI, and -EHI; four: MTV-MOF-5-ABCD and -ACEF; five: MTV-MOF-5-ABCHI; six: MTV-MOF-5-ABCGHI; seven: MTV-MOF-5-ABCEGHI; eight: MTV-MOF-5-ABCEFGHI. Reprinted with permission of reference[34]. Copyright 2010 Science.
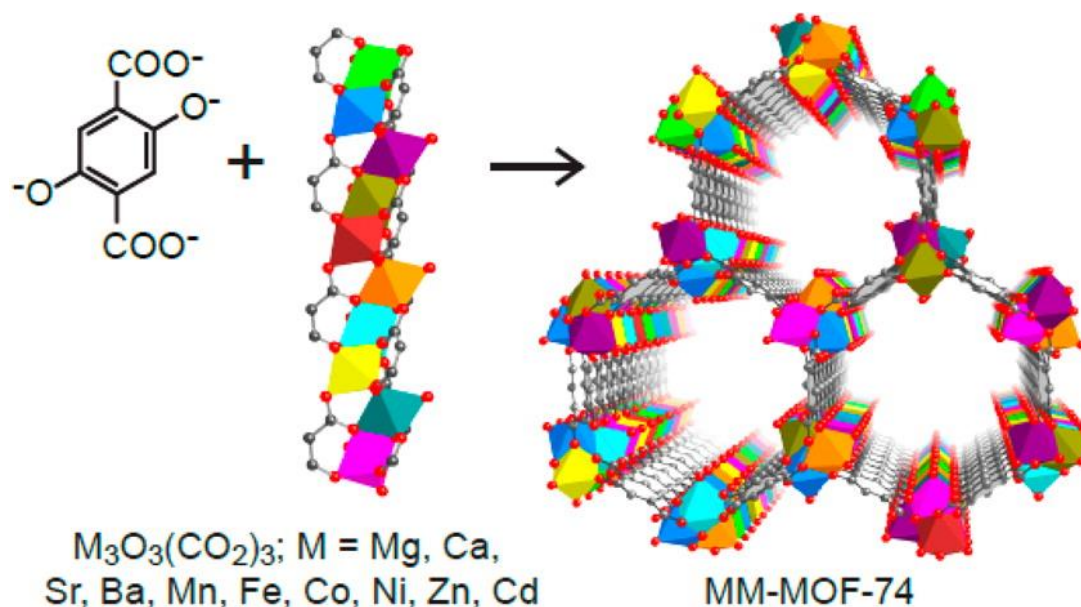
Figure 10 Crystal structure representation of MTV-MOF-74 with view along the crystallographic c-axis. The **etb** framework is formed by linking 1D $[M_3(O)_3(COO)_3]_\infty$ rod SBUs through DOT (DOT = dioxidoterephthalate) linkers. The resulting framework has hexagonal 1D channels running along the crystallographic c-axis. The SBUs of MTV-MOF-74 contain up to 10 different metals (Mg, Ca, Sr, Ba, Mn, Fe, Ni, Co, Zn, and Cd), out of which there are metals not present in binary MOF-74 structures. The metals are shown as their respective coordination polyhedra, each color represents a different metal. All hydrogen atoms are omitted for clarity. Color code: C, gray; O, red. Reprinted with permission from reference[45]. Copyright 2014 American Chemical society.

c. Aperiodic vacancies

Random vacancies can be added by introducing a defect into the structure manifested by a missing linker from the parent structure[47-49]. This can be accomplished using a higher concentration of a modulator molecule such as trifluoroacetic acid usually used in a typical solvothermal synthesis process. The modulator, usually structurally

related to the linkers[50-52] competes with the organic linker in incorporation which will lead to desired structures and properties (Figure 11). Another approach to create defects is the rapid formation of MOF structures by fast precipitation. This method is expected to yield disordered pores of the structure as in the typical solvothermal synthesis, the MOF is allowed more than 12 hours to crystallize while a fast precipitation yield a MOF structure in less than 1 minute[53-54].
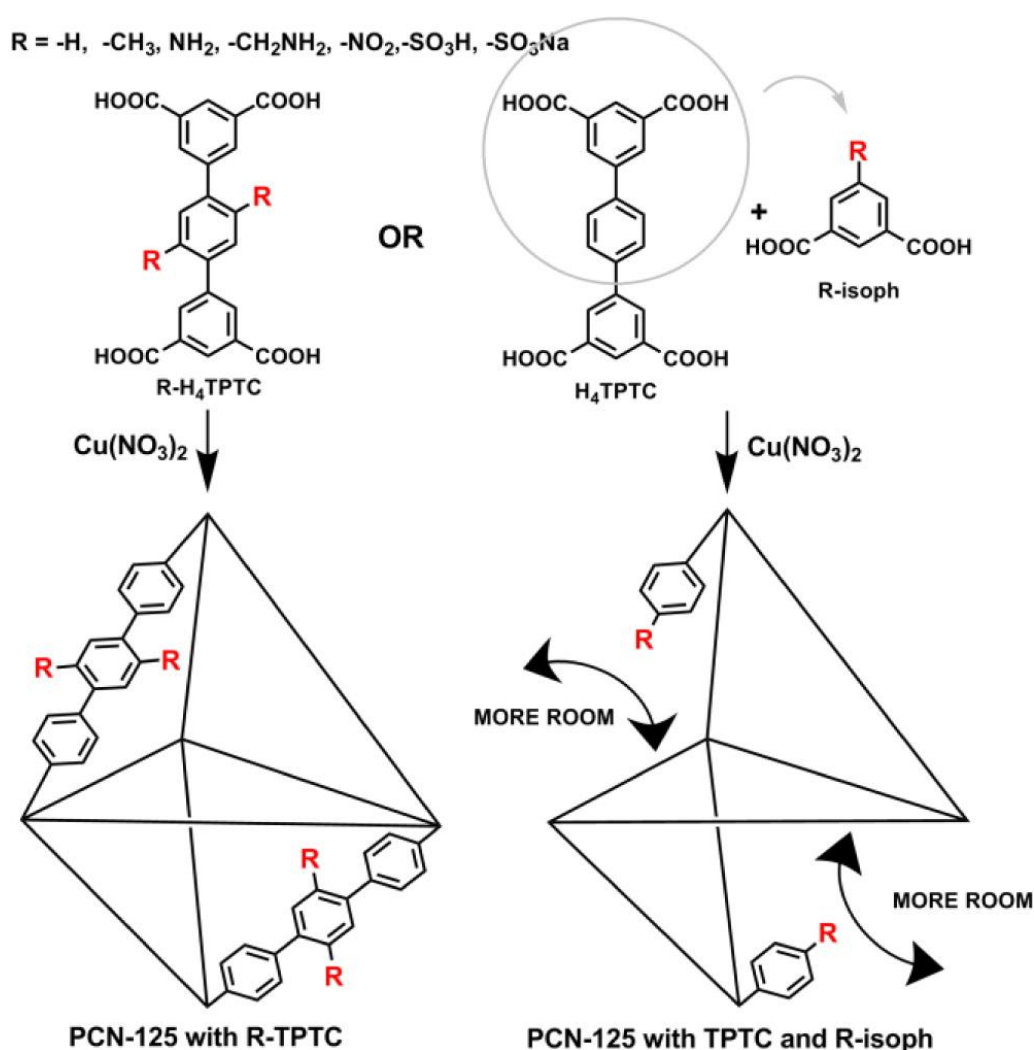
Figure 11 Schematic illustration of the ligand truncation method. When R-H₄TPTC reacts with Cu(NO₃)₂, the MOF has R groups pointing into pores (left), which might reduce the pore size. On the other hand, copolymerization of TPTC and R-isoph gives

the MOF having increased pore size due to the truncated ligands (right). Scaffold represents one of the pores of PCN-125 with R-TPTC (left) and with TPTC and R-isoph (right). Reprinted with permission from reference[52].Copyright 2012 American Chemical Society.

4. Functionalization of MOFs

It is of an utmost importance to study the geometry of the linkers and their embedded functionalities in order to introduce heterogeneity to MOFs. When applying a synthesis technique, many problems that may arise are solved differently and allowed to elaborate the newly emerging ways or synthesis routes detailed below. It is noteworthy to say, many functionalized MOFs are obtained directly through the typical solvothermal[55-56], mechanochemical[57-58], microwave assisted[59], electrochemical[60-61], template-guided[62-63], sonochemical[64] and slow-evaporation synthesis[65].

a. One-Pot Reaction

One-pot reaction also known as pre-synthetic functionalization is the trivial synthesis to be used by introducing derivatized organic linkers to the reaction medium prior to the MOF formation. The major concern that may arise is the interference of the added substituents with the formation of the intended MOF structure[66-67]. Nevertheless, this issue can be solved by using protected functional groups for the pre-synthetic incorporation of the intended functional groups as long as compatible with the synthesis conditions[68-69]. Under many conditions, the functionalities are well-introduced revealing much enhanced applications[70-72].

b. Post-synthetic Modifications

Due to the high demand on the functionalized MOFs which functional groups interfere with the formation of the intended MOF structure or their chemical or physical properties are not compatible with the synthetic conditions, the post-synthetic method (PSM) is found to be a suitable solution for the dilemma[73-74].

- Solvent-assisted Linker Exchange

The solvent-assisted ligand exchange (SALE) principle is based on the soaking of a MOF sample in a concentrated solution of a functionalized linker molecule with retention of the metrics of the parent MOF[75]. The exchange ratio can be tuned by adjusting the reaction conditions and after their incorporation these functionalized linkers can be further modified by carrying organic transformations[76].

- Post-Synthetic Linker Installation

As its name implies, this approach tends to install a new linker to a previously synthesized net. Therefore, linkers bearing appropriate binding groups are employed as pillars to bind similar SBUs resulting a much complex topology[77]. Sequential linker installation allows to construct diverse MOFs structures with precisely positioned functional groups[78].

5. *Applications of Functional MOFs*

Metal-organic frameworks' diverse properties open the door to a massive number of applications previously fulfilled by common porous materials. Moreover, the ability of functionalizing the networks of MOFs has led to a much more enhanced selectivity on the application level. Figure 12 illustrates the main domains which have encountered a tremendous progress for their applications by MTV-MOFs.
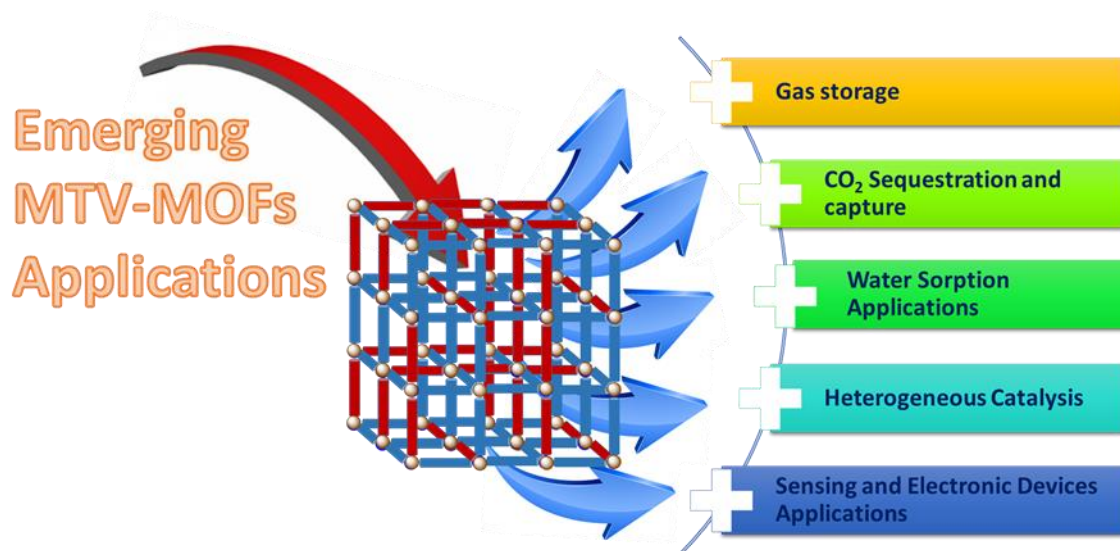
Figure 12 Enhanced emerging applications of multivariate metal-organic frameworks.

a. Gas storage

Metal-organic framework's properties that include their very high surface area, accessible and tunable pores and the potential functionalization of the pore surface make them ideal for gas storage applications[79-81]. Nevertheless, hydrogen (H_2) and methane (CH_4) are considered among the most studied systems for such application due to their

highly-seeked eco-friendly aspect and owing to the fact that their combustion yields only water and the smallest possible amounts of carbon dioxide (CO_2).

Hydrogen has had many challenges at the stage of its implementation as a clean energy resource. Hence, due to its low density at ambient temperature and pressure, its storage plays a vital role in its development. Indeed, hydrogen is either stored physically in the liquid state in expensive highly-pressurized tanks or chemically in kinetically unfavorable high cost materials such as boranes, metal hydrides or imidazolium ionic liquids. Lately, MOFs and especially pre-designed functional MOFs are voted as highly competitive candidates, because of the high interactions between their surface and hydrogen gas molecules[82-83]. It is observed that along with high surface area, hydrogen storage is increased in MOFs with a high number of small interdigitated pores and polar functional groups[84-85].

On the other hand, CH_4 with its nonpolar nature binds to most of the MOF materials having high surface area and regular pore shapes[86-88]. Moreover, CH_4 can be investigated for mobiles applications, because of its relatively easy storage in the solid materials, high working capacity and its potential recyclability for approximately the lifetime of a vehicle. For that, a MOF methane storage vehicle is actually developed by BASF and Yaghi group in 2016[89-90].

b. <u>CO_2 Sequestration and capture</u>

The increase of CO_2 emissions is considered to be one of the major causes of pollution that is kept being solved partially until today. Regardless of the huge

environmental awareness spread since the beginning of the twenty first century, CO_2 levels still are increasing due to the massive industrial development and the costly energy dissipating commercial capture materials e.g. aqueous alkanolamine solutions[91].

Research in MOF field especially in tunable and defect-containing structures has revealed a major advancement in material science. It is concluded that CO_2 binds to frameworks that exhibit open metal sites, and more selectively to hydroxyl and amino-functionalized MOFs. Noting that, it can be recycled several times approaching to practical and industrial large scale applications as well as its selective separation from gaseous mixtures[50, 92-94].

c. Water Sorption Applications

Water sorption applications in metal-organic frameworks are very diverse and can include the adsorption of pollutants from water, water desalination, humidity control in buildings and water harvesting from air. Even though each of the above mentioned applications require specific properties in the structure, all MOFs must show a stability in water, high adsorption capacity and a high selectivity. However, this water stability can be tuned through adding a steric hindrance in organic linkers or SBUs to prevent water accessing to the sites in question namely functionalizing the MOF structures[95-96]. Due to many crises the world facing nowadays more light is shed on the ecological catastrophes water pollution is causing to the balance of the ecosystems, where the pollution caused by organic dyes and industrial wastes is one of the major contributors. It is now evident that the removal of such organic pollutants is of an utmost importance and

more efforts will be focused on developing efficient and fast methods to reach this goal. While many purification methods and devices are currently developed, adsorption remains an easy, cost-effective, fast and efficient way. MOFs are heavily used as efficient adsorbent material, due to their very suitable properties for adsorption such as large accessible active adsorption sites, a wide range of possible interactions and lately their thermal and chemical stability[97]. Moreover, MOF structures can be tuned through functionalization in order to enhance their fit for specific applications[80, 98]. The functionalization can also aid to specially target the adsorbate by increased adsorbent-adsorbate interactions accompanied with an appropriate pore size and apertures to ensure the adsorbate trapping[97]. In this context, many examples stand out as efficient functionalization for the enhancement of MOF's behavior for organic dyes adsorption [99], heavy metals removal[100], and other micropollutants such as pharmaceuticals and drugs[101-102]. It is also concluded that adding specific functional groups usually boosts adsorption kinetics and increases the overall adsorption capacities[103].

d. Heterogeneous Catalysis

Owing to their very high surface area featuring adsorptive active sites either in channeled organic structures or open metal SBUs[104],MOF structures are extensively investigated for their application in catalysis for many years. Moreover, the creation of defects in such interesting frameworks makes MOFs the most suitable candidates for a specific catalytic activity, which has yielded many MOF structures with finely tuned pores to be more efficient for substrate diffusion between neighboring channels[105-106]. In

addition, the functionalization has played an enormous role in the growth of the field, where it is evident that adding functional groups that specifically attract the substrate to a highly porous and rigid structure to have an outstanding outcome[107]. Lastly, the great interest in metal-organic frameworks for catalysis along with their outranging flexibility has led to many structures with integrated or immobilized catalytic centers namely MOF-encapsulated catalysts, where the MOF's role is essential for the stability of the catalyst and an improved catalyst efficiency and reusability[108-109].

e. Sensing and Electronic Devices Applications

For a material to be an efficient sensor, many simultaneous properties must be present. A sensor needs to accommodate the analyte, interact with it and emit a specific response. MOFs with their permanent porosity, tunable pores and functional surface as well as their chemical and mechanical stability meets the above mentioned requirements. More importantly, based on size-selective recognition, many structures are constructed with finely-tuned small pore/apertures size, which enables the selective adsorption or release of adequately-sized guest molecules depending on the variation of the surrounding conditions[110]. Nevertheless, MOFs featuring wide channels or hierarchical large mesopores can even serve as excellent chemical sensors. By functionalizing such MOFs, many specific interactions or hydrogen bonds-based sensors can be selectively targeting the analytes by immobilizing open metal sites or implementing Lewis acidic/basic sites[111-112].

Moreover, MOF particles are reported as luminescent probes because of their unique hybrid composition of organic-inorganic building units that can both provide platforms to induce luminescence or even to be a solid the matrix for encapsulating luminescent guests such as fluorescent dyes, lanthanide ions or quantum dots[113].

Furthermore, MOFs were considered as insulators for a long period of time before the tremendous progress in the past years to construct porous structures featuring electrical conductivity or ion mobility. One of the most reported procedures is to add sulfur-bridging ligands that features strong interactions with metal clusters to form conductive materials[114], another is to add redox-active guest material to the MOF's pores implemented in conductive thin-film devices[115].

B. Reaction-Diffusion Framework

1. Introduction

As the first experiments for the first synthesis via reaction-diffusion process date back to 1800s, this extensively studied field is nearly mature. Thus, Reaction-diffusion often correlated with complex diffusion equations and eye-pleasing colored patterns is defined as the formation of an array organized structures repeated with defined or undefined symmetries without the intervention of external conditions, and arise far from equilibrium[116]. Indeed, reaction-diffusion process is widely observed in nature as illustrated in Figure 13, thus, it can range from regulatory processes in cells, tissues and organisms in biological systems to the layer by layer formation and deposition of cave

stalactites in wet environments, the dendritic formation on the limestone and the iris banding of the agate.

Inspired by such surrounding phenomena and until present, RDF scientists are succeeding in imitating nature's behavior and reconstructing many RDF patterns in labs. However, the underlying mathematical equations governing the diffusion laws coupled with the chemical reaction has led to the necessity of mandatory simulations and extensive modeling to deduce the initial conditions to create such state-of-art materails[117-118].
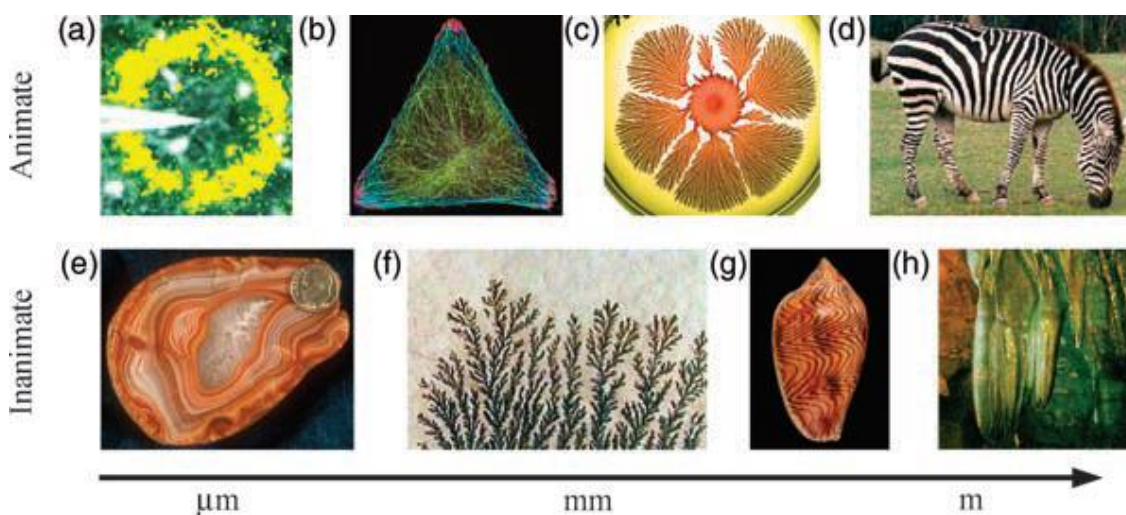
Figure 13 Examples of animate (a-d) and inanimate (e-h) RDF systems at different length scales (μm, nm and m) . Reprinted with permission from ref. [106]. Copyright 2009 John Wiley and Sons.

2. *RDF in chemistry*

In chemistry, the reaction-diffusion framework consists of the separation of the reaction medium into to compartments; namely the inner and the outer electrolyte. The inner electrolyte consisting the first reactant is entrapped in a gel medium while the outer

electrolyte is a solution containing the second reactant poured on top of the gel[119]. A higher concentration of the outer electrolyte versus that of the inner establishes a concentration gradient dictating the diffusion process. A supersaturation wave is created at the gel interface and decreases down the tube. Thus, the nucleation predominates near the interface where the supersaturation is at its highest followed by a gradual dominance of the crystal growth as we go further of the interface[120-121]. To this extent, RDF is governed by the diffusion of the electrolytes, nucleation and supersaturation and crystal growth.

- Diffusion

Fundamentally, diffusion is the mass transfer occurring between two adjacent mediums from one of a high concentration to one of a low concentration. The concentration gradient established between the outer and the inner electrolyte in the tubular reactor induces diffusion. Indeed, diffusion consists of three types: grain-boundary, bulk and surface diffusion. As the grain-boundary diffusion occurring in polycrystalline solids is not our case, surface diffusion seems also unattractive because it occurs at a very fast rate and the interface is usually removed due to its insolubility. Thus, the precipitation of MOF particles is mainly governed by bulk diffusion. Moreover, the kinetics of the diffusion is affected by many factors such as the temperature as the speed of precipitation increases as the temperature increases. In addition, the higher the margin between the concentration, the fastest the reaction as well as the distance procured by the formed particles.

- Nucleation and Supersaturation

The nucleation is the first assembly of the motif of the crystal. Once this motif is generated, further layering of the following atoms will be considered growth of the crystal. The nucleation process can be homogeneous or heterogeneous depending where the particles can be self-assembled forming the nuclei or formed on another surface such as impurities or dust particles[122].

For the nucleation to occur, a supersatured medium should be present meaning that the concentration of the outer electrolyte should be higher than that a liquid can normally accommodate. The supersaturation wave is at its highest near the interface hence it evokes many nucleation sites and many nuclei creation. The nonlinear coupling between the diffusing supersaturation and the crystal nucleation and growth may result in forming depleted regions hence alternating Lesigang bands may form[117, 123].

- Crystal growth

After a nucleus is formed, the neighboring gel region is depleted gradually from the reactants which will stop the nucleation. This will initiate diffusion of the reactants from other regions towards the formed nucleus. At this moment, if the solubility product of the reactants reaches a value higher than the reactants concentration multiplication product, growth will occur and the size of the nucleus will increase. This product is not always attained if the neighboring regions also manifests many enucleations thus small particles will form rapidly near the interface and a smaller number of larger crystals can be noticed down the tube[117].

3. *RDF in MOFs*

Owing to the low control over the results of the typical solvothermal synthesis of MOFs, several emerging innovative techniques to synthesize MOFs are highly researched[124]. Nevertheless, reaction diffusion process was never applied before to the field. Indeed, it is first employed to synthesize MOFs in our group back in 2017 where, HKUST-1 also known as MOF-199 is formed in a tubular reactor by separating the reacting species into two compartments; the inner electrolyte containing the BTC linker and the outer electrolyte containing the copper metal ions. Control over the crystal size and shape is successful by studying the effect of different gel types used, the reaction temperature, pH, and the concentrations of both reactants[125-126]. Subsequently, another successful synthesis via RDF is that of ZIF-8, ZIF-67 and their mixed-metal derivatives crystals. The spacing laws governing the alternating Lesigang bands and the mechanism of the formation of ZIF-8 crystals within the bands are extensively studied[123, 127]. Moreover, it is concluded that doping ZIF-8 with Co (II) enhances the photodegradation of methylene blue dye under visible light irradiation in the absence of hydrogen peroxide[123].

Early this year, Bartosz Grzybowski et al. start using the RDF approach to synthesize MOFs. By wet-stamping method, consisting of placing a hydrogel stamp that contains the solution of one or more reactants into a dry gel film doped with the other reactant, HKUST-1 is synthesized. A triethylamine modulator is added to the reaction medium to ensure the deprotonation and the nucleation, and several shapes are obtained

and studied between different bands. They also demonstrate the possibility of growth of metal-organic polyhedra (MOPs), several diffusing MOFs in one gel medium as well as a heterometallic MOF structure ensuring that RDF is a promising and a very advantageous route to synthesize MOFs[128].

C. Aim of the work

As previously mentioned, MOFs are a newly emerged class of rigid porous frameworks with permanent porosity and exceptional properties. Moreover, the advancement is huge in the field of reticular chemistry and crystal engineering in joint efforts to rationally design frameworks and optimize the knowledge of architecturally stitching building units to construct highly complex and multifunctional frameworks to fit predesigned applications. The best way to enhance the properties of an existing metal-organic framework to fit a specific intended application is to modify it lightly without causing its collapse nor altering its structure. MOF-199 seems to be the perfect candidate to test the effect of introducing a heterogeneity to an existing metal-organic structure owing to its robust structure, outstanding properties and most importantly being extensively studied. Also, its connectivity and possessing a square paddle-wheel SBU allows the substitution of one or more of the BTC linkers by one or more functionalized linkers with geometrical similarities. This field is grabbing more attention of the scientist as only some of them were able to synthesize MTV-MOFs without facing many challenges and they were found to have utmost enhancement of their properties and applications. By replacing BTC linker with defect-causing linkers, we are able to induce

defect in the structure and intimately insert new functional groups into the framework while preserving its metal structure (Figure 14). Herein, we report introducing heterogeneity to a well-known MOF-199 structure and its functionalization by several organic groups to form MTV-MOFs-199. Hence, two, three and four linkers are homogenously mixed together in the same framework without losing the crystalline order of MOF-199 (Figure 14). Furthermore, it is of a highly important manner to always search for greener synthesis approaches even when trying to synthesize the most intended and specific materials. Our outstanding RDF synthesis method allowed us to generate these MTV-MOFs at room temperature without employing any environmentally harmful organic solvents. In addition, we are able to go through many important parameters such as the particle size and the amount incorporated into the framework based on the position of the particles in tubular reactor. The MTV-MOFs are fully characterized by PXRD, SEM, BET, TGA, and the amount of introduced linkers incorporated in the structure is deduced by NMR. More importantly, the functionalized OH-MOF-199 is found to enhance the adsorption of Methylene Blue and NH_2-MOF-199 that of Rhodamine B as compared to MOF-199.
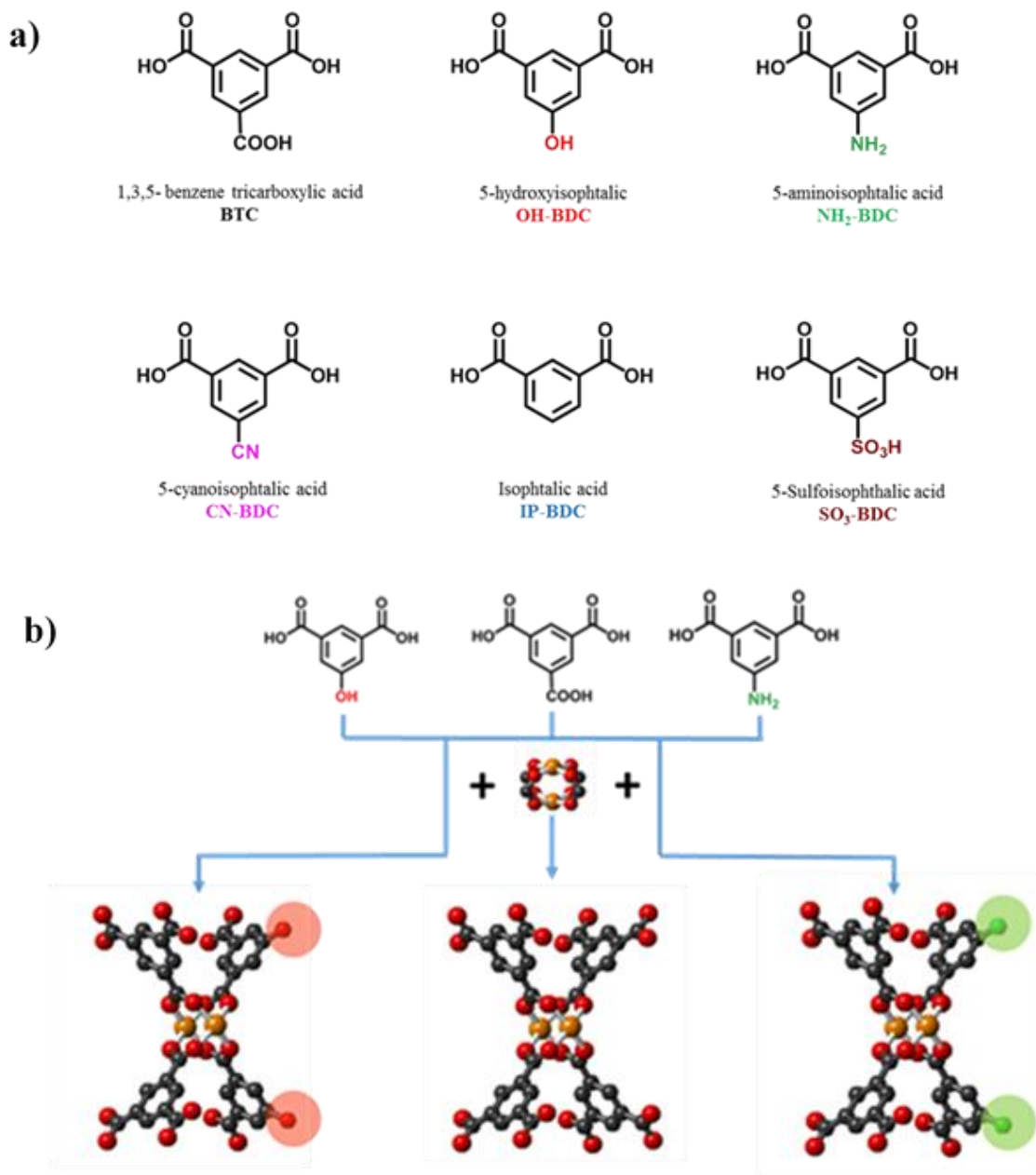
Figure 14 Different organic linkers used in the synthesis of MTV-MOFs-199 (a) Schematic presentation of the synthesis of MOF-199 and its mixed linkers derivatives through reacting Cu-paddle wheels with BTC linkers and OH-BDC or NH2-BDC while preserving the original MOF-199 crystal order (b).

CHAPTER II

MATERIALS AND METHODS

A. Materials

The chemical reagents, $Cu(OAc)_2.H_2O$ and 1,3,5-benzenetricarboxylic acid (BTC) are purchased from Acros Organics, Bacto Agar gel from Difco, Isophthalic acid (IP-BDC), 5-hydroxyisophthalic acid (OH-BTC), 5-aminoisophthalic acid (NH_2-BDC), 5-cyanoisophthalic acid (CN-BDC), 5-sulfoisophthalic acid (SO_3-BDC), N-N-Dimethyl Formamide (DMF), dichloromethane (DCM), methanol and ethanol absolute from Sigma Aldrich. All reagents are used as received and without any further purification.

B. Preparation via RDF

Our RDF method consists of the diffusion of an outer electrolyte solution into a gel matrix containing the inner electrolyte in a Pyrex test tube. For all our MTV-MOF-199 systems, the outer solution is formed of copper (II) ions diffusing into the gel containing two or more organic linkers forming the inner medium. It should be noted that the concentration of the outer solution should be 5 times higher than that of the inner one.

1. Preparation of MOF-199

A 10 mM solution of the organic linker BTC is prepared in 1:1 (v/v) mixture of ethanol and water as solvents to form the inner electrolyte. 1% (w/w) agar powder is then added and the mixture is heated up until the complete dissolution of the powder. The

31

mixture is poured hot into a Pyrex tube and covered to allow its jellification. The outer solution is prepared by dissolving $Cu(OAC)_2$ in 1:1 (v/v) mixture of ethanol and water as well. After the gel is solidified, the outer metal solution is poured into the Pyrex tube containing the inner material with gel, then covered to allow the diffusion and the precipitation of the blue MOF-199 crystals.

After 3 days of diffusion, the gel containing the crystals is collected by dividing each tube to three consecutive zones (zone 1, zone 2 and zone 3) according to their distance from the interface of the inner agar gel and the outer solution. The nearest to the interface is zone 1 and so on (Figure 15). Then, the gel is heated in an aqueous solution until its complete dissolution, the supernatant is removed and the crystals are collected by centrifugation. After that, the collected MOF-199 samples are washed with DMF for three days to dissolve any unreacted species and then activated with DCM by solvent exchange to clear the MOF pores. Consequently, the collected crystals are dried under vacuum for 12 hours to ensure the complete evacuation of the pore to be ready for the characterization.
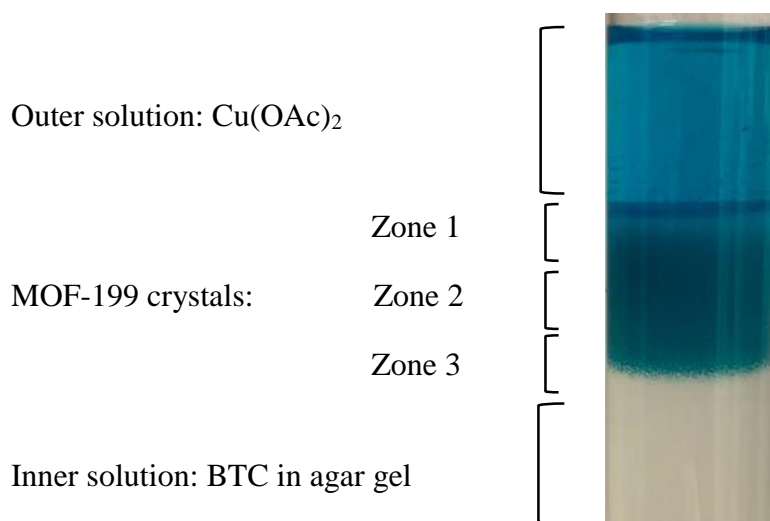
Figure 15 Schematic representation of MOF-199 synthesis via RDF.

2. Preparation of 2-linkers-MTV-MOFs-199

A mixture of a "functional group adding" organic linker X-BDC (OH-BDC, NH_2-BDC, IP-BDC, CN-BDC or SO_3-BDC) with BTC, at different starting molar ratios in a 1:1 (v/v) ethanol and water solution is prepared to form the inner electrolyte. Here, each one of the X-BDC linkers is mixed with BTC in a 1:1 starting molar ratio to form the corresponding X-BDC:BTC (1:1) or X-MOF-199 (1:1) as shown in Table 1. Moreover, the X-MOF-199 samples that are found to be more efficient for dyes removal are further investigated. Thus, the preparation of 1:3 and 3:1 starting ratios are done to form X-BDC:BTC (1:3) or X-MOF-199 (1:3) and X-BDC:BTC (3:1) or X-MOF-199 (3:1) respectively to check the effect of the concentration of the added functional group into the framework (Table 1). Noting that the same MOF-199 preparation procedure is employed, agar powder 1% (w/w) is added to the mixture and heated then poured and left to congeal where the same outer copper ions solution is added later on and the same collection process is also achieved (Figure 16).
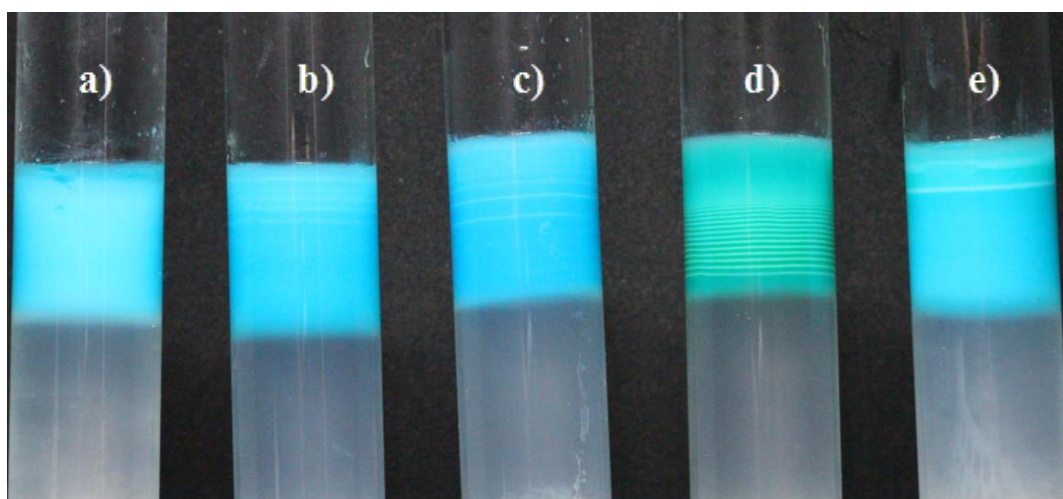
Figure 16 Schematic representation of 2-linkers MOF-199 synthesis via RDF: IP-MOF-199 (a), CN-MOF-199 (b), SO_3-MOF-199 (c), NH_2-MOF-199 (d), OH-MOF-199 (e).

X	X-BDC	BTC	Corresponding MTV-MOF-199
IP	10 Mm	10 mM	IP-MOF-199 (1:1)
CN	10 Mm	10 mM	CN-MOF-199 (1:1)
SO_3	10 Mm	10 mM	SO_3-MOF-199 (1:1)
NH_2	10 Mm	30 mM	NH_2-MOF-199 (1:3)
NH_2	10 mM	10 mM	NH_2-MOF-199 (1:1)
NH_2	30 mM	10 mM	NH_2-MOF-199 (3:1)
OH	10 Mm	30 mM	OH-MOF-199 (1:3)
OH	10 mM	10 mM	OH-MOF-199 (1:1)
OH	30 mM	10 mM	OH-MOF-199 (3:1)

Table 1 : The starting concentrations for the different 2- linkers MTV-MOFs and their corresponding nomenclature.

3. *Preparation of 3-linkers and 4-linkers MTV-MOFs-199*

After the successful synthesis of 2-linkers MOFs-199, both 3-linkers and 4-linkers MOF-199 systems are prepared by mixing two or three of the defect-introducing linkers X-BDC with BTC in an equimolar starting ratio to consist the inner electrolyte as shown in Table 2. The same procedure of preparation is then followed (Figure 17).

34

BTC	OH-BDC	NH$_2$-BDC	IP-BDC	Corresponding MTV-MOF-199
10 mM	10 mM	10 mM	-	OH-NH$_2$-MOF-199
10 mM	-	10 mM	10 mM	IP-NH$_2$-MOF-199
10 mM	10 mM	10 mM	-	IP-OH-MOF-199
10 mM	10 mM	10 mM	10 mM	IP-OH-NH$_2$-MOF-199

Table 2 : The starting concentrations for the different 3-linkers and 4-linkers MTV-MOFs and their corresponding nomenclature.
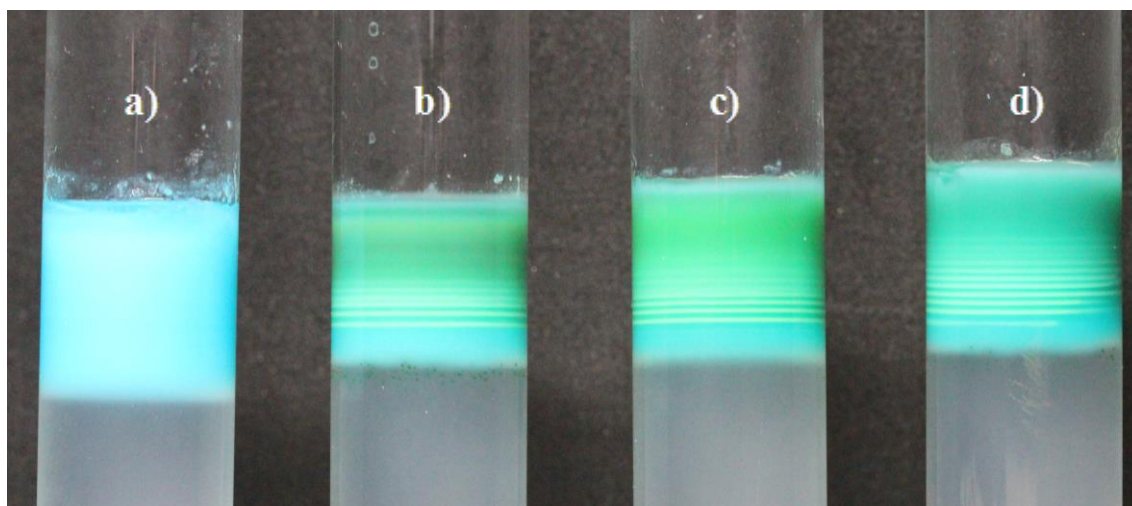
Figure 17 Schematic representation of the 3-linkers and 4-linkers MOF-199 synthesis via RDF: IP-OH-MOF-199 (a), IP-NH$_2$-MOF-199 (b), OH-NH$_2$-MOF-199 (c), IP-OH-NH$_2$-MOF-199 (d).

C. Characterization of MTV-MOFs

Following the activation process, the MOF samples are subjected to different characterization techniques including Powder X-ray diffraction (PXRD), Scanning Electron Microscopy (SEM), Nitrogen sorption Technique and Brunner Emmet Teller

(BET) calculations, Thermogravimetric analysis (TGA), and Nuclear Magnetic

Resonance Spectrometry (NMR).

1. *Powder X-ray Diffraction (PXRD)*

Powder X-ray diffraction (PXRD) is a non-destructive analysis technique that allows the unique identification of the sample structure through measuring the patterns diffracted after radiating X-ray on the powder sample. It is considered a fingerprint method to identify the sample structure and it could also be used to state the sample purity and to measure the sample size using Scherrer equation (I):

$$\tau = \frac{K\lambda}{\beta \cos \Theta} \qquad \text{(I)}$$

Where τ is the average crystallite size, K is the Scherrer constant, λ is the wavelength of the X-ray and β is the line broadening at the full width of the half maximum (FWHM).

PXRD are recorded on a Bruker D8 Advance X-ray diffractometer using the Cu-Kα radiation (λ= 1.5406 Å) at 40kV and 40 mA with a 2Θ ranging between 5° and 40° at a scanning rate of 0. 02°.min^{-1} and a total time of 12 hours.

2. *Scanning Electron Microscopy (SEM)*

The morphology of MTV-MOFs is shown by SEM images conducted on the MIRA3 by TESCAN SEM instrument. A small amount of MOF powder is dispersed in ethanol and few droplets are placed on a conductive carbon tape on top of the SEM stubs then left to dry completely at room temperature before coating the samples with a thin

layer of gold to avoid their charging during the screening. After that, SEM images are collected under definite magnifications

3. *Nitrogen sorption technique and BET calculations*

The specific surface areas of the MOF samples are calculated using the Brunner Emmet Teller (BET) theory using the Nitrogen sorption technique. The nitrogen adsorption isotherms are recorded on a NOVA 2200e Quantachrome analyzer. Prior to the analysis, 50-100 mg of the sample are degassed at 150 degrees for six hours to make sure that the MOF pores are clear from any residual solvent or adsorbed gas.

4. *Thermogravimetric analysis (TGA)*

In order to analyze the thermal stability of the samples, thermogravimetric analysis (TGA) are carried by determining the change in the weight of the MOF sample in response to the rising temperature. Nearly 5-10 mg of the MOF sample is placed in a crucible followed by moving it into an oven at a ramp rate of 5 °C/min from 30°C to 700°C under nitrogen atmosphere. The TGA profiles are recorded on NETZSCH TG 209F1 Libra TGA209F1D-0152-L.

5. *Nuclear Magnetic Resonance Spectroscopy (1H-NMR)*

In ^{1}H-NMR, the spectrum shows a characterizing frequency of a produced electromagnetic signal by each proton of the structures in response to a weak external oscillating magnetic field in the presence of another strong external magnetic field.

Hence, this allows to determine molecular structures, the purity of samples and to quantify the exact amounts in case of a known mixture. NMR is found to be a crucial technique to quantify the amount of the organic linkers incorporated in the MTV-MOF structures. Nearly 1-2 mg of the activated MTV-MOF samples are digested in few droplets of trifluoroacetic acid (TFA) and 0.5 ml of deuterated dimethyl sulfoxide (DMSO) to make sure that the MOF network is deterred and the organic linkers X-BDC and BTC are free again in the solution. The analysis is carried on using BRUKER Advance NMR Spectrometer (500 MHz). Note that the calculated numbers in the tables represent the mean values with a number of trials n=3.

D. Adsorption experiments

Prior to any adsorption experiment, the dried MOF sample is reactivated overnight under vacuum at 145°C. In a typical adsorption experiment, a known mass of the adsorbent (MOF) is added into a specific volume of the corresponding dye solution at a determined pH and temperature in a 30 ml glass vials and placed in a JULABO SW 23 thermal bath shaking at a constant rate of 200 rpm. At a specific time, t, aliquots are withdrawn and undergo filtration using filters of 0.2 μm to remove any MOF particles from the filtrate. It is important to note that the samples taken at time t = 0 are filtered as well. The remaining concentration of the equilibrium dye solution is measured on a Thermo Fisher Scientific Evolution Array UV-VIS spectrophotometer at λ=554 and 664 nm for methylene blue and rhodamine B respectively. The amount of the organic dye adsorbed at equilibrium is calculated by the following equation (II):

$$Q_e = \frac{(C_0 - C_e)V}{W} \qquad \text{(II)}$$

where C_o and C_e are the initial and the equilibrium concentrations (mg/L) of the dye respectively, V is the volume of the solution in Liters (L), W is the mass of the MOF in grams (g) and Q_e is the adsorption capacity (mg/g) of the adsorbent at equilibrium.

Similarly, the amount adsorbed of the dye at time t, is calculated by the equation (III):

$$Q_t = \frac{(C_t - C_e)V}{W} \qquad \text{(III)}$$

where C_t is the concentration (mg/L) of the dye at time t and Q_t is the adsorption capacity (mg/g) of the adsorbent at time t.

The effect of the pH and the initial dyes concentrations are investigated, as well as a kinetic study and a temperature effect study are conducted, and further analysis are done to calculate the corresponding adsorption parameters.

1. *pH effect:*

In order to examine the effect of the pH on the adsorption process, 10 mg of the MOF sample are added to 10 ml of 3.20 ppm MB or 10 ppm of Rh B dye solution in five separate tubes having solutions of different pHs ranging between 3 and 10, where the pH values of 6.3 and 6.1 corresponds to the MB and Rh B in deionized water without any additives. The initial solution's pH is adjusted by adding few droplets of a concentrated NaOH or HCl solution.

2. *Kinetic study:*

The adsorption study is conducted at different contact times (1, 3, 5, 10, 15, 25, 30, 60 and 120 minutes) by adding 10 mg of the MOF sample into 10 mL of a 10 ppm of each dye solution. Aliquots of 0.25 mL are withdrawn from each solution at the specific time t and measured using the spectrophotometer after filtration of the adsorbent MOF particles.

3. *Effect of the initial dyes concentrations*

In order to check the effect of the initial dyes concentration on the adsorption capacity, different adsorption experiments are done by varying the initial dyes concentrations. Where, 10 mg of the adsorbent MOF sample are added to 10 ml of the initial dye solution with concentrations ranging between 5 and 500 ppm. The contact time is 120 minutes, the samples are filtered and the remaining concentrations are measured on the UV-VIS spectrophotometer.

4. *Temperature effect:*

In order to study the effect of the temperature, the adsorption of MB and Rh B dyes by the MOF sample is carried out at four different temperatures: 25 °C, 35 °C, 45 °C and 55 °C. The adsorption conditions are of a typical experiment: 10 mg of the MOF,10 ml of 3.20 mg/L of the dye for MB and 10 ppm for Rh B, 120 min of contact time. The samples are filtered and the remaining concentration is measured as previously indicated.

5. *Co-adsorption Tests:*

In order to investigate the specify of the introduced functional group towards each dye and their relative behavior in the presence of both dyes in solution, additional adsorption tests are performed. Whereby, 10 mg of the optimal systems OH-MOF-199 or NH2-MOF-199 with 1:1 ratio are added to 10 ml of either Rh B or MB each of 10 ppm concentration and to 10 ml of a binary solution of 10 ppm of both Rh B and MB.

CHAPTER III

SYNTHESIS AND CHARACTERIZATION OF MULTIVARIATE MOF-199 VIA A REACTION DIFFUSION FRAMEWORK

A. Introduction

Various MTV-MOFs are synthesized via RDF and their characterization is detailed below. The effect of introducing defect on their crystal structure, morphology, thermal stability, nitrogen adsorption capacity and the control of the amount incorporated in each structure will be outlined. Moreover, RDF allows the live monitoring of the above parameters within the regions of the same tubular reactor.

B. Results and discussions

1. Powder X-ray diffraction of MTV-MOFs-199 by RDF

PXRD patterns for the as synthesized MOF-199 are recorded and compared to that of the simulated MOF-199. The sharp peaks of the collected blue crystals of MOF-199 perfectly match the ones of the simulated pattern with no additional peaks (Figure 18). Furthermore, to ensure the homogeneity of the system when adding a new linker to the system, the 2-linkers MTV-MOF-199 collected crystals are subjected to powder X-ray diffraction as well. Their PXRD patterns are also compared to that of MOF-199. It was noticed that these patterns are highly resolved and match the theoretical profile of MOF-199. This indicates introducing one functionalized linker did not affect the

formation of the MOF-199 lattice nor the homogeneity of the system as will be confirmed by the following SEM images. However, a broadening of the peaks is observed in the MTV-MOF-199 profiles increasing with an increased ratio of the introduced linker, owing to the small crystal size obtained in the latter (Figure 19).
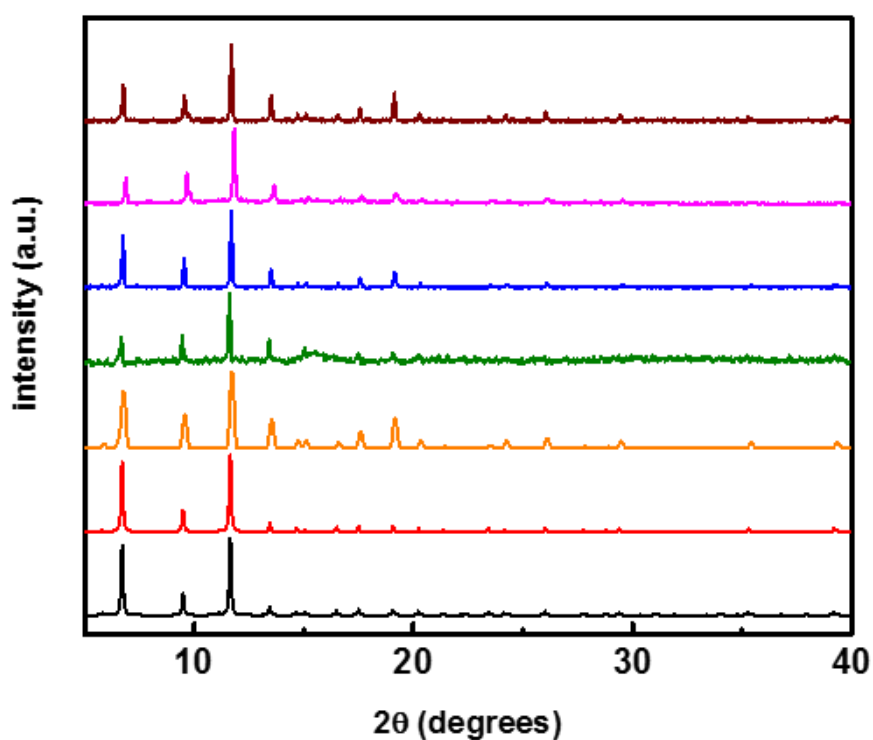
Figure 18 PXRD patterns of the simulated MOF-199 (black), synthesized MOF-199 (red), OH-MOF-199 (orange), NH_2-MOF-199 (green), IP-MOF-199 (blue), CN-MOF-199 (pink) and SO_3-MOF-199 (wine).

Moreover, the XRD patterns of the different 3-linkers systems reveal as well the conservation of the MOF-199 topology as shown in Figure 20. The same conclusion is also made when mixing up to 4 linkers in the same network. (Figure 20). However, some new minor peaks appear at 8.1°, 9.6°,18°, and 26.6° when more than three linkers where

mixed together in the presence of NH_2-BDC or in the case of NH_2-BDC was used in a higher ratio alone with BTC (NH_2-MOF-199 (3:1)).
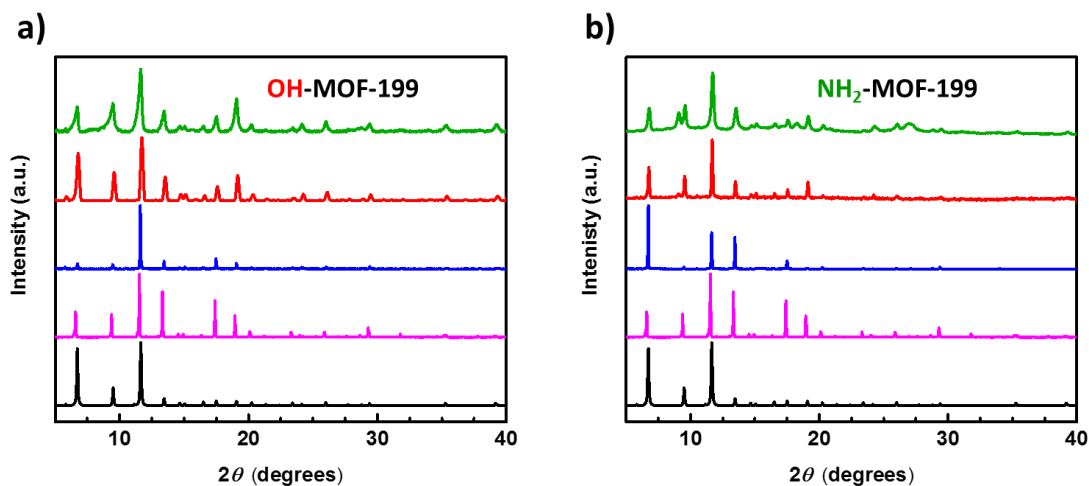
Figure 19 PXRD patterns of OH-BDC:BTC systems (a) and NH2-BDC:BTC systems (b); calculated MOF-199 (black), synthesized MOF-199 (pink), (1:3) (blue), (1:1) (red) and (3:1) (green).

Further experiments were carried out to investigate the reason behind these peaks. Interestingly, when NH_2-BDC crystallizes alone in the same growth conditions, it generates a green powder with a very low crystallinity showing similar peaks in its XRD pattern (Figure 21). Similar results are obtained in a related study as our systems[129].The presence of crystallized NH_2-BDC may be behind the extra peaks. Hence, they might be present in a very minor amount, so that they can be noticed by SEM or cause a major phase heterogeneity as shown in the following section.
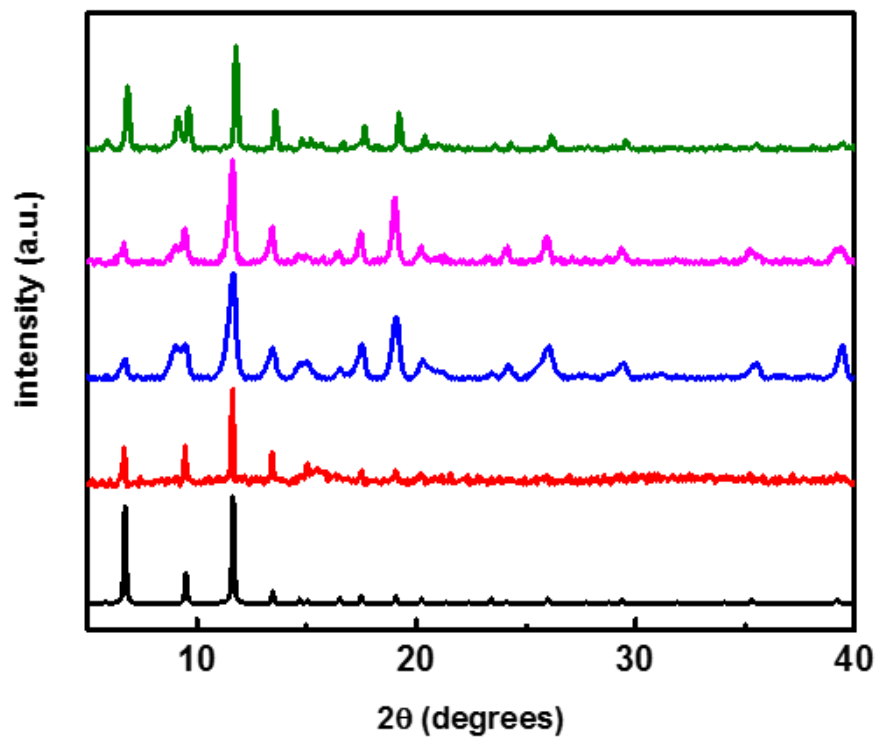
Figure 20 PXRD patterns of the simulated MOF-199 (black),IP-OH-MOF-199 (red), IP-NH$_2$-MOF-199 (blue), OH-NH$_2$-MOF-199 (pink), IP-OH-NH$_2$-MOF-199 (green).
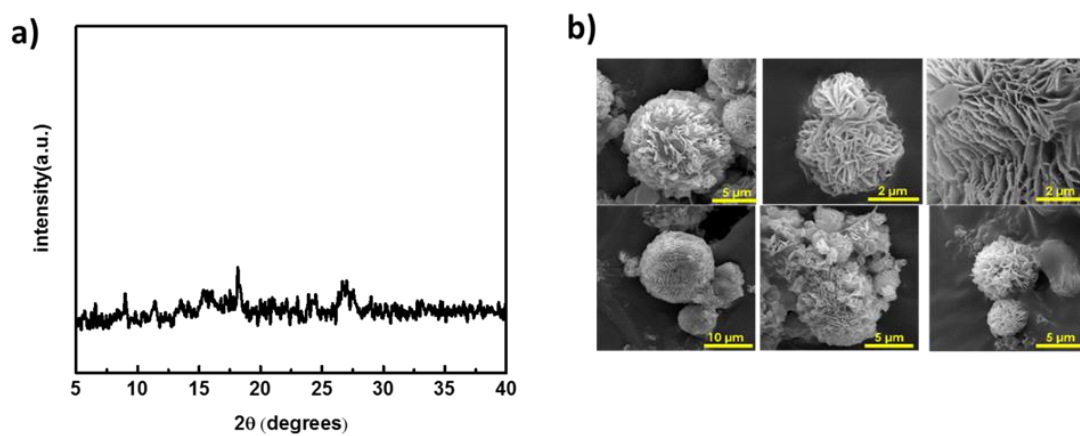
Figure 21 NH$_2$-BDC hierarchical structures XRD pattern (a) and SEM images (b).

2. *Scanning Electron Microscopy Analysis*

The phase purity of the synthesized MOF-199 and its MTV-MOF derivatives is confirmed by SEM images. Moreover, RDF allows us to lively monitor the formation of the precipitated particles by dividing each tube to three consecutive zones (zone 1, zone 2 and zone 3) according to their distance from the interface of the inner agar gel and the outer solution. The nearest to the interface is zone 1 and so on. SEM images of each zone are collected and representative images are shown in table 3. The obtained images reveal one of main features of RDF which is the evolution of the crystals relatively to the distance from the interface as an increase in the size which is consistent with the domination of the nucleation over growth near the interface that it is observed as we go farther from the gel-outer solution interface.

As shown in table 3, the pure MOF-199 particles are cubes when no functionalized X-BDC is added in the reaction system. Upon introducing any of the X-BDC linkers, the cubic morphology changes to spheres or octahedrons depending on the type of the linker introduced. In a (1:1) ratio, IP-BDC and OH-BDC with BTC generates interconnected spheres while CN-BDC and SO_3-BDC with BTC gives octahedral-shaped MOFs and NH_2-BDC in his turn with BTC shows cuboctahedra particles.

Zones	MOF-199	IP-MOF-199	CN-MOF-199	SO₃-MOF-199
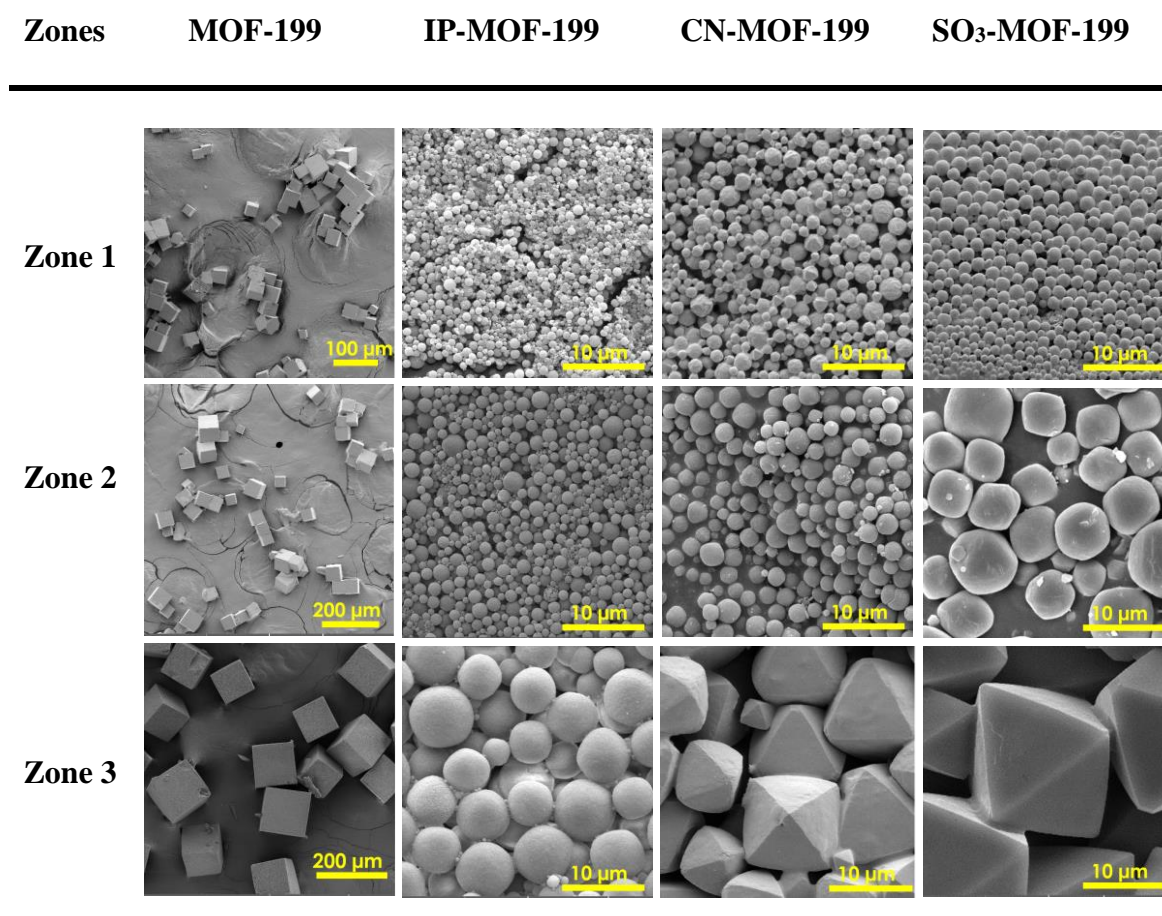
Table 3 SEM images of the different 2-linkers MOF systems (1:1) extracted from three consecutive zones of each of the reaction tube.

In order to investigate this morphology change, SEM images of different starting ratios of OH-MOF-199 and NH_2-MOF-199 are obtained and shown in table 4. In the case of pure MOF-199, when no functionalized X-BDC is added in the reaction system, it can be seen that all the crystals in all zones are cubes with $6 \times (100)$ facets. When OH-BDC is introduced into the system in a OH-BDC:BTC ratio of (1:3), in the region close to the interface, the particle morphology changed to a cuboctahedron consisting of $6 \times (100)$ and 8 (111) facets. Away from the interface, the facets of (111) become larger and the

cuboctahedron is transformed to octahedron. However, when we increase the starting concentration of OH-BDC (OH-BDC:BTC (1:1 or 3:1)), interconnected spheres are formed which is consistent with highly defected frameworks[130]. The interconnection between the particles could be responsible for the mesoporous behavior of the material. Likewise, in the case of the amino-functionalized MOF-199, relatively large cubeoctahedral crystals are obtained for NH2-BDC:BTC (1:1 and 1:3). Interestingly, for higher starting ratio NH2-BDC:BTC (3:1), a hierarchical structure can be observed which could explain the mesoporous behavior and the decrease in the surface area (Figure 21).

| Zones | MOF-199 | OH-BDC:BTC | | | NH$_2$-BDC:BTC | | |
		1:3	1:1	3:1	1:3	1:1	3:1
Zone 1							
Zone 2							
Zone 3							
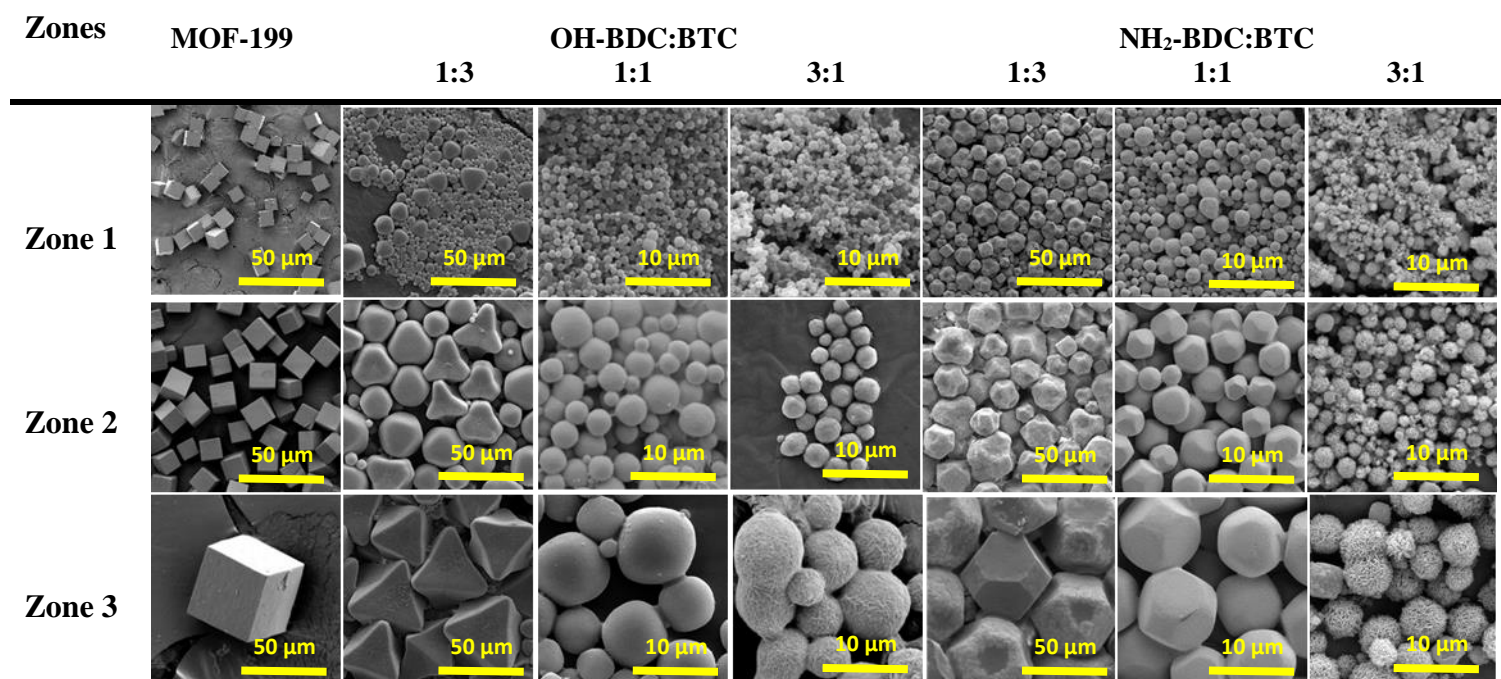
Table 4 SEM images of the different MOF samples extracted from three consecutive zones of the reaction tubes.

Regarding the 3-linkers MOF systems, the concurrence between the ligands led to different morphologies. Spherical particles are only obtained in case of IP-OH-MOF-199 system as expected, while the systems containing NH$_2$-BDC (IP-NH$_2$-MOF-199,

OH-NH$_2$-MOF-199 and IP-OH-NH$_2$-MOF-199) all showed small aggregates with octahedral morphology (Table 5). All the previous demonstrates that the morphology of the defected MTV-MOF-199 is highly dependent on the type of the introduced ligand and its corresponding concentration in the framework.

System	IP-OH-MOF-199	IP-NH$_2$-MOF-199	OH-NH$_2$-MOF-199	IP-OH-NH$_2$-MOF-199
Zone 1				
Zone 2				
Zone 3				
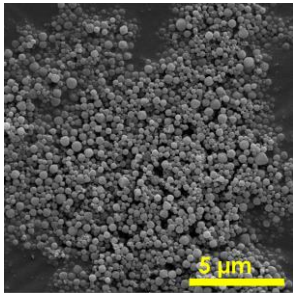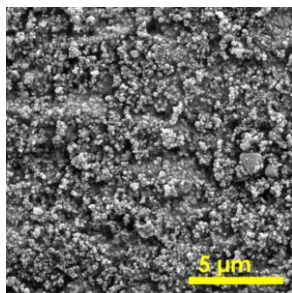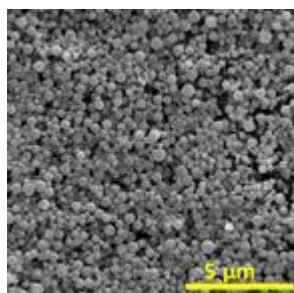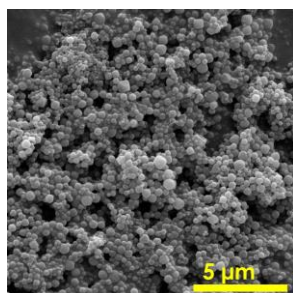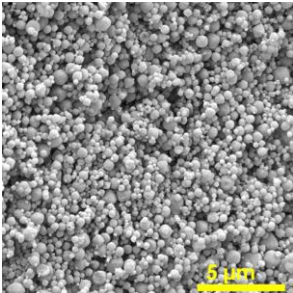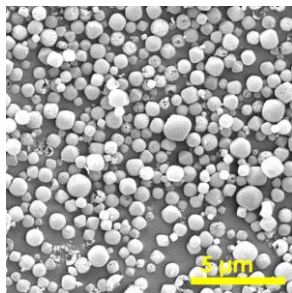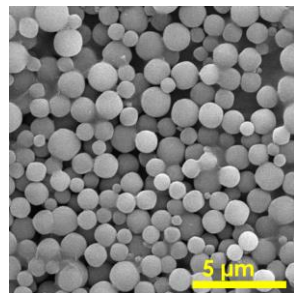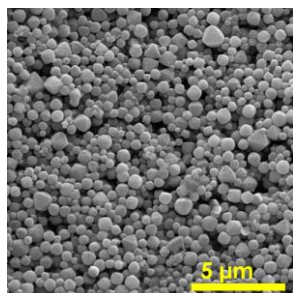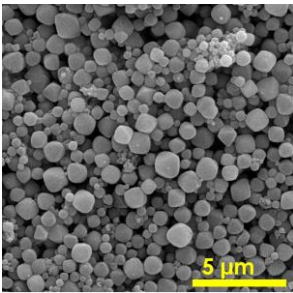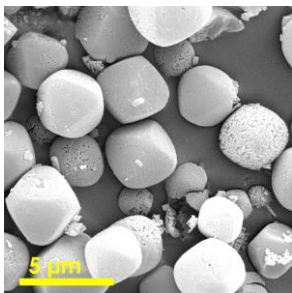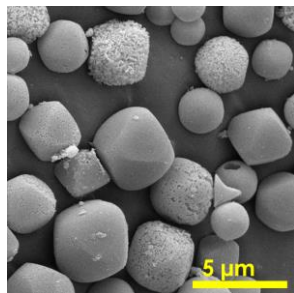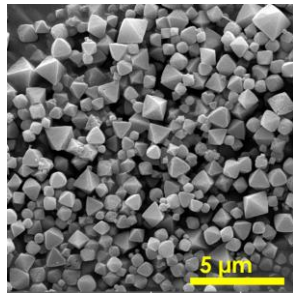
Table 5 SEM images of the different 3-linkers and 4-linkers MOF systems extracted from three consecutive zones of each of the reaction tube.

3. *Nitrogen adsorption isotherms results*

In order to evaluate the effect of introducing defects on the porosity of MOF-199, nitrogen isotherms are recorded and the corresponding surface areas are reported using the BET calculation method as well as the pore volume using the BJH method. As shown in Figure 22, MOF-199 profile exhibits a type I isotherm which is associated with the presence of micropores with a surface area of 1230 m^2/g. Interestingly, when adding X-BDC to the framework, the profiles of nitrogen adsorption corresponding to the all the MTV-MOFs (1:1) shows a type IV isotherm with a characteristic hysteresis loop signifying the creation of mesopores. Moreover, H4 hysteresis loop appears to be the case in all these systems indicating the presence of micropores expect the case of SO_3-MOF-199 where a H2 hysteresis loop is observed indicating a severe defect where the pore size and pore distribution are hard to predict[131]. The corresponding surface areas and pore volume shown in Table 6 shows a general decrease in the surface area usually related to the creation of mesopores[37, 50].
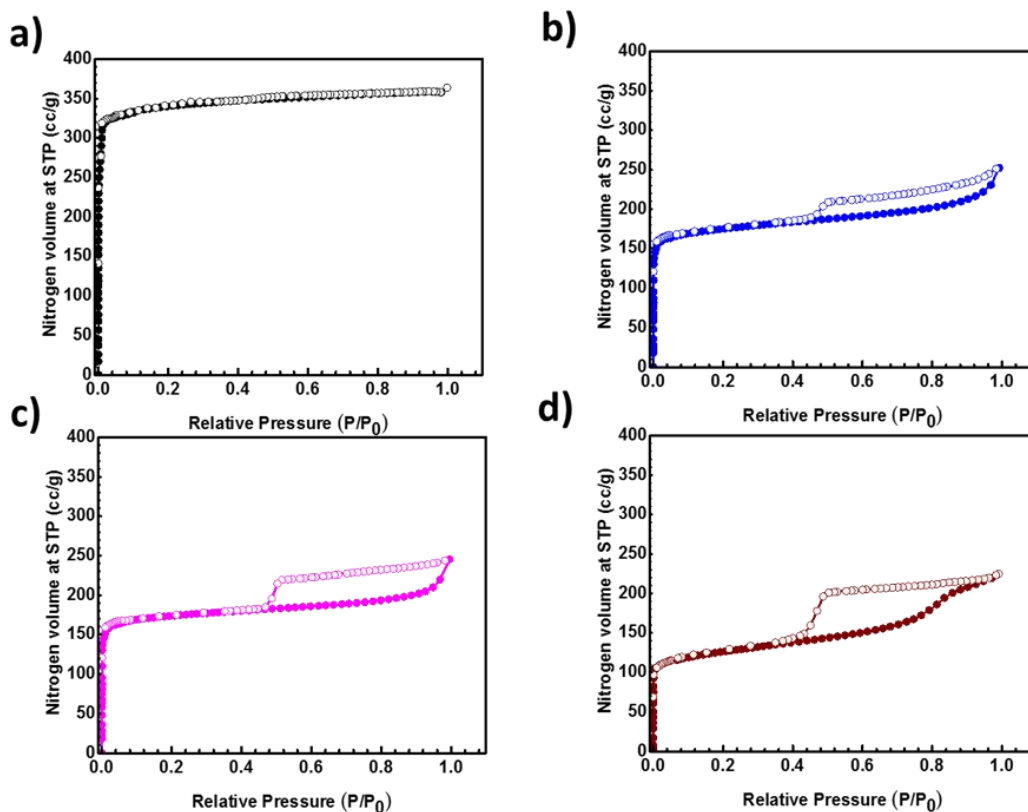
Figure 22 Nitrogen adsorption profiles of MOF-199 (a), IP-MOF-199 (b), CN-MOF-199 (c), SO_3-MOF-199 (d).

Looking more closely to the effect of the amount of X-BDC introduced, when having BTC in excess X-BDC:BTC (1:3) exhibit Type I isotherm similar to that of MOF-199, with a surface area of 900 and 800 m^2/g for OH-BDC and NH_2-BDC respectively (Figure 23). Interestingly, when we increase the concentration of X-BDC to equate that of BTC (1:1), the obtained isotherm revealed a deviation from type I into type IV (Figure 23), signifying the introducing of mesopores into the framework. The calculated surface areas are 420 and 410 m^2/g for the hydroxyl-functionalized (OH-MOF-199) and amino-functionalized (NH_2-MOF-199), respectively, which are much lower than that of the as-synthesized MOF-199 which could be probably explained by the introduction of the new

51

functional groups thus leading to a decrease in the total pore volume (Table 6). By further increasing the concentration of OH-BDC and NH_2-BDC to be in excess with respect to BTC (3:1), a slight disappearance in the hysteresis loop is observed. This implies that there is a change in the pore size distribution induced by the major shape change of the material as shown in the SEM images due to the domination of the defect within the MOF-199 structure rendering a lower surface area of 360 and 400 m^2/g for OH-BDC and NH_2-BDC respectively.
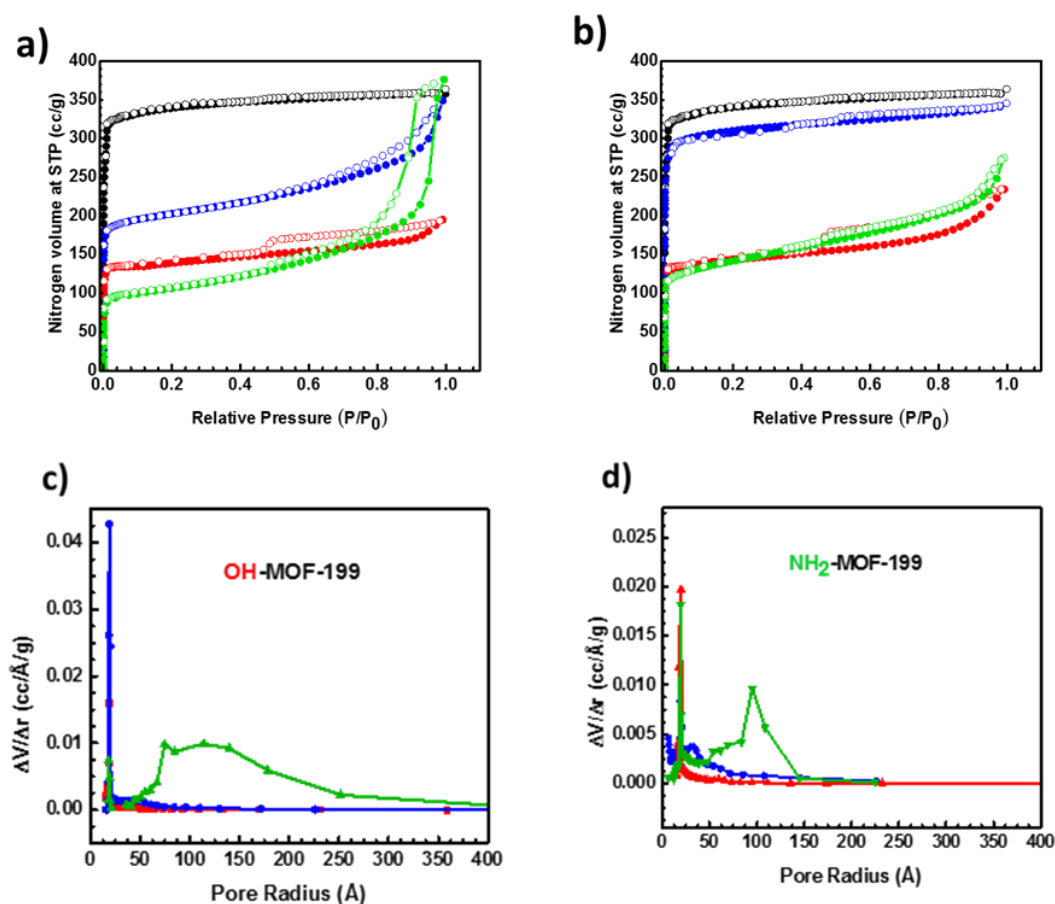
Figure 23 Nitrogen adsorption isotherms of OH-BDC:BTC systems (a) and NH_2-BDC:BTC systems (b) Pore Size Distribution of OH-BDC:BTC systems (c) and NH2-BDC:BTC systems (d) MOF-199 (black), (1:3) (blue), (1:1) (red) and (3:1) (green).
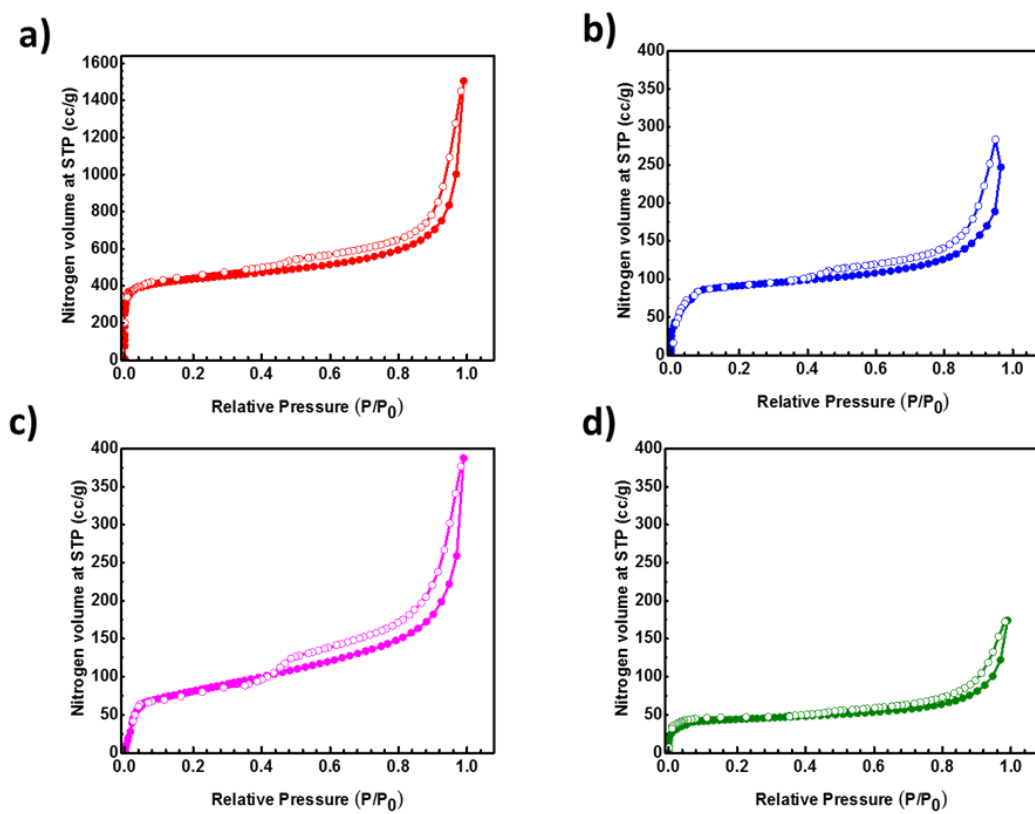
Figure 24 Nitrogen adsorption isotherms of IP-OH-MOF-199 (a), IP-NH$_2$-MOF-199 (b), OH-NH$_2$-MOF-199 (c), IP-OH-NH$_2$-MOF-199 (d).

Regarding the 3-linkers and 4-linkers systems, the surface area kept decreasing as shown in Table 6 as more defect is introduced. Interestingly, the type IV isotherm is obtained but now with hysteresis loop type H3 (Figure 24) which is usually associated with nonrigid aggregates of particles[131] that are in compliance with the SEM results. Surprisingly, when combining IP-BDC and OH-BDC in one framework with BTC, the obtained network shows a very high surface area of 1296 m^2/g and higher total pore volume of 2.25 cm^3/g that is associated with missing a cluster from the framework due to the severe defect[50].

MOF System	Ratio X-BDC:BTC	BET specific surface area (m^2/g)	BJH Total Pore Volume (cc/g)
MOF-199	-	1230	0.87
OH-MOF-199	1:3	900	0.54
	1:1	420	0.36
	3:1	360	0.52
NH$_2$-MOF-199	1:3	800	0.54
	1:1	410	0.30
	3:1	400	0.58
IP-MOF-199	1:1	514	0.39
CN-MOF-199	1:1	497	0.38
SO$_3$-MOF-199	1:1	380	0.30
IP-OH-MOF-199	1:1:1	1296	2.25
IP-NH$_2$-MOF-199	1:1:1	314	0.44
OH-NH$_2$-MOF-199	1:1:1	268	0.58
IP-OH-NH$_2$-MOF-199	1:1:1:1	132	0.27

Table 6 BET surface areas and the total pore volume for the different MTV-MOF systems.

4. Thermal stability of the synthesized MTV-MOFs-199

The effect of the incorporation of defects within the MOF-199 topology on its thermal stability is evaluated through TGA analysis. The developed MTV-MOFs systems showed the curves in Figure 25.
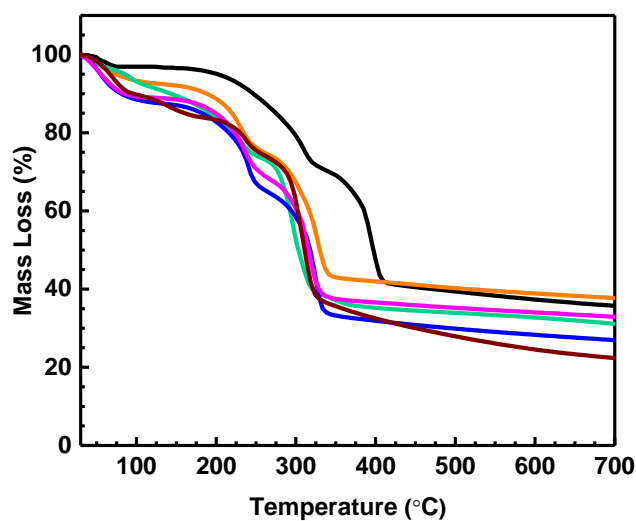
Figure 25 TGA profiles for MOF-199 (black) and the 2-linkers MTV-MOFs (1:1): OH-MOF-199 (orange), NH_2-MOF-199 (green), IP-MOF-199 (blue), CN-MOF-199 (pink) and SO_3-MOF-199 (wine).

It is clear that there is a slight decrease in the thermal stability of the MTV-MOFs-199 (1:1) when compared to the as-synthesized MOF-199 as expected. Nevertheless, the TGA profiles of MTV-MOFs-199 resemble that of MOF-199, where two main weight losses are observed. The first is at around 100 °C ranging from 5 to 20% loss, probably corresponding to the loss or the escape of water molecules from the exposed metal sites of the SBUs. The second is near 300 °C with around 50% mass loss indicating the thermal decomposition of the corresponding MOF (Figure 26).
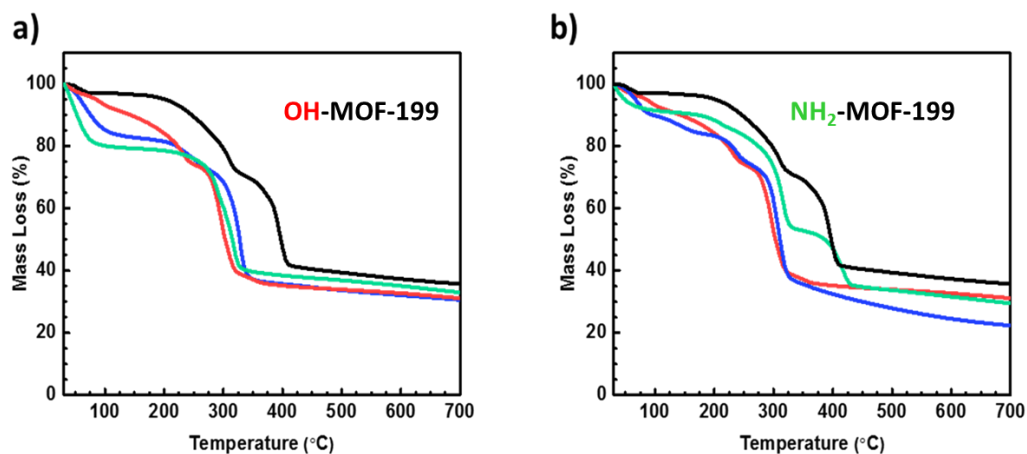
Figure 26 Thermogravimetric analysis of OH-BDC:BTC systems (a) and NH2-BDC:BTC systems (b): MOF-199 (black), (1:3) (blue), (1:1) (red) and (3:1) (green).

This can be explained by a decrease in the number of covalent bonds because each incorporated functional ligand is substituting two carboxylate covalent bonds with the corresponding metal site within the mixed linker MOF structure. The same trend is obtained with the 3-linkers and 4-linkers MOF systems as shown in Figure 27.
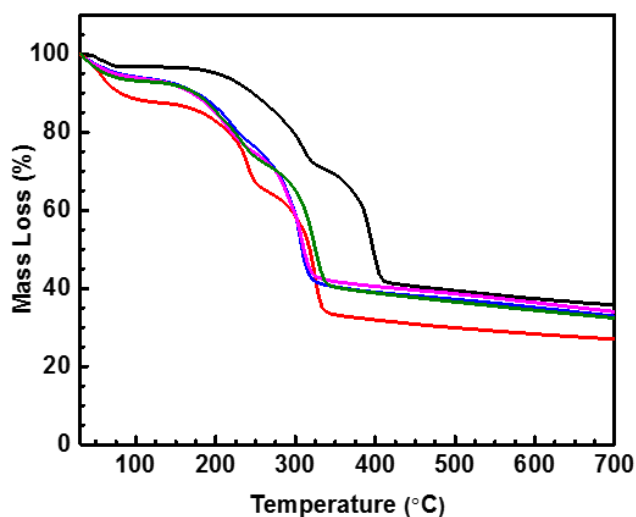
Figure 27 TGA profiles for MOF-199 (black), IP-OH-MOF-199 (red), IP-NH$_2$-MOF-199 (blue), OH-NH$_2$-MOF-199 (pink), IP-OH-NH$_2$-MOF-199 (green)

5. ^{1}H-NMR Analysis of the obtained MTV-MOFs-199

^{1}H-NMR analysis on the digested crystals of the MTV-MOFs allows us to validate the presence of X-BDC and BTC linkers and to quantify their relative amounts incorporated in the MOF structure determined by the ratio of their aromatic hydrogen peaks in the NMR spectrum. Representative NMR spectra are shown in the supplementary information and the results of their integrations illustrated in Figure 28 showing that the final proportion of the linkers incorporated in the MOF structure is lower than the initial proportions used in the reaction mixture. Moreover, the MOF-199 functionalization along the tube is also monitored via RDF and a very interesting trend is obtained in all the studied systems. In which, the amount of the functionalized linker incorporated decreases with decreasing supersaturation by going farther from the interface as shown in Figure 28.

System	Linker	Average X-BDC (%)
	CN-BDC	15
	SO3-BDC	17
X-BDC:BTC (1:1)	OH-BDC	26
	NH2-BDC	41
	IP-BDC	35
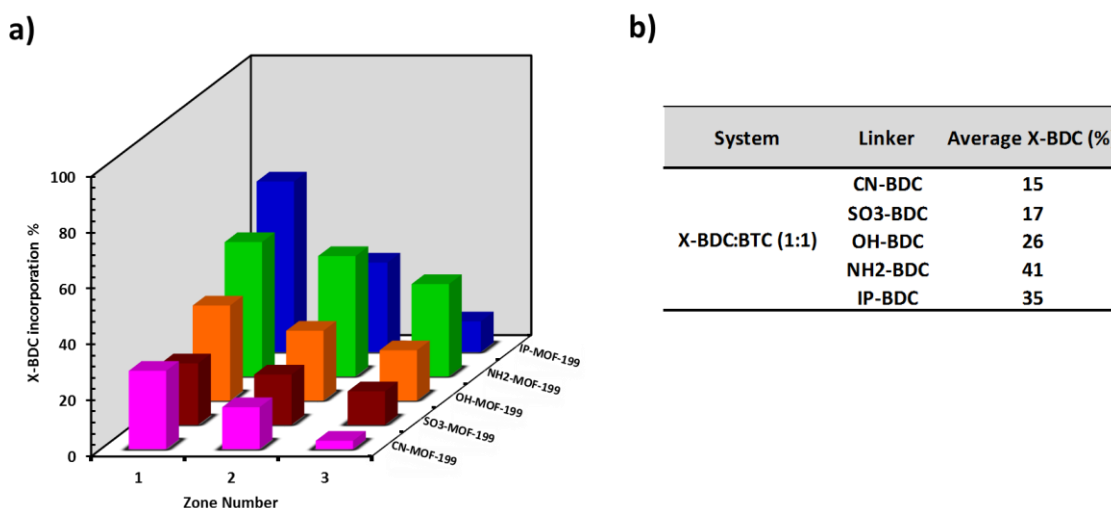
Figure 28 Percentages of X-BDC incorporated within X-MOF-199 (1:1) crystals extracted from three consecutive zones: CN-BDC (pink), SO$_3$-BDC (wine), OH-BDC (orange), NH$_2$-BDC (green) and IP-BDC (blue) (a) and their corresponding average values in the framework as a function of the linker X-BDC (b).

Although there is always a competition between BTC and X-BDC linkers, where, it is noticed that depending on the functionality, some X-BDC are more efficiently incorporated than others. Then, the final average amounts are calculated to be 15%, 17%, 26%, 35% and 41% for the functional linker CN-BDC, SO3-BDC, OH-BDC, NH2-BDC and IP-BDC respectively (Figure 28).

Regarding the different starting ratios, the final amounts of OH-BDC and NH_2-BDC in each tube are calculated to be 32%, 26% and 16% for initial ratios OH-BDC:BTC (3:1), (1:1) and (1:3) respectively, and 52%, 41% and 23% for initial ratios NH_2-BDC:BTC (3:1), (1:1) and (1:3), respectively. This indicates that the higher the starting ratio, the higher the defect is incorporated within each system with a decreasing trend along the zones (Figure 29).
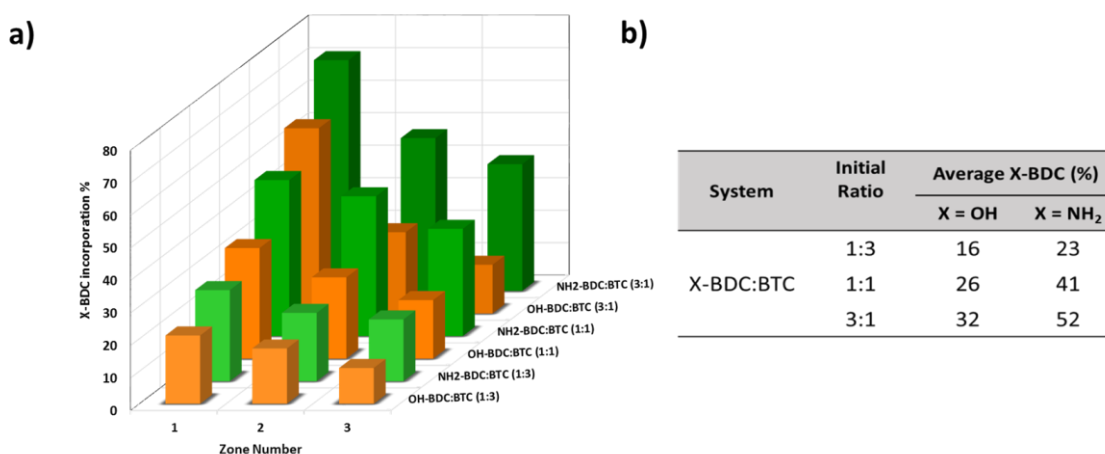
Figure 29 . Percentages of OH-BDC (orange) and NH2-BDC (green) incorporated within OH-MOF-199 and NH2-MOF-199 crystals extracted from three consecutive zones (a) and their corresponding average values as a function of the starting ratios (b).

It is very interesting to study the behavior of each X-BDC linker and its relative amount in the framework in the presence of 3 or more linkers (Figure 30). Initially, it is found that OH-BDC and IP-BDC are incorporated equally in the framework in the presence of BTC with a final average amount of 13% in the IP-OH-MOF-199 framework. Regarding NH_2-BDC, it is more incorporated than OH-BDC in the presence of BTC with average final amounts of 24% and 20% for NH_2-BDC and OH-BDC respectively in the OH-NH_2-MOF-199 system, while it is less incorporated than IP-BDC in the presence of BTC with average final amounts of 13% and 17% for NH_2-BDC and IP-BDC respectively the IP-NH_2-MOF-199 system.

Meanwhile, for IP-BDC, OH-BDC and NH_2-BDC in the presence of BTC in the IP-OH-NH_2-MOF-199 system, NH_2-BDC is the most incorporated with a final average amount of 26 % while IP-BDC and OH-BDC are less incorporated with a final average amount of 13% for both. It is noteworthy to say that most of the zones maintained the same trend of incorporating the highest defect in the first zone and a nearly zero incorporation in the last zone in the case of 3 or more linkers in the same system.

a)

b)

System	Linker	Average X-BDC (%)
IP-OH-MOF-199	IP-BDC	13
	OH-BDC	13
IP-NH2-MOF-199	IP-BDC	17
	NH2-BDC	13
OH-NH2-MOF-199	OH-BDC	20
	NH2-BDC	24
IP-OH-NH2-MOF-199	IP-BDC	13
	OH-BDC	13
	NH2-BDC	29
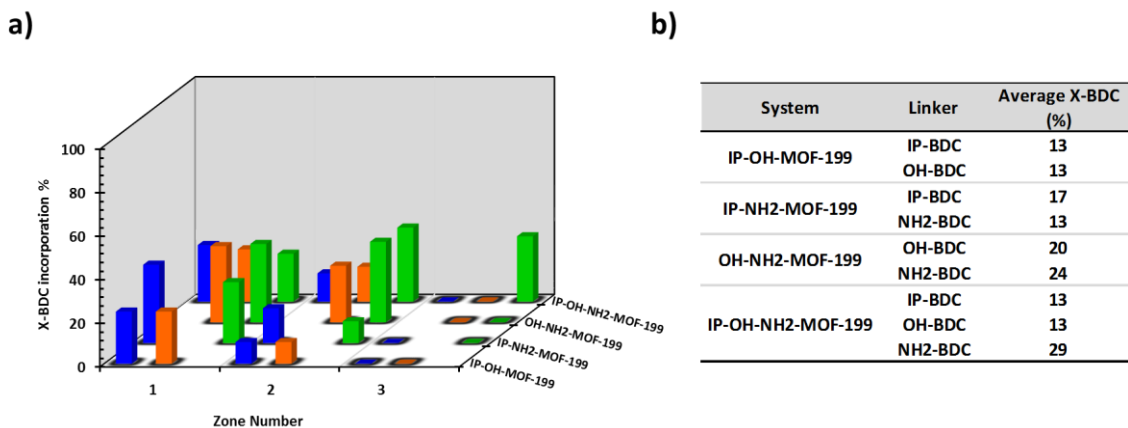
Figure 30 Percentages of IP-BDC (blue),OH-BDC (orange) and NH2-BDC (green) incorporated within the different 3-linkers and 4-linkers MTV-MOF crystals extracted from three consecutive zones (a) and their corresponding average values as a function of the linker X-BDC (b).

CHAPTER IV

ADSORPTION OF ORGANIC DYES ON MOF-199 AND MTV-MOFS-199

A. Introduction

In this work, to demonstrate the importance of the functionalization and defects incorporated within MOF-199 structure, MTV-MOF-199 samples are employed as adsorbents for MB and Rh B removal from water. In this chapter, a full adsorption study for MB and Rh B on hydroxyl- and amino-functionalized MOF-199 will be discussed to prove the enhancement of the adsorption properties brought by introducing the functionalization the MOF-199 structure (Figure 31).
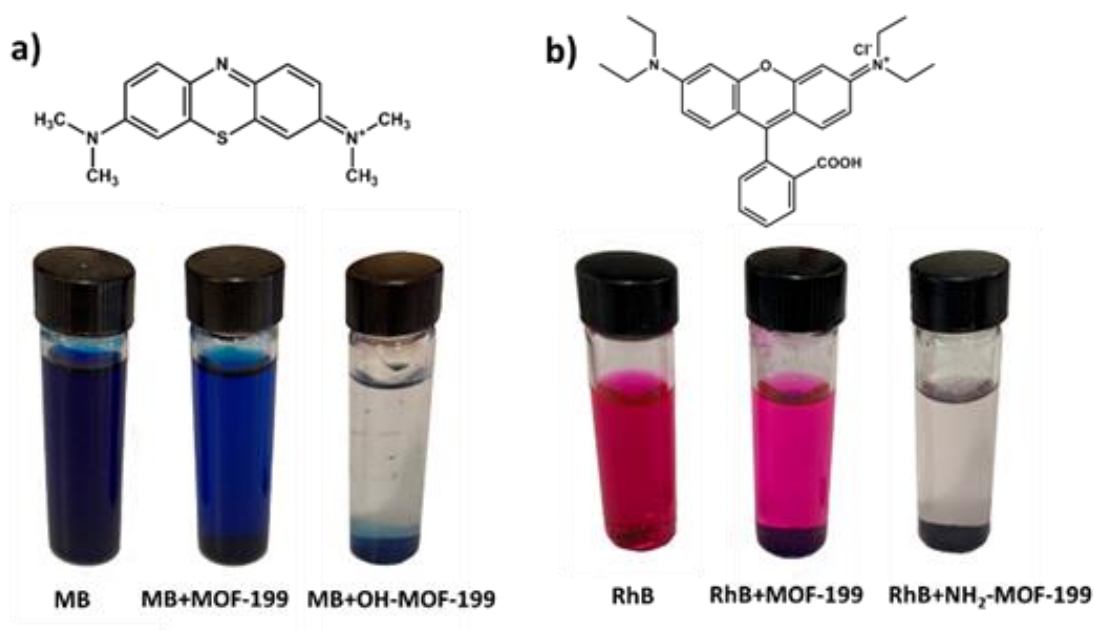
Figure 31 Adsorption of methylene blue (a) and rhodamine B (b) dyes by the functionalized and defected MOF-199 compared to pure MOF-199.

B. Results and Discussion

1. *Adsorption isotherms of the MTV-MOFs-199*

The Hydroxyl-functionalized version showed high affinity toward MB, however NH_2-MOF-199 is found to be good adsorbent for Rh B. More importantly, both defected systems are found to perform much better than MOF-199. In our study, Langmuir isotherm equation is found to have highest R-squared values as compared to the Freundlich model as shown in Table 7. The plots in Figure 32 are fitted in accordance to the non-linearized form of Langmuir equation:

$$q_e = \frac{q_{max} K_L C_e}{1 + K_L C_e} \tag{3}$$

Where K_L is the Langmuir equilibrium constant (L/mg) and q_{max} is the monolayer adsorption capacity of the adsorbent (mg/g).

It is clear from Table 7 that the MTV-MOFs with starting rations of OH-BDC:BTC (1:1) and NH_2-BDC:BTC (1:1) have the highest values of q_{max} 263 and 156 mg/g for MB and Rh B respectively when compared to MOF-199 and other defected structures. These highest values mean that the adsorption process is most favorable on these functionalized MOF-199 adsorbents.

MOF system	X-BDC:BTC Ratio	q_{max} (mg/g)	K_L(L/mg)	Langmuir R-squared	Freundlich R-squared
Methylene Blue					
MOF-199	-	84	0.0149	0.9809	0.9517
OH-MOF-199	1:3	111	0.0171	0.9742	0.9653
	1:1	263	0.117	0.9798	0.9345
	3:1	147	0.0454	0.9518	0.8951
Rhodamine B					
MOF-199	-	74	0.00873	0.9876	0.9385
NH$_2$-MOF-199	1:3	131	0.00846	0.9920	0.9590
	1:1	156	0.0314	0.9915	0.9524
	3:1	143	0.0147	0.9917	0.9235

Table 7 Langmuir isotherm parameters q_{max}, K_L, and Langmuir R-squared values versus Freundlich R- squared for OH-BDC:BTC systems with MB and NH$_2$-BDC:BTC systems with Rh B.

Furthermore, since our adsorption studies fits the Langmuir model, thus, a physical adsorption process on the surface of the MOF is proposed in such case. In order to validate the newly synthesized MTV-MOFs efficiency, their maximum adsorption capacity is compared to numerous common adsorbent materials and is shown to perform better than many of them as shown in Table 8. Our strategy of introducing defects and functionalities into MOF-199 demonstrates the effectiveness of the heterogeneity within order to enhance the performance of the MOF adsorbents.
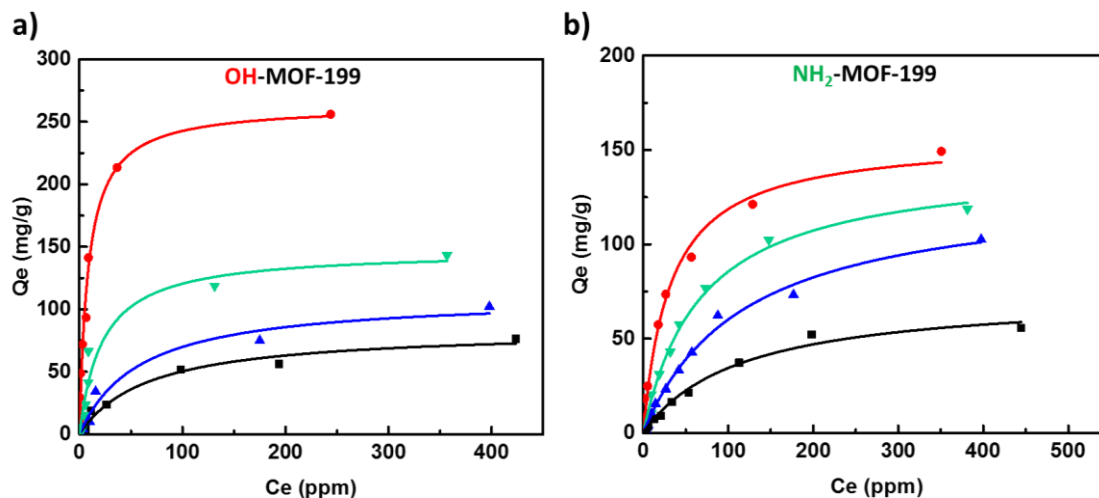
Figure 32 Langmuir adsorption isotherms for OH-BDC:BTC systems (a) and NH2-BDC:BTC systems (b) and MOF-199 (black), (1:3) (blue), (1:1) (red) and (3:1) (green).

Type of adsorbent	Dye	Q_{max} (mg/g)	Reference
Montmorillonite clay	MB	289.12	[132]
Commercial Activated carbon	MB	319	[133]
MOF-199/GO	MB	183	[134]
MOF-199	MB	84	This work
OH-MOF-199 (1:1)	MB	263	This work
OH-MOF-199 (3:1)	MB	147	This work
OH-MOF-199 (1:3)	MB	111	This work
Sodium montmorillonite	Rh B	42.19	[135]
Activated carbon	Rh B	16.12	[136]
MIL-125(Ti)	Rh B	180	[137]
MOF-199	Rh B	74	This work
NH₂-MOF-199 (1:1)	Rh B	156	This work
NH₂-MOF-199 (3:1)	Rh B	143	This work
NH₂-MOF-199 (1:3)	Rh B	131	This work

Table 8 Uptake capacity of OH-MOF-199 and NH₂-MOF-199 compared to other adsorbents.

2. *Effect of the initial pH of the solution*

The pH of the solution is an imperative factor as it affects the transmission of the adsorbate from the aqueous solution towards the adsorbent via altering the adsorbent's surface charge. The corresponding adsorption experiments are conducted at different pHs ranging between 3 and 10 and the results are shown in Figure 33. When the pHs increase from 3 to 6, the quantity adsorbed of MB onto OH-BDC:BTC and Rh B onto NH_2-BDC:BTC increases until reaching their maximum values at the optimum pHs (6.3 and 6.1) which correspond to MB and Rh B in the de-ionized water. However, for higher pHs (7-10), it decreases significantly for Rh B and modestly for MB.
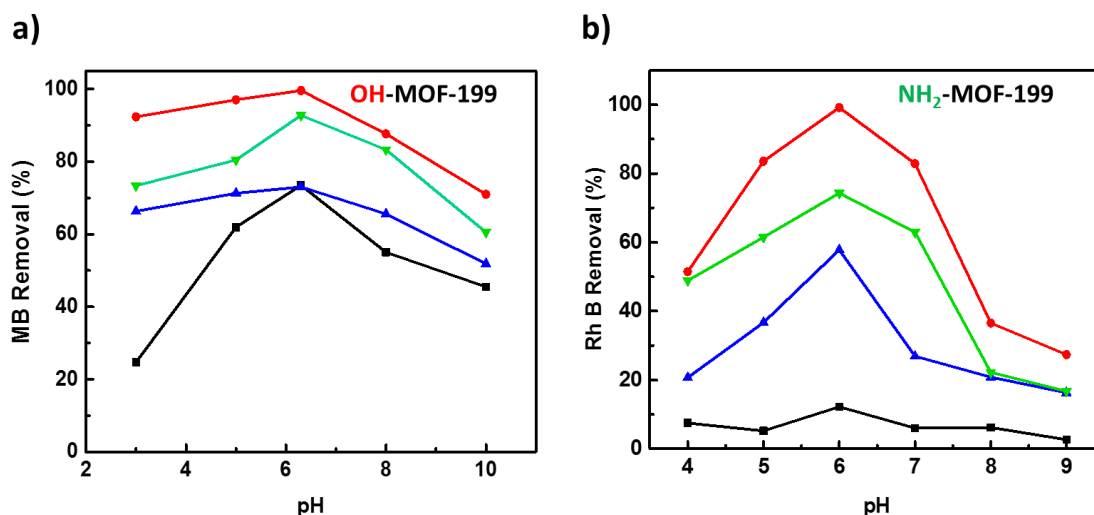
Figure 33 pH effect on the methylene blue and rhodamine B removal for OH-BDC:BTC systems (a) and NH_2-BDC:BTC systems (b) respectively: MOF-199 (black), (1:3) (blue), (1:1) (red) and (3:1) (green).

In order to understand the mechanism behind these changes, Zeta potential measurements of the best performing samples (OH-BDC:BTC (1:1) and NH_2-BDC:BTC (1:1)) are reported in Figure 34. It is obvious that the surface charge is always negative

on the wide range of pH, which explains the adsorption of the positively charged dyes MB and Rh B. More precisely, the surface charge becomes less negative on the acidic range of pH until reaching its peaks coherently with the peak of the uptake. This can be explained by the electrostatic attraction between the positively charged dyes and the negatively charged surfaces. For the higher alkaline pH values, the results slightly differ where the adsorption of Rh B decreases dramatically. This is due to Rh B being in its zwitterion form at this pH range. Therefore its possibility to form dimers that aggregates consequently[138] which may lower the uptake values to this limit along with the slight increase of the negative charge of the surface. For the MB, the adsorption also decreases moderately knowing that MB is always in its positive form and the surface charge is increasing moderately in the negative range. On the other hand, the adsorption of some organic pollutants could be related to the ionic strength because of the electrostatic screening effect[139-140], which implies that the surface of the MOF becomes more positively charged than in deionized water due to the accumulation of the H^+ ions from the solution in acidic mediums, thereby rendering an electrostatic repulsion with the positive charge of the dyes and decreasing the amount of the MB and Rh B adsorbed. Likewise, at high pH values beyond 6.3, the amount of the dyes adsorbed on the surface of the MOF decreases, however this may be due the increasing number on Na^+ ions from the solution, which could compete with the cationic MB and Rh B in their basic forms for the equivalent active adsorption sites in the MOF.
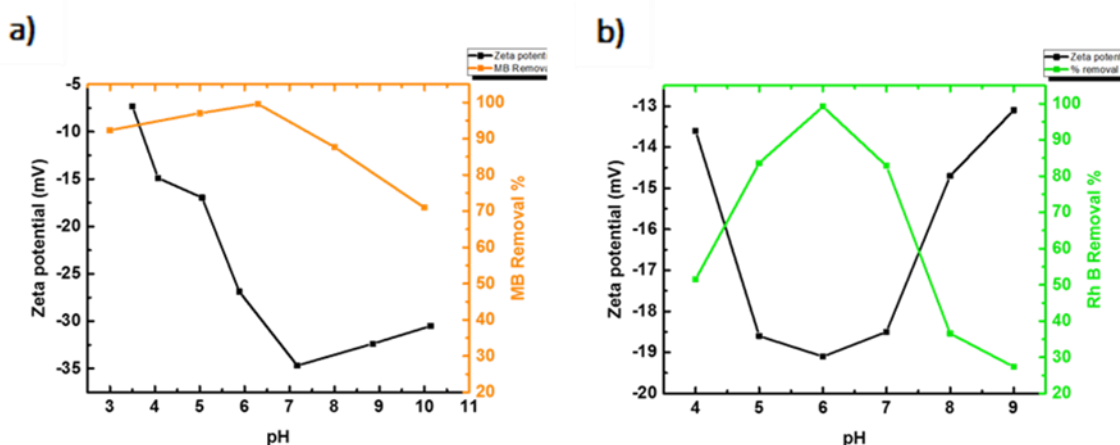
Figure 34 Zeta potential measurement and the corresponding dye uptake for OH-MOF-199 (1:1) (a) and NH2-MOF-199 (1:1) (b).

3. *Thermodynamic Study: Effect of Temperature*

To perceive the effect of the temperature, the adsorption studies of MB and Rh B over MOF-199 and its mixed-linker counterparts are carried out at four different temperatures: 298K, 308K, 318K, 328K. The results for the thermodynamic calculations are indicated in Table 9. The thermodynamic parameters including enthalpy ($\Delta H°$) in $kJ \cdot mol^{-1}$, entropy ($\Delta S°$) in $J \cdot K^{-1} \cdot mol^{-1}$ and the Gibbs free energy ($\Delta G°$) in $kJ \cdot mol^{-1}$ are estimated through the Van't Hoff plot in accordance to the equations below:

$$\Delta G° = \Delta H° - T\Delta S° \tag{4}$$

$$Ln\ K = (\Delta S°/R) - (\Delta H°/RT) \tag{5}$$

where K is the equilibrium constant, R is the ideal gas constant ($8.314\ J \cdot mol^{-1} \cdot K^{-1}$).

Adsorbent	$\Delta G°$ (kJ·mol^{-1})				$\Delta H°$(kJ ·mol^{-1})	$\Delta S°$(J·K^{-1} ·mol^{-1})
	T=298 K	T=308 K	T=318 K	T=328 K		
Methylene Blue						
MOF-199	-1.96	-2.25	-2.54	-2.83	7	29
OH-BDC:BTC (1:3)	-1.91	-2.50	-3.10	-3.69	16	60
OH-BDC:BTC (1:1)	-6.38	-9.03	-11.7	-14.3	73	265
OH-BDC:BTC (3:1)	-2.89	-3.55	-4.21	-4.88	17	66
Rhodamine B						
MOF-199	2.04	1.58	1.11	0.65	16	46
NH₂-BDC:BTC (1:3)	-1.80	-2.57	-3.33	-4.09	21	76
NH₂-BDC:BTC (1:1)	-7.46	-9.16	-10.85	-12.54	43	169
NH₂-BDC:BTC (3:1)	-3.06	-3.94	-4.81	-5.69	23	87

Table 9 Thermodynamic parameters $\Delta G°$ (kJ·mol^{-1}) at four different temperatures, $\Delta H°$ (kJ·mol^{-1}) and $\Delta S°$ (J·K^{-1}·mol^{-1}) for NH₂-BDC:BTC and OH-BDC:BTC systems.

The negative values of $\Delta G°$ signifies that the adsorption process is feasible and spontaneous. Furthermore, the increase in the magnitude of $\Delta G°$ with the rise in temperature indicates that the extent of spontaneity is escalating at higher temperatures.

68

The second parameter is $\Delta S°$, which reveals the disorder at the adsorbent/adsorbate interface. It is clear from Table 9 that the values of $\Delta S°$ are positive suggesting the high degree of disorderliness and the high affinity of the MOFs towards MB and Rh B especially the mixed-linker systems (1:1) which have the highest $\Delta S°$ value as compared to (3:1), (1:3) and MOF-199 systems. This is actually compatible with the highest adsorption uptake as the dyes are adsorbed and desorbed continuously on the molecular level. Another important parameter is the enthalpy $\Delta H°$, which is positive for MOF-199 and all MTV-MOFs systems. This demonstrates that the adsorption process is endothermic and a stronger interaction exists between pre-adsorbed water and the adsorbent as compared to the one between the corresponding dye and the adsorbent which is evident from their high hydrophilic character, which agrees with the increase of MB and Rh B adsorption at higher temperatures. By comparing all the thermodynamic parameters of all of the four MOF systems, it is obvious that the MTV-MOFs (1:1) has the uppermost values and exhibits a good adsorption performance, with MB and Rh B removal up to 99% superior to the other systems.
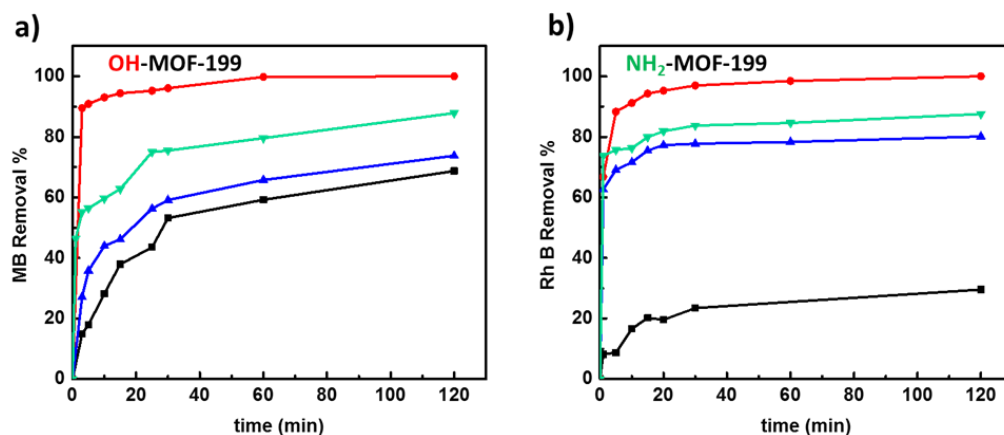
Figure 35 . Kinetic curves for the methylene blue and rhodamine B removal as a function of time by OH-BDC:BTC systems (a) and NH$_2$-BDC:BTC systems (b) respectively: MOF-199 (black), (1:3) (blue), (1:1) (red) and (3:1) (green).

4. Kinetic Study

The removal efficiency of MB and Rh B by OH-MOF-199 and NH$_2$-MOF-199 as a function of contact time is shown in Figure 35. It can be clearly seen that the highest efficiency and the most active systems are the ones with 1:1 starting ratios. By applying the linear regression of both kinetic models (pseudo-first and pseudo-second order), the correlation coefficients obtained for the pseudo-second order are much higher than those corresponding to the pseudo-first order in all of the four adsorbents for both dyes as shown in Table 10. The illustrations of the pseudo-first and pseudo-second order kinetic model are shown in Figure 36. Therefore, it is a bimolecular reaction and the rate determining step depends on the concentration of both the adsorbent (MOF) and the adsorbate (dye).
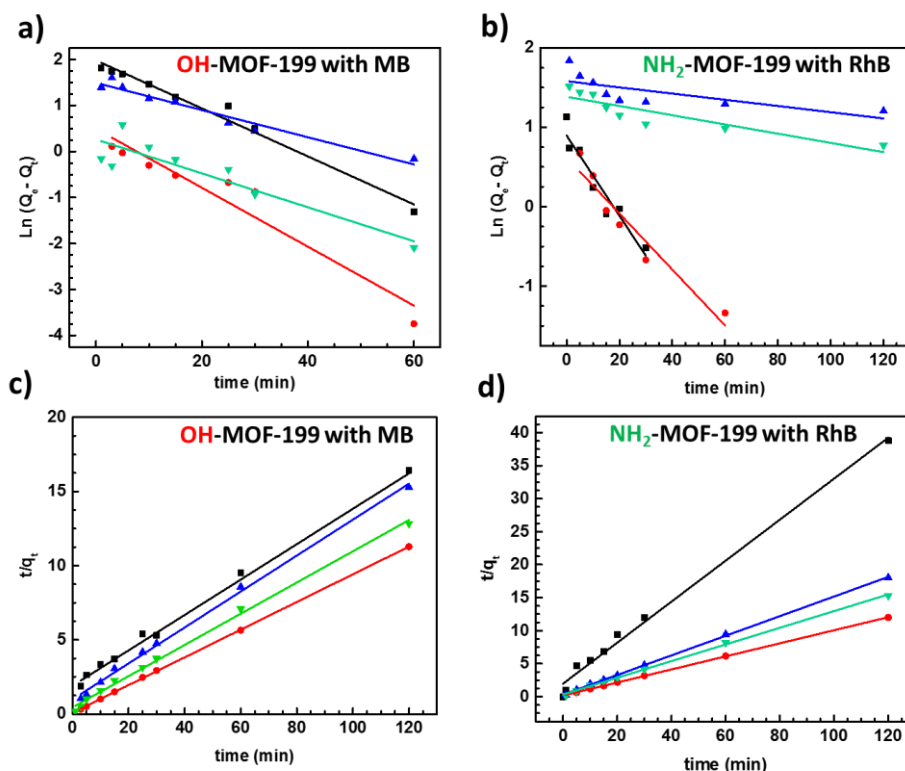
Figure 36 Pseudo-first order (a and b) and pseudo-second order (c and d) plots for OH-BDC:BTC systems (a and c) and NH_2-BDC:BTC systems (b and d): MOF-199 (black), (1:3) (blue), (1:1) (red) and (3:1) (green).

System	Pseudo-first order (R^2)	Pseudo-second order (R^2)
Methylene blue		
MOF-199	0.976	0.996
OH-MOF-199 (1:3)	0.948	0.997
OH-MOF-199 (1:1)	0.913	0.999
OH-MOF-199 (3:1)	0.909	0.999
Rhodamine B		
MOF-199	0.911	0.991
NH₂-MOF-199 (1:3)	0.964	1
NH₂-MOF-199 (1:1)	0.977	0.999
NH₂-MOF-199 (3:1)	0.966	0.999

Table 10 Correlation coefficients obtained for the pseudo-first order and pseudo-second order for OH-BDC:BTC systems and NH_2-BDC:BTC systems.

5. *Adsorption Mechanism: Intra-particle Diffusion*

In order to deeply understand the adsorption mechanism, the probability of intra-particle diffusion is investigated by applying the following equation:

$$q_t = K_p t^{0.5} + C \qquad (6)$$

where K_p is the intra-particle diffusion rate constant ($mg \cdot g^{-1} \cdot min^{-0.5}$) and C is a constant that defines the boundary layer effect. The graphs in Figure 37 reveals that the plots are not linear over the entire time interval, though it displays a dual linearity. This validates the presence of two consecutive adsorption stages of mass transport with a diminution in the rate. The first stage is the boundary layer effect whereas the second stage refers to the intra-particle diffusion, therefore a linear fit of the second stage permits the estimation of the values of the intra-particle rate constant k and the constant C. It is known that the effect of the intra-particle diffusion is more dominant when the value of C is lower and if C reaches zero, then the adsorption process is merely controlled by intra-particle diffusion[132]. However, this is not the case as demonstrated in Figure 37.
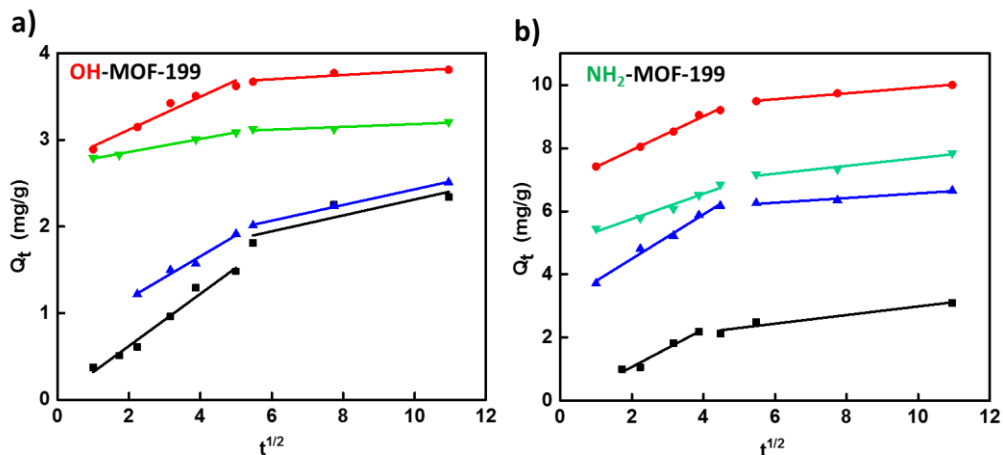
Figure 37 Intra-particle diffusion graphs for OH-BDC:BTC systems (a) and NH2-BDC:BTC systems (b); MOF-199 (black), (1:3) (blue), (1:1) (red) and (3:1) (green).

It is clear that the linear plot of q_t vs $t^{1/2}$ the of the second part didn't pass through the origin and the intercept values were 1.4, 1.5, 3 and 3.5 for MOF-199, OH-BDC:BTC (1:3), OH-BDC:BTC (3:1) and OH-BDC:BTC (1:1) respectively and 5.8, 6.4 and 9.0 for NH_2-BDC:BTC (1:3), NH_2-BDC:BTC (3:1) and NH_2-BDC:BTC (1:1) respectively. This indicates that the intra-particle diffusion is not the rate-determining step and is governed by linear diffusion.

6. *Recycling and reusability*

Figure 38 shows the recycling capability of OH-BDC:BTC (1:1) and NH_2-BDC:BTC (1:1) for MB and Rh B, respectively in the same adsorption conditions (1 mg of adsorbent /10 ml of 10 ppm dye solution). It is clear from the histograms that both MTV-MOFs systems are recyclable with less than 10% loss in efficiency after three consecutive cycles of adsorption and desorption. Moreover, the desorption process is achieved by stirring the loaded MTV-MOFs in a methanol solution for 30 mins. XRD patterns were also collected after the third cycle of desorption showing an intact crystalline structure for both systems as also shown in Figure 38.
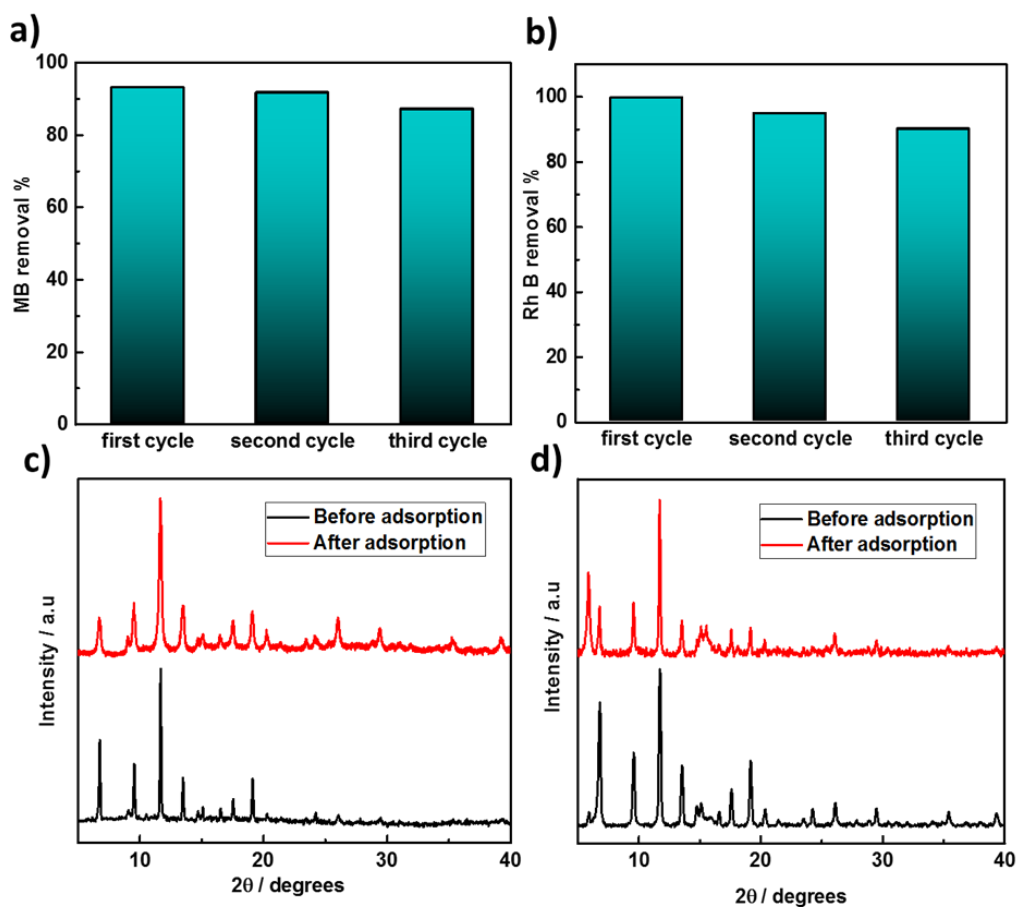
Figure 38 Recycling of OH-BDC:BTC (1:1) (a) and NH2-BDC:BTC (1:1) (b) and their corresponding PXRD patterns before and after adsorption respectively (c) and (d).

7. *Selectivity and co-adsorption studies*

In order to investigate the specify of the introduced functional group towards the adsorbed dye, additional experiments are performed on the optimal OH-MOF-199 (1:1) with Rh B and NH2-MOF-199 (1:1) with MB as well as each system with an equimolar binary solution of MB and Rh B. The results in Figure 39 showing the percentage of removal reflects the adsorption capacity since the conditions are that of a typical adsorption experiment. This demonstrate that while the OH-functionalized MOF-199

adsorbs less Rh B than the NH_2-functionalized MOF-199 and the latter adsorbs MB as good as the OH-functionalized-MOF-199. This can be explained by realizing that the MB molecule possesses a sulfur atom which is probably attracted to the metal cation of the adsorbent through acid-base interactions[141] while Rh B is less electron donor due to its stable zwitterion form in solution. On the other hand, the greater affinity of Rh B towards NH_2-MOF-199 might be due to greater hydrogen bonding between the oxygen in Rh B and the amino group of the MOF.

In any case, it is noteworthy to first state that the defect introduced in the MTV structures enhances the uptake regardless of the functional group when compared to the parent MOF-199 uptake. Hence, the enhanced adsorption obtained is due to the dual effect of introducing the functional group along with the creation of mesopores in the microporous MOF-199 structure allowing for more favorable adsorbent/adsorbate interactions. Moreover, the percentage of dye adsorption from the binary solution of MB and Rh B is higher for both systems which could be associated to the possibility there are newly created disparate specific adsorption sites for each of the dyes on the MTV-MOF, which do not generally compete with each other. These sites are accessible by the dyes, due to their small size, through any pore with a size greater than 1 nm via $\pi - \pi$ interactions.[142] This can be seen in Figure 39 where the adsorption of MB and Rh B in a binary solution is only slightly affected when compared to that in the individual solutions. The slight variations in both panels of Figure 39 could be due to the interaction of MB and Rh B due to π-stacking of the aromatic rings in a binary solution of the dyes.
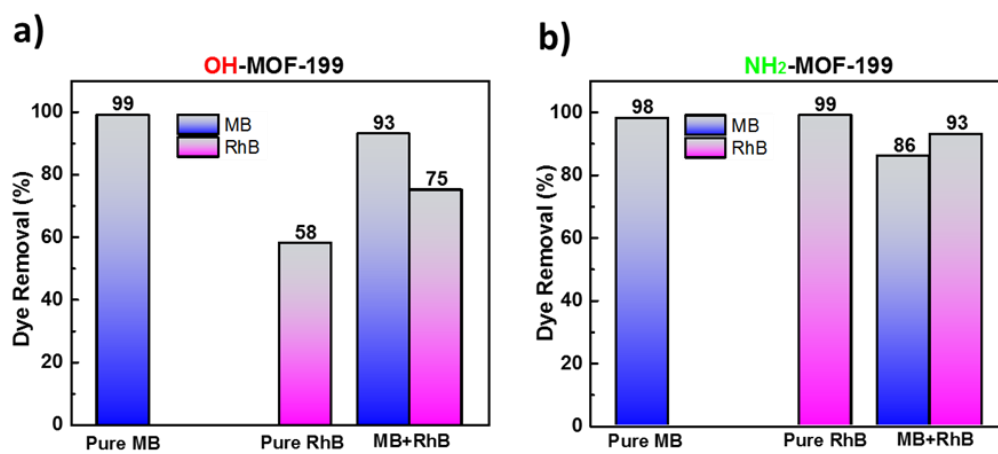
Figure 39 Dye removal percentage from individual and binary solutions of MB and Rh B by each of NH2-MOF-199 (a) and OH-MOF-199 (b).

CHAPTER V

CONCLUSION AND FUTURE WORK

A. Conclusion

A novel RDF technique is used to synthesize MOFs in a green environmentally friendly route. It consists of the diffusion of the outer metal solution throughout an inner gel matrix entrapping the organic linkers. The precipitation of the MOFs crystals inside the gel is initiated since the interface between the outer and the inner electrolytes, then propagates with the diffusion of the metal solution inside the gel, where nucleation dominates at the zones near the interface versus a dominating crystal growth as we go further in the tubular reactor. Hence, RDF allows a control over the size of the crystal and provide a live monitoring of the crystal shape throughout the tube. As MOF-199 is successfully synthesized in our lab by precipitating BTC linker with copper (II) via RDF, several organic linkers presenting geometric similarities to BTC are as well mixed to generate a series of multivariate MTV-MOFs-199. Namely, each of Isophthalic acid (IP-BDC), 5-hydroxyisophthalic acid (OH-BTC), 5-aminoisophthalic acid (NH_2-BDC), 5-cyanoisophthalic acid (CN-BDC), 5-sulfoisophthalic acid (SO_3-BDC) is mixed along with BTC in the inner agar gel to form MTV-MOFs incorporating 2-linkers, 3-linkers and 4-linkers-MTV-MOFs in one single MOF-199 framework without losing the crystalline order. A full characterization of the obtained MTV-MOFs is performed. PXRD patterns matched the inherited MOF-199 structure while SEM images beautifully revealed the progress of defect incorporated gradually in the structures turning the MOF-199 crystal

77

from a cubic structure to defective octahedrons and spherical particles in severe defect cases. In addition, the BET surface area is generally decreased as expected due to the incorporation of functionalized linkers to the structure and the creation of mesopores as well as the thermal stability that shows a slight decrease. More importantly, NMR experiments allows to calculate the actual amount of the functional linker introduced and reveals that this amount is decreasing down the tube regardless of the type of the functionality which enlarges the advantages of using RDF technique to grow multivariate MOFs for its ability to provide over the exact amount incorporated with the constructed frameworks.

On the application level, OH-MOF-199 is found to enhance the adsorption of the organic methylene blue dye and NH_2-MOF-199 to enhance that of Rh B dye from an aqueous solution compared to MOF-199. Thus, 3 different starting ratios 1:3, 1:1 and 3:1 are synthesized and activated then tested for adsorption and the 1:1 starting ratio is found to be the optimal system in both cases. Langmuir model shows the best fit model for the adsorption results and the corresponding adsorption capacities are 263 mg/g and 156 mg/g for MB and Rh B onto OH-MOF-199 (1:1) and NH_2-MOF-199 (1:1) respectively. The effect of pH is also investigated where the optimal pH is found to be that of the dye in water without any additives. In addition, the effect of the temperature is monitored and the thermodynamics parameters $\Delta H°$, $\Delta S°$ and $\Delta G°$ are calculated where the adsorption is found to endothermic and spontaneous at the ambient temperature. Moreover, the kinetic study shows that the adsorption phenomenon depends on both of the adsorbent and adsorbate as the pseudo-second order plots are the ones to show the lowest R-squared

values. The mechanism study and the intra-particle diffusion plots indicates that the adsorption happens in a double step process and the mechanism is governed by film diffusion rather than intra-particle diffusion. The reusability is also tested where the optimal MTV-MOFs systems are proved recyclable up to three times with minimal loss in effiency and crystallinity. Finally, the possibility of the adsorption of each of the dyes from a binary solution of MB and Rh B is also tested and proves the selectivity and effiency in the adsorption process where the percentage of adsorption is higher for both dyes adsorbed from a binary solution indicating the possibility of creation of specific adsorption sites of both dyes within each of the MTV-MOFs and this slight increase might be due to a higher interaction between the dyes themselves through $\pi - \pi$ stacking.

B. Future work

1. Investigate new structures via RDF

After the synthesis of several successful structures in the lab via RDF, the advantages are proving to be countless. RDF in MOFs is getting more attention worldwide and should be implemented as an alternative technique to the typical solvothermal synthesis that dissipates a lot of energy and uses harmful organic solvents. It would be very interesting to grow more famous MOF structures such as MOF-5, UIO-66, and many others and to compare the outcome with the solvothermal synthesis crystals. Noting that the RDF reaction conditions such as the concentrations, type of the gel, pH and the temperature can be finely tuned to optimize the obtained MOF's properties. Moreover, Metal-organic polyhedra (MOP), which are defined as discrete cages, are

formed in the absence of BTC when 1,3-dicarboxylate ligands are precipitated alone. MOPs are extremely important because of their tunable pore volume in terms of functionality and active metal sites[143]. Indeed, IP-BDC when precipitated alone via RDF in the same reaction conditions forms the famous MOP-1 structure (Figure 40) and it possible functionalization is also achieved by mixing it with NH_2-BDC while conserving the sharp cubic homogeneous structure. Noting that, the incorporation of NH_2-BDC is obvious because of the characteristic green color granted by NH_2-BDC in the similar MTV-MOFs. Further experimental characterization and future applications would be very interesting to be done.

a)   **b)**
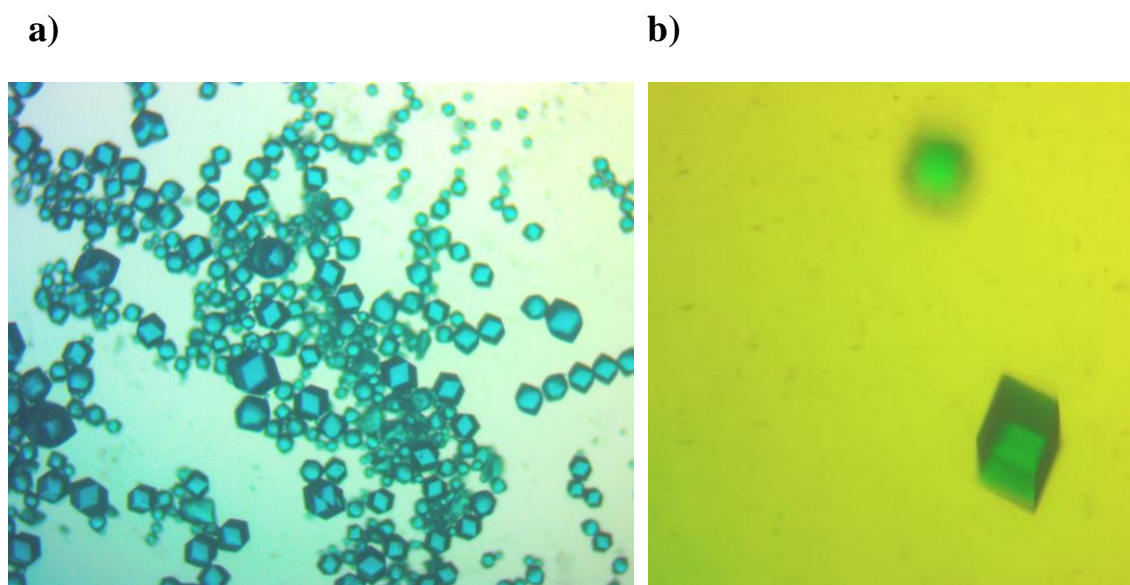
Figure 40 Microscopic pictures of the as synthesized IP-BDC-MOP (a) and IP-NH_2-BDC-MOP (b)

2. *Investigate in more heterogeneity via RDF*

Introducing a defect into a MOF's structure is a very challenging task to accomplish as it is usually faced with a phase separation or a loss of crystallinity in several

80

cases. In such cases, most of the scientists adopt the solvothermal synthesis in order to grant a homogenous outcome without taking into consideration the environmental side effects. The fact that RDF did succeed the test in producing MTV-MOFs structures in a green approach extends the hopes to many more successful syntheses. First of all, mixing of different metals into the same MOF-199 structure and optimizing the conditions to obtain a homogeneous solution is to be done owing to the fact that many metals such as Co^{2+}, Zn^{2+}, Ni^{2+} and others are already mixed in the backbone of MOF-199. Furthermore, mixing both organic linkers with mixed metals produces highly defective structures that may have outstanding properties in terms of the applications. Indeed, one of the synthesized MTV-MOFs of this work showed a very high surface area when both IP-BDC and OH-BDC are incorporated in one structure.

Moreover, defect incorporation is an unlimited field of study as more complex structures may be generated. The Mixing of geometrically distinct linkers and metals leading to different can now be tested after the successful synthesis of MTV-MOFs with similar linkers. Finally, MOPs also known as tertiary building units, in case where complex structures may be generated, as MOP building units may be stitched by relatively long linkers to form multifunctional heterogeneous frameworks.

SUPPORTING INFORMATION
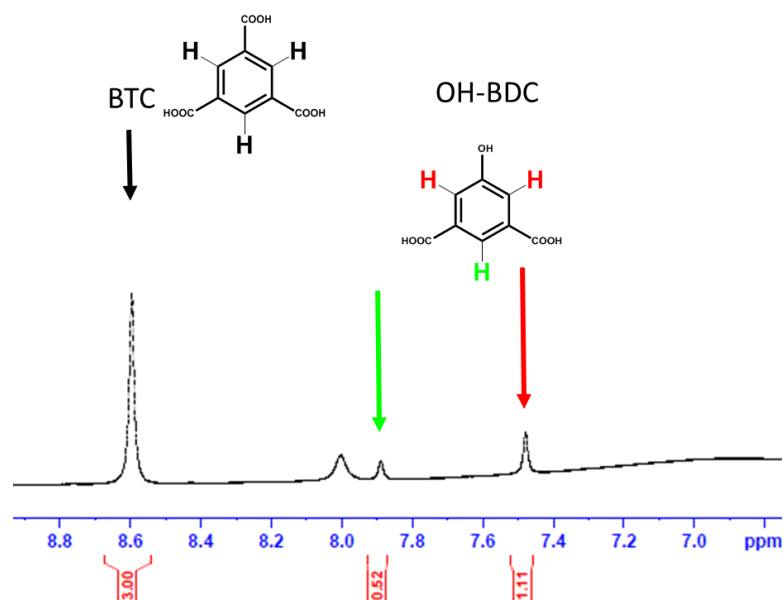
Figure S1 Representative NMR spectrum of the OH-MOF-199 system. Note that the peak at 8 ppm corresponds to remaining DMF in the framework accompanied by another peak at 3 ppm having double its intensity.
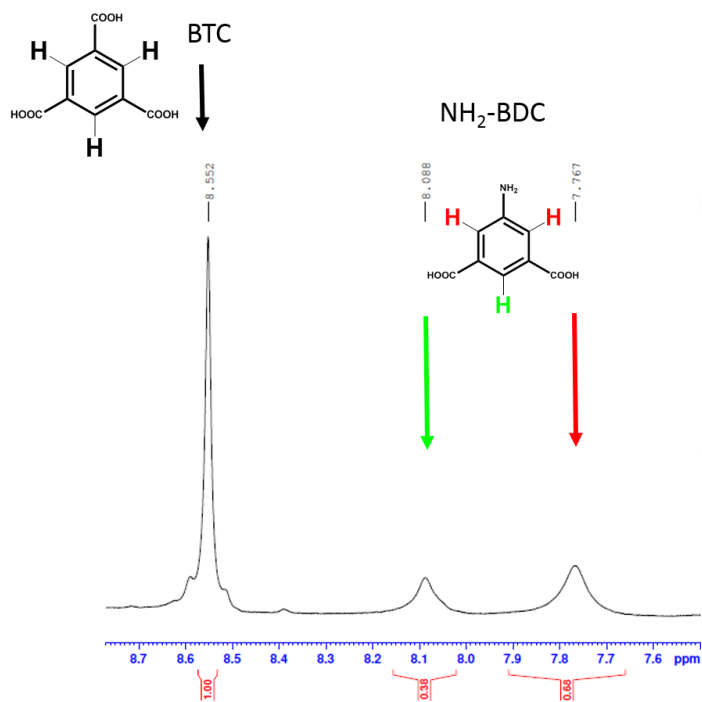
Figure S2 Representative NMR spectrum of the NH$_2$-MOF-199 system.
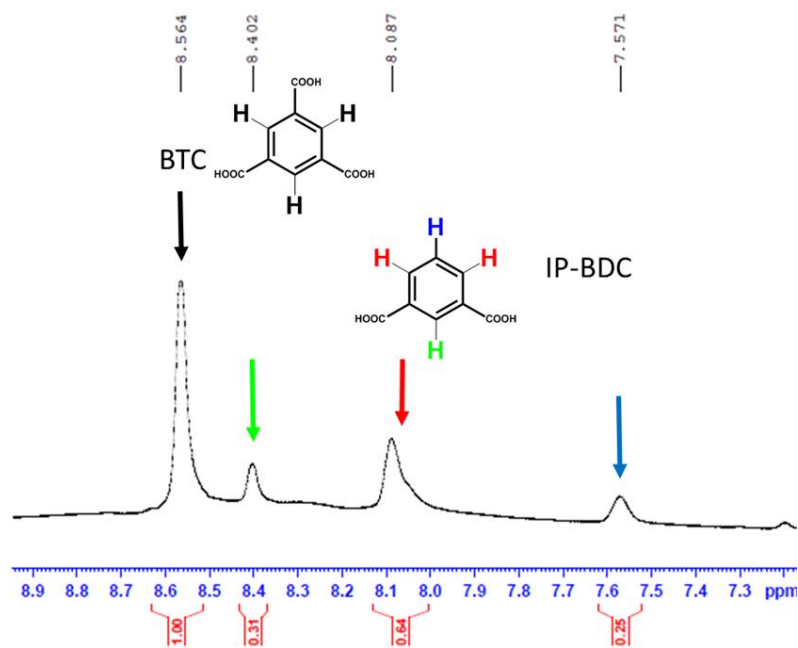
Figure S3 Representative NMR spectrum of the IP-MOF-199 system.
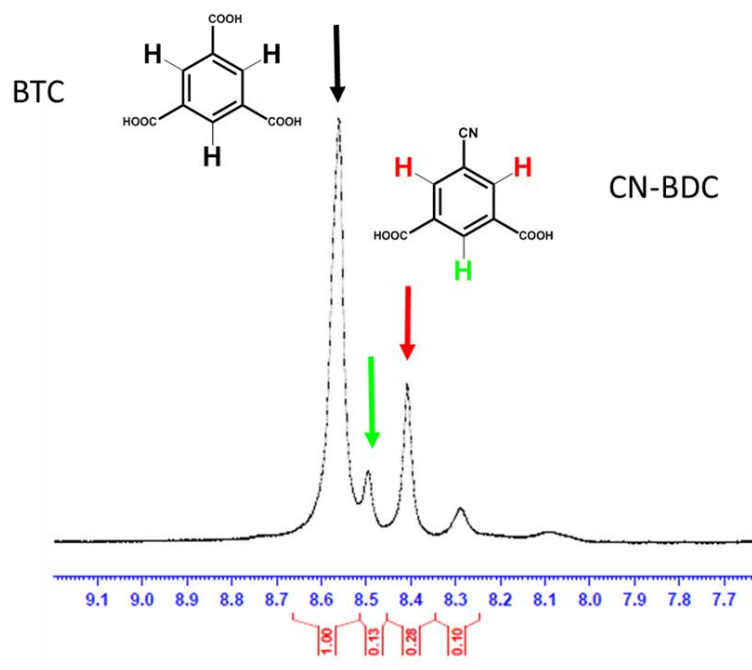
Figure S4 Representative NMR spectrum of the CN-MOF-199 system.
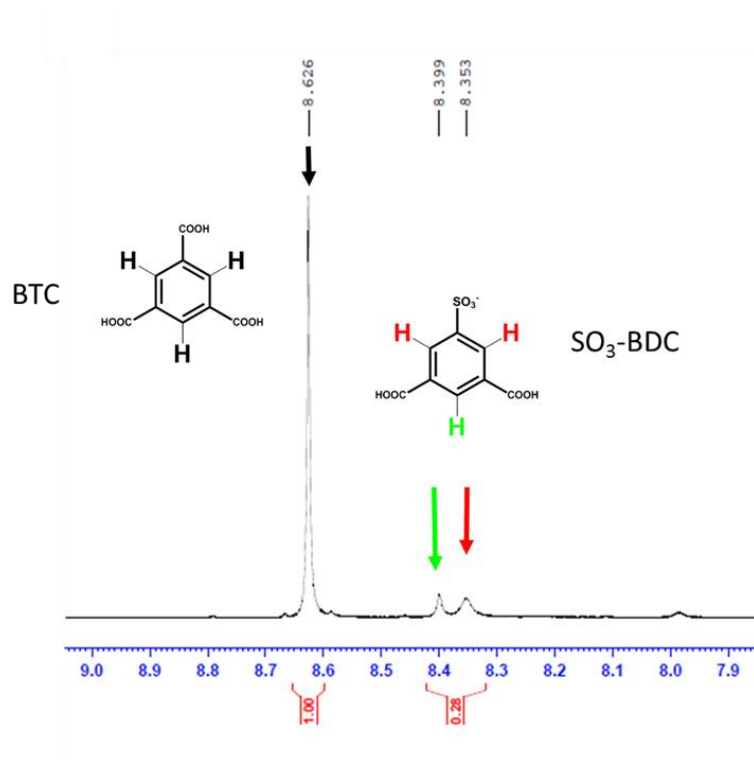
Figure S5 Representative NMR spectrum of the SO$_3$-MOF-199 system.
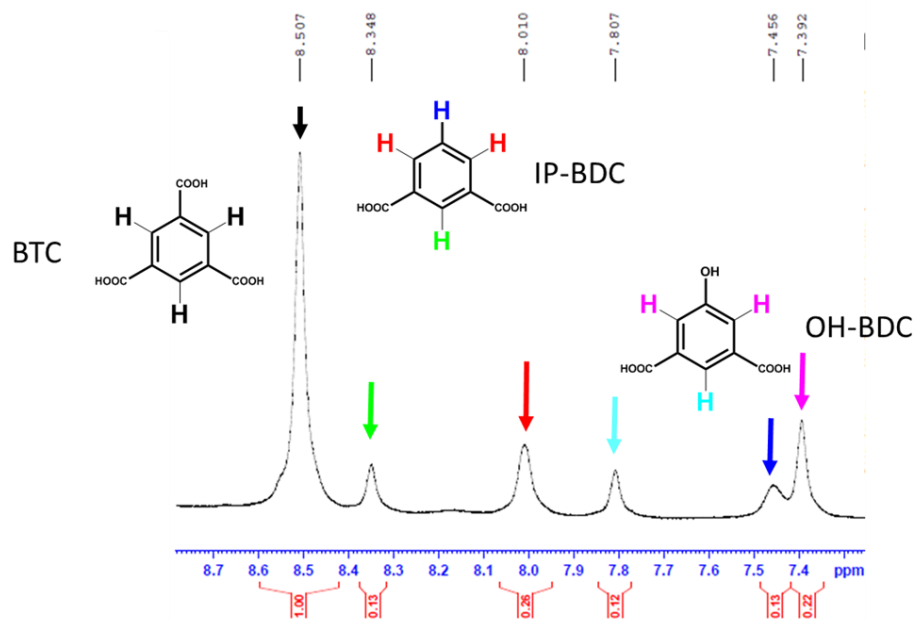
Figure S6 Representative NMR spectrum of the IP-OH-MOF-199 system.
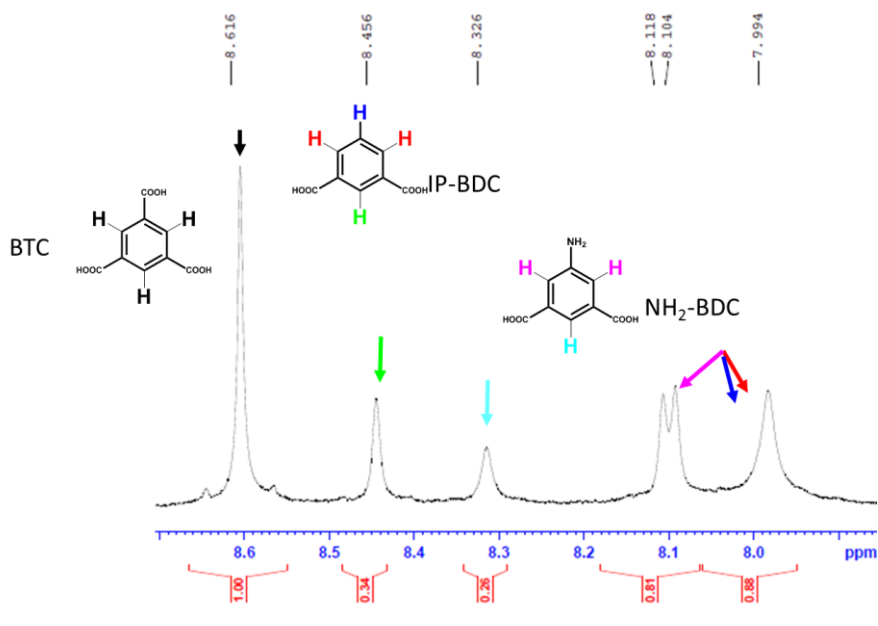
Figure S7 Representative NMR spectrum of the IP-NH$_2$-MOF-199 system. Note that some overlapping peaks are excluded from the calculations.
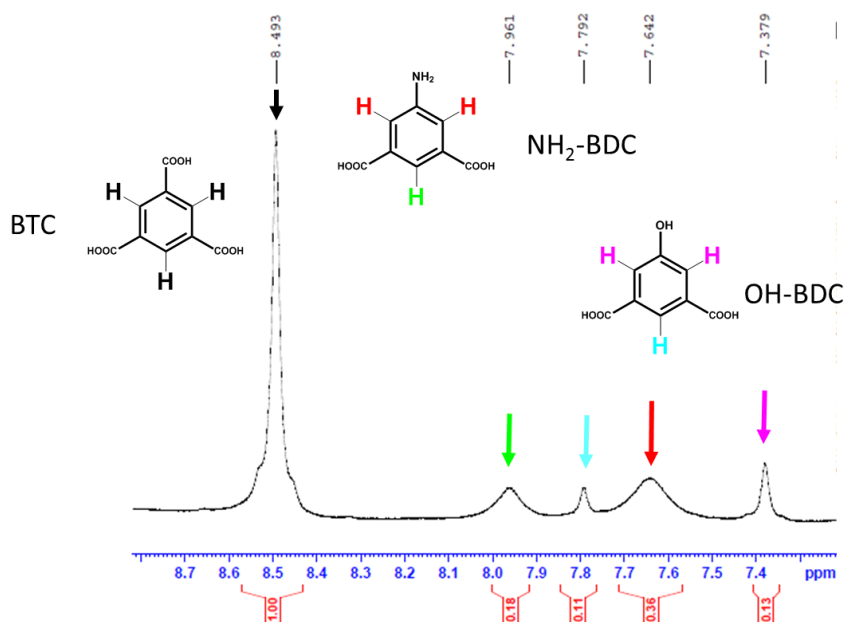
Figure S8 Representative NMR spectrum of the OH-NH$_2$-MOF-199 system.
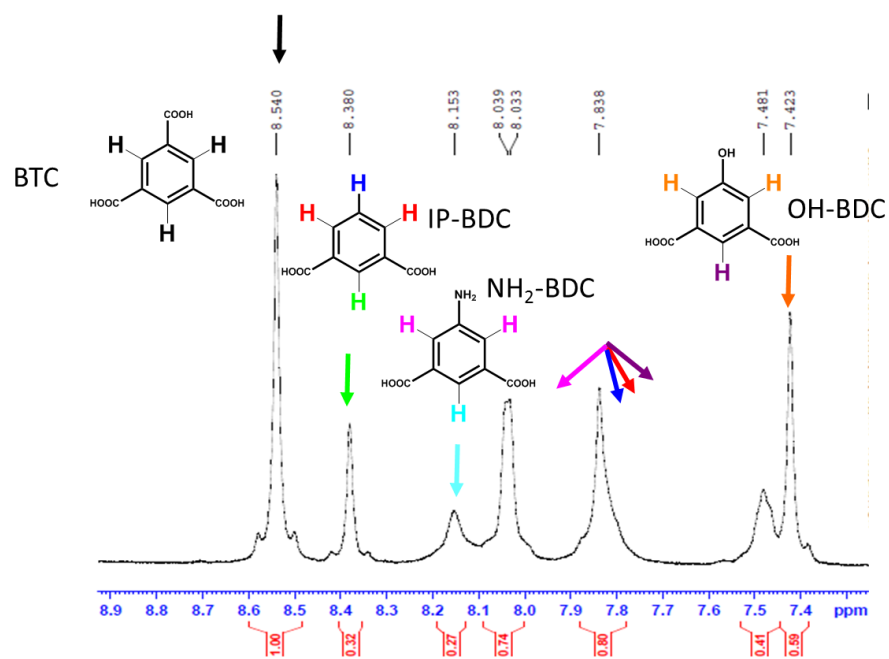
Figure S9 Representative NMR spectrum of the OH-NH$_2$-MOF-199 system. Note that some overlapping peaks are excluded from the calculations.

REFERENCES

1.   Karyakin, A. A., Prussian blue and its analogues: electrochemistry and analytical applications. *Electroanalysis: An International Journal Devoted to Fundamental and Practical Aspects of Electroanalysis* **2001,** *13* (10), 813-819.

2.   Kinoshita, Y.; Matsubara, I.; Higuchi, T.; Saito, Y., The crystal structure of bis (adiponitrilo) copper (I) nitrate. *Bulletin of the Chemical Society of Japan* **1959,** *32* (11), 1221-1226.

3.   Kwong, H.-L.; Lee, W.-S.; Ng, H.-F.; Chiu, W.-H.; Wong, W.-T., Chiral bipyridine–copper (II) complex. Crystal structure and catalytic activity in asymmetric cyclopropanation. *Journal of the Chemical Society, Dalton Transactions* **1998,** (6), 1043-1046.

4.   Yaghi, O. M.; Li, G.; Li, H., Selective binding and removal of guests in a microporous metal–organic framework. *Nature* **1995,** *378* (6558), 703-706.

5.   Li, H.; Eddaoudi, M.; Groy, T. L.; Yaghi, O., Establishing microporosity in open metal− organic frameworks: gas sorption isotherms for Zn (BDC)(BDC= 1, 4-benzenedicarboxylate). *Journal of the American Chemical Society* **1998,** *120* (33), 8571-8572.

6.   Li, H.; Eddaoudi, M.; O'Keeffe, M.; Yaghi, O. M., Design and synthesis of an exceptionally stable and highly porous metal-organic framework. *nature* **1999,** *402* (6759), 276.

7.   Chui, S. S.-Y.; Lo, S. M.-F.; Charmant, J. P.; Orpen, A. G.; Williams, I. D., A chemically functionalizable nanoporous material [Cu3 (TMA) 2 (H2O) 3] n. *Science* **1999,** *283* (5405), 1148-1150.

8.   Zhang, S.-Y.; Li, D.; Guo, D.; Zhang, H.; Shi, W.; Cheng, P.; Wojtas, L.; Zaworotko, M. J., Synthesis of a chiral crystal form of MOF-5, CMOF-5, by chiral induction. *Journal of the American Chemical Society* **2015,** *137* (49), 15406-15409.

9.   Saha, D.; Bao, Z.; Jia, F.; Deng, S., Adsorption of CO2, CH4, N2O, and N2 on MOF-5, MOF-177, and zeolite 5A. *Environmental science & technology* **2010,** *44* (5), 1820-1826.

10.   Salehi, S.; Anbia, M., High CO2 adsorption capacity and CO2/CH4 selectivity by nanocomposites of MOF-199. *Energy & Fuels* **2017,** *31* (5), 5376-5384.

11.   Mahmoodi, N. M.; Abdi, J., Nanoporous metal-organic framework (MOF-199): Synthesis, characterization and photocatalytic degradation of Basic Blue 41. *Microchemical Journal* **2019,** *144*, 436-442.

12.   Eddaoudi, M.; Moler, D. B.; Li, H.; Chen, B.; Reineke, T. M.; O'Keeffe, M.; Yaghi, O. M., Modular Chemistry: Secondary Building Units as a Basis for the Design of Highly Porous and Robust Metal−Organic Carboxylate Frameworks. *Accounts of Chemical Research* **2001,** *34* (4), 319-330.

13.   O'Keeffe, M.; Kim, J.; Yaghi, O. M.; Ockwig, N. W.; Chae, H. K.; Eddaoudi, M., Reticular synthesis and the design of new materials. *Nature* **2003,** *423* (6941), 705-714.

14.   Furukawa, H.; Cordova, K. E.; O'Keeffe, M.; Yaghi, O. M., The Chemistry and Applications of Metal-Organic Frameworks. *Science* **2013,** *341* (6149).

15.   Wang, C.; Liu, X.; Keser Demir, N.; Chen, J. P.; Li, K., Applications of water stable metal-organic frameworks. *Chemical Society Reviews* **2016,** *45* (18), 517-5134.

16.   Yaghi, O. M., Reticular Chemistry—Construction, Properties, and Precision Reactions of Frameworks. *Journal of the American Chemical Society* **2016,** *138* (48), 15507-15509.

17.   Kitagawa, S., Metal–organic frameworks (MOFs). *Chemical Society Reviews* **2014,** *43* (16), 5415-5418.

18.   Takaya, O.; Iyoki, K.; Fukushima, T.; Kajikawa, Y., Landscape of Research Areas for Zeolites and Metal-Organic Frameworks Using Computational Classification Based on Citation Networks. *Materials* **2017,** *10*, 1428.

19.   Tranchemontagne, D. J.; Mendoza-Cortés, J. L.; O'Keeffe, M.; Yaghi, O. M., Secondary building units, nets and bonding in the chemistry of metal–organic frameworks. *Chemical Society Reviews* **2009,** *38* (5), 1257-1283.

20.   Janiak, C.; Vieth, J. K., MOFs, MILs and more: concepts, properties and applications for porous coordination networks (PCNs). *New Journal of Chemistry* **2010,** *34* (11), 2366-2388.

21.   Furukawa, H.; Ko, N.; Go, Y. B.; Aratani, N.; Choi, S. B.; Choi, E.; Yazaydin, A. Ö.; Snurr, R. Q.; O'Keeffe, M.; Kim, J.; Yaghi, O. M., Ultrahigh Porosity in Metal-Organic Frameworks. *Science* **2010,** *329* (5990), 424-428.

22.   Bazzicalupi, C.; Bencini, A.; Lippolis, V., Tailoring cyclic polyamines for inorganic/organic phosphate binding. *Chemical Society Reviews* **2010,** *39* (10), 3709-3728.

23.   Tan, J. C.; Bennett, T. D.; Cheetham, A. K., Chemical structure, network topology, and porosity effects on the mechanical properties of Zeolitic Imidazolate Frameworks. *Proceedings of the National Academy of Sciences* **2010,** *107* (22), 9938-9943.

24.   Titov, A. A.; Filippov, O. A.; Epstein, L. M.; Belkova, N. V.; Shubina, E. S., Macrocyclic copper (I) and silver (I) pyrazolates: Principles of supramolecular assemblies with Lewis bases. *Inorganica Chimica Acta* **2018,** *470*, 22-35.

25.   Tăbăcaru, A.; Pettinari, C.; Galli, S., Coordination polymers and metal-organic frameworks built up with poly (tetrazolate) ligands. *Coordination Chemistry Reviews* **2018,** *372*, 1-30.

26.   Hmadeh, M.; Lu, Z.; Liu, Z.; Gándara, F.; Furukawa, H.; Wan, S.; Augustyn, V.; Chang, R.; Liao, L.; Zhou, F., New porous crystals of extended metal-catecholates. *Chemistry of Materials* **2012,** *24* (18), 3511-3513.

27.   Yaghi, O. M.; Kalmutzki, M. J.; Diercks, C. S., *Introduction to Reticular Chemistry: Metal-Organic Frameworks and Covalent Organic Frameworks*. John Wiley & Sons: 2019.

28.   Lu, W.; Wei, Z.; Gu, Z.-Y.; Liu, T.-F.; Park, J.; Park, J.; Tian, J.; Zhang, M.; Zhang, Q.; Gentle III, T., Tuning the structure and function of metal–organic frameworks via linker design. *Chemical Society Reviews* **2014,** *43* (16), 5561-5593.

29.   Rocío-Bautista, P.; Taima-Mancera, I.; Pasán, J.; Pino, V., Metal-Organic Frameworks in green analytical chemistry. *Separations* **2019,** *6* (3), 33.

30.   Eddaoudi, M.; Moler, D. B.; Li, H.; Chen, B.; Reineke, T. M.; O'keeffe, M.; Yaghi, O. M., Modular chemistry: secondary building units as a basis for the design of highly porous and robust metal− organic carboxylate frameworks. *Accounts of chemical research* **2001,** *34* (4), 319-330.

31.   Kalmutzki, M. J.; Hanikel, N.; Yaghi, O. M., Secondary building units as the turning point in the development of the reticular chemistry of MOFs. *Science advances* **2018,** *4* (10), eaat9180.

32.   Howarth, A. J.; Liu, Y.; Li, P.; Li, Z.; Wang, T. C.; Hupp, J. T.; Farha, O. K., Chemical, thermal and mechanical stabilities of metal–organic frameworks. *Nature Reviews Materials* **2016,** *1* (3), 1-15.

33.   Furukawa, H.; Müller, U.; Yaghi, O. M., "Heterogeneity within order" in metal–organic frameworks. *Angewandte Chemie International Edition* **2015,** *54* (11), 3417-3430.

34.   Deng, H.; Doonan, C. J.; Furukawa, H.; Ferreira, R. B.; Towne, J.; Knobler, C. B.; Wang, B.; Yaghi, O. M., Multiple functional groups of varying ratios in metal-organic frameworks. *Science* **2010,** *327* (5967), 846-850.

35.   Helal, A.; Yamani, Z. H.; Cordova, K. E.; Yaghi, O. M., Multivariate metal-organic frameworks. *National Science Review* **2017,** *4* (3), 296-298.

36.   Furukawa, H.; Cordova, K. E.; O'Keeffe, M.; Yaghi, O. M., The chemistry and applications of metal-organic frameworks. *Science* **2013,** *341* (6149), 974-974.

37.   Fang, Z.; Dürholt, J. P.; Kauer, M.; Zhang, W.; Lochenie, C.; Jee, B.; Albada, B.; Metzler-Nolte, N.; Pöppl, A.; Weber, B.; Muhler, M.; Wang, Y.; Schmid, R.; Fischer, R. A., Structural Complexity in Metal–Organic Frameworks: Simultaneous Modification of Open Metal Sites and Hierarchical Porosity by Systematic Doping with Defective Linkers. *Journal of the American Chemical Society* **2014,** *136* (27), 9627-9636.

38.   Li, B.; Wen, H. M.; Cui, Y.; Zhou, W.; Qian, G.; Chen, B., Emerging Multifunctional Metal–Organic Framework Materials. *Advanced Materials* **2016,** *28* (40), 8819-8860.

39.   Yuan, S.; Qin, J.-S.; Li, J.; Huang, L.; Feng, L.; Fang, Y.; Lollar, C.; Pang, J.; Zhang, L.; Sun, D., Retrosynthesis of multi-component metal− organic frameworks. *Nature communications* **2018,** *9* (1), 1-11.

40.   Zhang, Y.-B.; Furukawa, H.; Ko, N.; Nie, W.; Park, H. J.; Okajima, S.; Cordova, K. E.; Deng, H.; Kim, J.; Yaghi, O. M., Introduction of functionality, selection of topology, and enhancement of gas adsorption in multivariate metal–organic framework-177. *Journal of the American Chemical Society* **2015,** *137* (7), 2641-2650.

41.   Schrimpf, W.; Jiang, J.; Ji, Z.; Hirschle, P.; Lamb, D. C.; Yaghi, O. M.; Wuttke, S., Chemical diversity in a metal-organic framework revealed by fluorescence lifetime imaging. *Nature Communications* **2018,** *9* (1), 1647-10.

42.   Park, T.-H.; Koh, K.; Wong-Foy, A. G.; Matzger, A. J., Nonlinear properties in coordination copolymers derived from randomly mixed ligands. *Crystal growth & design* **2011,** *11* (6), 2059-2063.

43.   Botas, J. A.; Calleja, G.; Sánchez-Sánchez, M.; Orcajo, M. G., Cobalt doping of the MOF-5 framework and its effect on gas-adsorption properties. *Langmuir* **2010,** *26* (8), 5300-5303.

44.   Brozek, C. K.; Dincă, M., Ti3+-, V2+/3+-, Cr2+/3+-, Mn2+-, and Fe2+-substituted MOF-5 and redox reactivity in Cr-and Fe-MOF-5. *Journal of the American Chemical Society* **2013,** *135* (34), 12886-12891.

45.   Wang, L. J.; Deng, H.; Furukawa, H.; Gándara, F.; Cordova, K. E.; Peri, D.; Yaghi, O. M., Synthesis and characterization of metal–organic framework-74 containing 2, 4, 6, 8, and 10 different metals. *Inorganic chemistry* **2014,** *53* (12), 5881-5883.

46.   Liu, Q.; Cong, H.; Deng, H., Deciphering the spatial arrangement of metals and correlation to reactivity in multivariate metal–organic frameworks. *Journal of the American Chemical Society* **2016,** *138* (42), 13822-13825.

47.   Fang, Z.; Dürholt, J. P.; Kauer, M.; Zhang, W.; Lochenie, C.; Jee, B.; Albada, B.; Metzler-Nolte, N.; Pöppl, A.; Weber, B., Structural complexity in metal–organic frameworks: Simultaneous modification of open metal sites and hierarchical porosity by systematic doping with defective linkers. *Journal of the American Chemical Society* **2014,** *136* (27), 9627-9636.

48.   Wu, H.; Chua, Y. S.; Krungleviciute, V.; Tyagi, M.; Chen, P.; Yildirim, T.; Zhou, W., Unusual and highly tunable missing-linker defects in zirconium metal–organic framework UiO-66 and their important effects on gas adsorption. *Journal of the American Chemical Society* **2013,** *135* (28), 10525-10532.

49.   Vermoortele, F.; Bueken, B.; Le Bars, G. l.; Van de Voorde, B.; Vandichel, M.; Houthoofd, K.; Vimont, A.; Daturi, M.; Waroquier, M.; Van Speybroeck, V., Synthesis modulation as a tool to increase the catalytic activity of metal–organic frameworks: the unique case of UiO-66 (Zr). *Journal of the American Chemical Society* **2013,** *135* (31), 11465-11468.

50.   Barin, G.; Krungleviciute, V.; Gutov, O.; Hupp, J. T.; Yildirim, T.; Farha, O. K., Defect Creation by Linker Fragmentation in Metal–Organic Frameworks and Its Effects on Gas Uptake Properties. *Inorganic Chemistry* **2014,** *53* (13), 6914-6919.

51.   Vermoortele, F.; Ameloot, R.; Alaerts, L.; Matthessen, R.; Carlier, B.; Fernandez, E. V. R.; Gascon, J.; Kapteijn, F.; De Vos, D. E., Tuning the catalytic performance of metal–organic frameworks in fine chemistry by active site engineering. *Journal of Materials Chemistry* **2012,** *22* (20), 10313-10321.

52.   Park, J.; Wang, Z. U.; Sun, L.-B.; Chen, Y.-P.; Zhou, H.-C., Introduction of Functionalized Mesopores to Metal–Organic Frameworks via Metal–Ligand–Fragment Coassembly. *Journal of the American Chemical Society* **2012,** *134* (49), 20110-20116.

53.   Huang, L.; Wang, H.; Chen, J.; Wang, Z.; Sun, J.; Zhao, D.; Yan, Y., Synthesis, morphology control, and properties of porous metal–organic coordination polymers. *Microporous and mesoporous materials* **2003,** *58* (2), 105-114.

54.   Jrad, A.; Tarboush, B. J. A.; Hmadeh, M.; Ahmad, M., Tuning acidity in zirconium-based metal organic frameworks catalysts for enhanced production of butyl butyrate. *Applied Catalysis A: General* **2019,** *570*, 31-41.

55. Sun, Y.; Sun, L.; Feng, D.; Zhou, H. C., An in situ one‑pot synthetic approach towards multivariate zirconium MOFs. *Angewandte Chemie International Edition* **2016,** *55* (22), 6471-6475.

56. Bunck, D. N.; Dichtel, W. R., Mixed Linker Strategies for Organic Framework Functionalization. *Chemistry – A European Journal* **2013,** *19* (3), 818-827.

57. Ayoub, G.; Karadeniz, B.; Howarth, A. J.; Farha, O. K.; Đilović, I.; Germann, L. S.; Dinnebier, R. E.; Užarević, K.; Friscic, T., Rational Synthesis of Mixed-Metal Microporous Metal–Organic Frameworks with Controlled Composition Using Mechanochemistry. *Chemistry of Materials* **2019,** *31* (15), 5494-5501.

58. Masoomi, M. Y.; Stylianou, K. C.; Morsali, A.; Retailleau, P.; Maspoch, D., Selective CO2 Capture in Metal–Organic Frameworks with Azine-Functionalized Pores Generated by Mechanosynthesis. *Crystal Growth & Design* **2014,** *14* (5), 2092-2096.

59. Monterde, C.; Navarro, R.; Iglesias, M.; Sánchez, F., Fluorine-Phenanthroimidazole Porous Organic Polymer: Efficient Microwave Synthesis and Photocatalytic Activity. *ACS Applied Materials & Interfaces* **2019,** *11* (3), 3459-3465.

60. Wei, J.-Z.; Gong, F.-X.; Sun, X.-J.; Li, Y.; Zhang, T.; Zhao, X.-J.; Zhang, F.-M., Rapid and low-cost electrochemical synthesis of UiO-66-NH2 with enhanced fluorescence detection performance. *Inorganic chemistry* **2019,** *58* (10), 6742-6747.

61. Lu, M.; Deng, Y.; Luo, Y.; Lv, J.; Li, T.; Xu, J.; Chen, S.-W.; Wang, J., Graphene Aerogel–Metal–Organic Framework-Based Electrochemical Method for Simultaneous Detection of Multiple Heavy-Metal Ions. *Analytical chemistry* **2018,** *91* (1), 888-895.

62. Yue, Y.; Fulvio, P. F.; Dai, S., Hierarchical Metal–Organic Framework Hybrids: Perturbation-Assisted Nanofusion Synthesis. *Accounts of Chemical Research* **2015,** *48* (12), 3044-3052.

63. Duan, C.; Li, F.; Zhang, H.; Li, J.; Wang, X.; Xi, H., Template synthesis of hierarchical porous metal–organic frameworks with tunable porosity. *RSC Advances* **2017,** *7* (82), 52245-52251.

64. Razavi, S. A. A.; Masoomi, M. Y.; Morsali, A., Ultrasonic assisted synthesis of a tetrazine functionalized MOF and its application in colorimetric detection of phenylhydrazine. *Ultrasonics Sonochemistry* **2017,** *37*, 502-508.

65. Masoomi, M. Y.; Morsali, A.; Dhakshinamoorthy, A.; Garcia, H., Mixed-Metal MOFs: Unique Opportunities in Metal–Organic Framework (MOF) Functionality and Design. *Angewandte Chemie International Edition* **2019,** *58* (43), 15188-15205.

66. Yaghi, O. M., Reticular Chemistry in All Dimensions. *ACS Central Science* **2019,** *5* (8), 1295-1300.

67. Ibrahim, S. Synthesis and Applications of Novel Coordination Polymers and their Derivatives. Quaid-i-Azam University, Islamabad., 2019.

68. Deshpande, R. K.; Waterhouse, G. I.; Jameson, G. B.; Telfer, S. G., Photolabile protecting groups in metal–organic frameworks: preventing interpenetration and masking functional groups. *Chemical Communications* **2012,** *48* (10), 1574-1576.

69. Fu, Y.; Sun, D.; Chen, Y.; Huang, R.; Ding, Z.; Fu, X.; Li, Z., An Amine-Functionalized Titanium Metal–Organic Framework Photocatalyst with Visible-Light-Induced Activity for CO2 Reduction. *Angewandte Chemie International Edition* **2012,** *51* (14), 3364-3367.

70.   Cui, Y.; Li, B.; He, H.; Zhou, W.; Chen, B.; Qian, G., Metal–Organic Frameworks as Platforms for Functional Materials. *Accounts of Chemical Research* **2016,** *49* (3), 483-493.

71.   Fan, Y.-H.; Zhang, S.-W.; Qin, S.-B.; Li, X.-S.; Qi, S.-H., An enhanced adsorption of organic dyes onto NH2 functionalization titanium-based metal-organic frameworks and the mechanism investigation. *Microporous and Mesoporous Materials* **2018,** *263*, 120-127.

72.   Kirchon, A.; Feng, L.; Drake, H. F.; Joseph, E. A.; Zhou, H.-C.; Energy Frontier Research Centers . Center for Gas Separations Relevant to Clean Energy, T.; Univ. of California, O. C. A.; Texas, A.; M Univ, C. S. T. X., From fundamentals to applications: a toolbox for robust and multifunctional MOF materials. *Chemical Society Reviews* **2018,** *47* (23), 8611-8638.

73.   Cohen, S. M., Postsynthetic methods for the functionalization of metal–organic frameworks. *Chemical reviews* **2011,** *112* (2), 970-1000.

74.   Islamoglu, T.; Goswami, S.; Li, Z.; Howarth, A. J.; Farha, O. K.; Hupp, J. T., Postsynthetic tuning of metal–organic frameworks for targeted applications. *Accounts of chemical research* **2017,** *50* (4), 805-813.

75.   Yu, D.; Shao, Q.; Song, Q.; Cui, J.; Zhang, Y.; Wu, B.; Ge, L.; Wang, Y.; Zhang, Y.; Qin, Y., A solvent-assisted ligand exchange approach enables metal-organic frameworks with diverse and complex architectures. *Nature communications* **2020,** *11* (1), 1-10.

76.   Kim, M.; Cahill, J. F.; Su, Y.; Prather, K. A.; Cohen, S. M., Postsynthetic ligand exchange as a route to functionalization of 'inert' metal-organic frameworks. *Chemical Science* **2012,** *3* (1), 126-130.

77.   Yuan, S.; Lu, W.; Chen, Y.-P.; Zhang, Q.; Liu, T.-F.; Feng, D.; Wang, X.; Qin, J.; Zhou, H.-C., Sequential Linker Installation: Precise Placement of Functional Groups in Multivariate Metal–Organic Frameworks. *Journal of the American Chemical Society* **2015,** *137* (9), 3177-3180.

78.   Cui, P.; Wang, P.; Zhao, Y.; Sun, W.-Y., Fabrication of Desired Metal–Organic Frameworks via Postsynthetic Exchange and Sequential Linker Installation. *Crystal Growth & Design* **2019,** *19* (2), 1454-1470.

79.   Czaja, A. U.; Trukhan, N.; Müller, U., Industrial applications of metal–organic frameworks. *Chemical Society Reviews* **2009,** *38* (5), 1284-1293.

80.   Sosa, J.; Bennett, T.; Nelms, K.; Liu, B.; Tovar, R.; Liu, Y., Metal–Organic Framework Hybrid Materials and Their Applications. *Crystals* **2018,** *8* (8), 325.

81.   Alezi, D.; Belmabkhout, Y.; Suyetin, M.; Bhatt, P. M.; Weseliński, Ł. J.; Solovyeva, V.; Adil, K.; Spanopoulos, I.; Trikalitis, P. N.; Emwas, A.-H., MOF crystal chemistry paving the way to gas storage needs: aluminum-based soc-MOF for CH4, O2, and CO2 storage. *Journal of the American Chemical Society* **2015,** *137* (41), 13308-13318.

82.   Chouhan, N.; Liu, R.-S.; Zhang, J., *Photochemical Water Splitting: Materials and Applications*. CRC Press: 2017.

83.   Sun, D.; Ma, S.; Ke, Y.; Collins, D. J.; Zhou, H.-C., An interweaving MOF with high hydrogen uptake. *Journal of the American Chemical Society* **2006,** *128* (12), 3896-3897.

84.   Alkordi, M. H.; Belmabkhout, Y.; Cairns, A.; Eddaoudi, M., Metal–organic frameworks for H2 and CH4 storage: insights on the pore geometry–sorption energetics relationship. *IUCrJ* **2017,** *4* (Pt 2), 131.

85.   Sun, X.; Ma, Y.; Zhao, J.; Li, D.-S.; Li, G.; Zhang, L.; Liu, Y., Tuning the gate opening pressure of a flexible doubly interpenetrated metal–organic framework through ligand functionalization. *Dalton Transactions* **2018,** *47* (37), 13158-13163.

86.   Li, B.; Wen, H.-M.; Zhou, W.; Xu, J. Q.; Chen, B., Porous metal-organic frameworks: promising materials for methane storage. *Chem* **2016,** *1* (4), 557-580.

87.   Alezi, D.; Belmabkhout, Y.; Eddaoudi, M., Methane Storage in Metal-Organic Frameworks: Insights into the Storage Performance and the Intrinsic Property Relationships for Enhanced Adsorbed Natural Gas Storage. World Scientific: 2018.

88.   Belmabkhout, Y.; Mouttaki, H.; Eubank, J. F.; Guillerm, V.; Eddaoudi, M., Effect of pendant isophthalic acid moieties on the adsorption properties of light hydrocarbons in HKUST-1-like tbo-MOFs: application to methane purification and storage. *RSC Advances* **2014,** *4* (109), 63855-63859.

89.   Cordova, K. E.; Yaghi, O. M., The 'folklore'and reality of reticular chemistry. *Materials Chemistry Frontiers* **2017,** *1* (7), 1304-1309.

90.   Peplow, M., Materials science: the hole story. *Nature News* **2015,** *520* (7546), 148.

91.   Edenhofer, O., *Climate change 2014: mitigation of climate change*. Cambridge University Press: 2015; Vol. 3.

92.   Fracaroli, A. M.; Furukawa, H.; Suzuki, M.; Dodd, M.; Okajima, S.; Gándara, F.; Reimer, J. A.; Yaghi, O. M., Metal–organic frameworks with precisely designed interior for carbon dioxide capture in the presence of water. *Journal of the American Chemical Society* **2014,** *136* (25), 8863-8866.

93.   Nugent, P.; Belmabkhout, Y.; Burd, S. D.; Cairns, A. J.; Luebke, R.; Forrest, K.; Pham, T.; Ma, S.; Space, B.; Wojtas, L., Porous materials with optimal adsorption thermodynamics and kinetics for CO 2 separation. *Nature* **2013,** *495* (7439), 80-84.

94.   Trickett, C. A.; Helal, A.; Al-Maythalony, B. A.; Yamani, Z. H.; Cordova, K. E.; Yaghi, O. M., The chemistry of metal–organic frameworks for CO 2 capture, regeneration and conversion. *Nature Reviews Materials* **2017,** *2* (8), 1-16.

95.   Furukawa, H.; Gandara, F.; Zhang, Y.-B.; Jiang, J.; Queen, W. L.; Hudson, M. R.; Yaghi, O. M., Water adsorption in porous metal–organic frameworks and related materials. *Journal of the American Chemical Society* **2014,** *136* (11), 4369-4381.

96.   DeCoste, J. B.; Peterson, G. W.; Jasuja, H.; Glover, T. G.; Huang, Y.-g.; Walton, K. S., Stability and degradation mechanisms of metal–organic frameworks containing the Zr 6 O 4 (OH) 4 secondary building unit. *Journal of Materials Chemistry A* **2013,** *1* (18), 5642-5650.

97.   Jiang, D.; Chen, M.; Wang, H.; Zeng, G.; Huang, D.; Cheng, M.; Liu, Y.; Xue, W.; Wang, Z., The application of different typological and structural MOFs-based materials for the dyes adsorption. *Coordination Chemistry Reviews* **2019,** *380*, 471-483.

98.   Jiao, J.; Gong, W.; Wu, X.; Yang, S.; Cui, Y., Multivariate crystalline porous materials: Synthesis, property and potential application. *Coordination Chemistry Reviews* **2019,** *385*, 174-190.

99.   Li, C.; Xiong, Z.; Zhang, J.; Wu, C., The strengthening role of the amino group in metal–organic framework MIL-53 (Al) for methylene blue and malachite green dye adsorption. *Journal of Chemical & Engineering Data* **2015,** *60* (11), 3414-3422.

100.   Yuan, Q.; Li, N.; Chi, Y.; Geng, W.; Yan, W.; Zhao, Y.; Li, X.; Dong, B., Effect of large pore size of multifunctional mesoporous microsphere on removal of heavy metal ions. *Journal of hazardous materials* **2013,** *254*, 157-165.

101.   Alsbaiee, A.; Smith, B. J.; Xiao, L.; Ling, Y.; Helbling, D. E.; Dichtel, W. R., Rapid removal of organic micropollutants from water by a porous β-cyclodextrin polymer. *Nature* **2016,** *529* (7585), 190.

102.   Shetty, D.; Jahovic, I.; Raya, J.; Asfari, Z.; Olsen, J.-C.; Trabolsi, A., Porous Polycalix[4]arenes for Fast and Efficient Removal of Organic Micropollutants from Water. *ACS Applied Materials & Interfaces* **2018,** *10* (3), 2976-2981.

103.   Adeyemo, A. A.; Adeoye, I. O.; Bello, O. S., Metal organic frameworks as adsorbents for dye adsorption: overview, prospects and future challenges. *Toxicological & Environmental Chemistry* **2012,** *94* (10), 1846-1863.

104.   Yoon, M.; Srirambalaji, R.; Kim, K., Homochiral metal–organic frameworks for asymmetric heterogeneous catalysis. *Chemical reviews* **2012,** *112* (2), 1196-1231.

105.   Canivet, J.; Vandichel, M.; Farrusseng, D., Origin of highly active metal–organic framework catalysts: defects? Defects! *Dalton Transactions* **2016,** *45* (10), 4090-4099.

106.   Yuan, S.; Zou, L.; Qin, J.-S.; Li, J.; Huang, L.; Feng, L.; Wang, X.; Bosch, M.; Alsalme, A.; Cagin, T., Construction of hierarchically porous metal–organic frameworks through linker labilization. *Nature communications* **2017,** *8* (1), 1-10.

107.   Xu, C.; Fang, R.; Luque, R.; Chen, L.; Li, Y., Functional metal–organic frameworks for catalytic applications. *Coordination Chemistry Reviews* **2019,** *388*, 268-292.

108.   Feng, D.; Liu, T.-F.; Su, J.; Bosch, M.; Wei, Z.; Wan, W.; Yuan, D.; Chen, Y.-P.; Wang, X.; Wang, K.; Lian, X.; Gu, Z.-Y.; Park, J.; Zou, X.; Zhou, H.-C., Stable metal-organic frameworks containing single-molecule traps for enzyme encapsulation. *Nature Communications* **2015,** *6* (1), 5979.

109.   Qiu, X.; Zhong, W.; Bai, C.; Li, Y., Encapsulation of a metal–organic polyhedral in the pores of a metal–organic framework. *Journal of the American Chemical Society* **2016,** *138* (4), 1138-1141.

110.   Lei, J.; Qian, R.; Ling, P.; Cui, L.; Ju, H., Design and sensing applications of metal–organic framework composites. *TrAC Trends in Analytical Chemistry* **2014,** *58*, 71-78.

111.   Shustova, N. B.; Cozzolino, A. F.; Reineke, S.; Baldo, M.; Dincă, M., Selective turn-on ammonia sensing enabled by high-temperature fluorescence in metal–organic frameworks with open metal sites. *Journal of the American Chemical Society* **2013,** *135* (36), 13326-13329.

112.   Hu, Z.; Deibert, B. J.; Li, J., Luminescent metal–organic frameworks for chemical sensing and explosive detection. *Chemical Society Reviews* **2014,** *43* (16), 5815-5840.

113.   Cui, Y.; Yue, Y.; Qian, G.; Chen, B., Luminescent functional metal–organic frameworks. *Chemical reviews* **2012,** *112* (2), 1126-1162.

114.   Sun, L.; Miyakai, T.; Seki, S.; Dincă, M., Mn2 (2, 5-disulfhydrylbenzene-1, 4-dicarboxylate): a microporous metal–organic framework with infinite (− Mn–S−) ∞ chains and high intrinsic charge mobility. *Journal of the American Chemical Society* **2013,** *135* (22), 8185-8188.

115.   Talin, A. A.; Centrone, A.; Ford, A. C.; Foster, M. E.; Stavila, V.; Haney, P.; Kinney, R. A.; Szalai, V.; El Gabaly, F.; Yoon, H. P., Tunable electrical conductivity in metal-organic framework thin-film devices. *Science* **2014,** *343* (6166), 66-69.

116.   Donnelly, R. J.; Herman, R.; Prigogine, I., *Non-equilibrium thermodynamics: variational techniques and stability*. University of Chicago Press: 1966.

117.   Grzybowski, B. A., *Chemistry in motion: reaction-diffusion systems for micro- and nanotechnology*. John Wiley & Sons: 2009.

118.   Al-Ghoul, M.; Sultan, R., Front propagation in patterned precipitation. 1. Simulation of a migrating Co (OH) 2 Liesegang pattern. *The Journal of Physical Chemistry A* **2001,** *105* (34), 8053-8058.

119.   Al-Ghoul, M.; Ammar, M.; Al-Kaysi, R. O., Band propagation, scaling laws and phase transition in a precipitate system. I: Experimental study. *The Journal of Physical Chemistry A* **2012,** *116* (18), 4427-4437.

120.   Al-Ghoul, M.; Ammar, M. In *Polymorphic and Morphological Transformation during the Transition from a Propagating Band to Static Bands in the Nickel Hydroxide/Ammonia Liesegang System*, Defect and Diffusion Forum, Trans Tech Publ: 2011; pp 800-805.

121.   Al Akhrass, G. A.; Ammar, M.; El-Rassy, H.; Al-Ghoul, M., Self-assembled lanthanum hydroxide microspheres within a reaction-diffusion framework: Synthesis, characterization, control and application. *RSC Advances* **2016,** *6* (5), 3433-3439.

122.   Kashchiev, D., *Nucleation*. Elsevier: 2000.

123.   Saliba, D.; Ammar, M.; Rammal, M.; Al-Ghoul, M.; Hmadeh, M., Crystal Growth of ZIF-8, ZIF-67, and Their Mixed-Metal Derivatives. *Journal of the American Chemical Society* **2018,** *140* (5), 1812-1823.

124.   Yu, J.; Mu, C.; Yan, B.; Qin, X.; Shen, C.; Xue, H.; Pang, H., Nanoparticle/MOF composites: preparations and applications. *Materials Horizons* **2017,** *4* (4), 557-569.

125.   Al-Ghoul, M.; Issa, R.; Hmadeh, M., Synthesis, size and structural evolution of metal–organic framework-199 via a reaction–diffusion process at room temperature. *CrystEngComm* **2017,** *19* (4), 608-612.

126.   Issa, R.; Hmadeh, M.; Al-Ghoul, M., Control of Particle Size and Morphology of MOF-199 Crystals via a Reaction-Diffusion Framework. *Defect and Diffusion Forum* **2017,** *380*, 39-47.

127.   Zakhia Douaihy, R.; Al‐Ghoul, M.; Hmadeh, M., Liesegang Banding for Controlled Size and Growth of Zeolitic‐Imidazolate Frameworks. *Small* **2019,** *15* (28), 1901605.

128.   Park, J. H.; Paczesny, J.; Kim, N.; Grzybowski, B. A., Shaping Microcrystals of Metal–Organic Frameworks by Reaction–Diffusion. *Angewandte Chemie International Edition* **2020**.

129.   Peterson, G. W.; Au, K.; Tovar, T. M.; Epps, T. H., Multivariate CuBTC Metal–Organic Framework with Enhanced Selectivity, Stability, Compatibility, and Processability. *Chemistry of Materials* **2019,** *31* (20), 8459-8465.

130.   Lee, H. J.; We, J.; Kim, J. O.; Kim, D.; Cha, W.; Lee, E.; Sohn, J.; Oh, M., Morphological and Structural Evolutions of Metal–Organic Framework Particles from Amorphous Spheres to Crystalline Hexagonal Rods. *Angewandte Chemie International Edition* **2015,** *54* (36), 10564-10568.

131.   Sing, K. S., Reporting physisorption data for gas/solid systems with special reference to the determination of surface area and porosity (Recommendations 1984). *Pure and applied chemistry* **1985,** *57* (4), 603-619.

132.   Xiong, L.; Yang, Y.; Mai, J.; Sun, W.; Zhang, C.; Wei, D.; Chen, Q.; Ni, J., Adsorption behavior of methylene blue onto titanate nanotubes. *Chemical Engineering Journal* **2010,** *156* (2), 313-320.

133.   Raposo, F.; De La Rubia, M. A.; Borja, R., Methylene blue number as useful indicator to evaluate the adsorptive capacity of granular activated carbon in batch mode: Influence of adsorbate/adsorbent mass ratio and particle size. *Journal of Hazardous Materials* **2009,** *165* (1), 291-299.

134.   Li, L.; Liu, X. L.; Geng, H. Y.; Hu, B.; Song, G. W.; Xu, Z. S., A MOF/graphite oxide hybrid (MOF: HKUST-1) material for the adsorption of methylene blue from aqueous solution. *Journal of Materials Chemistry A* **2013,** *1* (35), 10292-10299.

135.   Selvam, P. P.; Preethi, S.; Basakaralingam, P.; N.Thinakaran; Sivasamy, A.; Sivanesan, S., Removal of rhodamine B from aqueous solution by adsorption onto sodium montmorillonite. *Journal of Hazardous Materials* **2008,** *155* (1), 39-44.

136.   Kadirvelu, K.; Karthika, C.; Vennilamani, N.; Pattabhi, S., Activated carbon from industrial solid waste as an adsorbent for the removal of Rhodamine-B from aqueous solution: Kinetic and equilibrium studies. *Chemosphere* **2005,** *60* (8), 1009-1017.

137.   Guo, H.; Lin, F.; Chen, J.; Li, F.; Weng, W., Metal–organic framework MIL-125(Ti) for efficient adsorptive removal of Rhodamine B from aqueous solution. *Applied Organometallic Chemistry* **2015,** *29* (1), 12-19.

138.   Eftekhari, S.; Habibi-Yangjeh, A.; Sohrabnezhad, S., Application of AlMCM-41 for competitive adsorption of methylene blue and rhodamine B: Thermodynamic and kinetic studies. *Journal of Hazardous Materials* **2010,** *178* (1), 349-355.

139.   Dukhin, S., J. Lyklema Fundamentals of Interface and Colloid Science vol. IV 2005 Academic Press New York-Toronto. Elsevier B.V: 2006; Vol. 119, pp 69-70.

140.   Fontecha-Cámara, M. A.; López-Ramón, M. V.; Álvarez-Merino, M. A.; Moreno-Castilla, C., Effect of Surface Chemistry, Solution pH, and Ionic Strength on the Removal of Herbicides Diuron and Amitrole from Water by an Activated Carbon Fiber. *Langmuir* **2007,** *23* (3), 1242-1247.

141.   Blanco-Brieva, G.; Campos-Martin, J.; Al-Zahrani, S.; Fierro, J., Removal of refractory organic sulfur compounds in fossil fuels using MOF sorbents. *Global Nest J* **2010,** *12* (12), 296-304.

142.   Banerjee, A.; Gokhale, R.; Bhatnagar, S.; Jog, J.; Bhardwaj, M.; Lefez, B.; Hannoyer, B.; Ogale, S., MOF derived porous carbon–Fe 3 O 4 nanocomposite as a high

performance, recyclable environmental superadsorbent. *Journal of Materials Chemistry* **2012,** *22* (37), 19694-19699.

143. Tranchemontagne, D. J.; Ni, Z.; O'Keeffe, M.; Yaghi, O. M., Reticular chemistry of metal–organic polyhedra. *Angewandte Chemie International Edition* **2008,** *47* (28), 5136-5147.